REAL-TIME IMAGE PROCESSING USING ACOUSTO-OPTIC BRAGG DIFFRACTION

by

Derrek Butler Dunn

Dissertation submitted to the Graduate Faculty of
Virginia Polytechnic Institute and State University
in partial fulfillment of the requirements for the degree of

Doctor of Philosophy
in
Electrical Engineering

APPROVED:

_____
Dr. Ting-Chung Poon, Chairman

_____ _____
Dr. Ioannis M. Besieris Dr. Ahmad Safaai-Jazi

_____ _____
Dr. Wayne A. Scales Dr. Carl L. Prather

January 7, 1998

Blacksburg, Virginia

Keywords: Image Processing, Bragg Diffraction, Acousto-Optics, Transfer Function

REAL-TIME IMAGE PROCESSING
USING
ACOUSTO-OPTIC BRAGG DIFFRACTION

by

Derrek Butler Dunn

Ting-Chung Poon, Chairmen

Electrical Engineering Department

(ABSTRACT)

Optical image processing systems using an acousto-optic cell have been studied previously. However, these previous studies have been limited to two diffracted order in the Bragg regime and two spatial dimensions. Some comparisons between experimental data and theoretical predictions have been made.

This dissertation studies image processing by acousto-optic Bragg diffraction to perform image enhanment. Theoretical results involving two diffracted orders in three spatial dimensions is presented. Experimental data is presented that confirms the validity of the theoretical results. Detailed analysis of several optical image processing system using acousto-optic modulators is presented. Also, the methodology use to derive an analytically expression in three spatial dimension for the interaction of an arbitrary light profile and a rectangular sound column in an acousto-optic cell is presented.

Lastly, the ability to change the characteristics of the derived transfer function that mathematically represents the interaction of light and sound inside the acousto-optic cell is discussed and future research topics is given.

Grant Information

I would also like to acknowledge the support of Office of Naval Research and The Historically Black Engineering College fellowship (grant # N000014-92-J-1252-VPI-002).

Dedication

I dedicate this dissertation to my mother, Roxie, my father, Samuel, my sister, Denise, my brothers, DeRome and Derrell, my sister-in-law, Rhonda and my nieces Danielle, Gabrielle and Samantha and my friend Nicole. All of you have given me the strength to accomplish this great task.

Author's Acknowledgments

This dissertation was made possible with the support and cooperation of several key people on my committee. Dr. Ting-Chung Poon, deserves special credit for his intellect, patience and guidance. He has been there with me through it all and has been a wonderful influence, I will cherish this time always.

There is a special place in my heart for Dr. Wayne Scales, his vast knowledge of electromagnetic theory helped guide me in the right direction, so to you I say thanks.

To Dr. Yannis Besieris, you were one of the very first professors I had when I arrived at Virginia Tech. You stuck by me during the rocky times and gave me invaluable advice. I consider you to be one of the best professors I have had, at this university, out of the approximately thirty faculty members I have had during my stay. To you, I say thank you for being with me my entire tenure at Tech.

To Dr. Carl Prather and Dr. Ahmad Safaai-Jazi, I wish to thank you for all the administrative assistance and emotional guidance you have given me while I pursued this degree.

To Mr. Jiangang Xia, your assistance while you were a visiting professor in the Optical Image Processing(OIP) Laboratory was invaluable.

To Mr. Brad Schilling, your friendship while you were a doctoral student in the OIP Laboratory was a tremendous asset to me. I will miss our discussions about corporate stocks and mutual funds.

Last but not least, I wish to thank my family for their love, patience and understanding.

Table of Contents

1.0 Introduction..... 1

2.0 Literature Review..... 2

3.0 Fundamentals of Acousto-Optic Interaction..... 7

3.1 Sound-Field Configuration and Plane-Wave interaction model..... 7

3.2 Raman-Nath Diffraction..... 8

3.3 Bragg Diffraction..... 9

4.0 The Scalar Wave Equation and its application to Acousto-Optic interaction..... 12

5.0 Analytical Solutions to the Acousto-Optic interaction Problem..... 17

5.1 2-D Solution of Acousto-Optic interaction Equations..... 17

5.1.1 Using Exponential Fourier Transform Theory..... 18

5.2 3-D Solution of Acousto-Optic interaction Equations..... 20

5.2.1 Using Exponential Fourier Transform Theory..... 21

6.0 The Function of the Sound Wave in an Acousto-Optic Image Processing System..... 23

6.1 Calculation of the Peak Phased Delay Parameter..... 23

6.2 Calculation of the Cook-Klien Parameter..... 24

6.3 Effect of the Peak Phase Delay Parameter and the Cook-Klien Parameter on the AO transfer function..... 25

7.0 Coordinate System Transformations and Image Separation..... 40

7.1 Coordinate System Transformations..... 40

7.2 Image Separation..... 44

8.0 Detailed Analysis of Single Acousto-Optic Image Processing System..... 58

8.1 Realization of image processing using the zeroth diffracted order 58

8.2 Realization of image processing using the minus one diffracted order..... 61

8.3 Results from single acousto-optic image processing system..... 65

9.0 Detailed Analysis of the Series Acousto-Optic Cells Image Processing System..... 81

9.1 Realization of zeroth order image processing..... 81

9.2 Realization of minus one order image processing..... 84

9.3 Results from Series Acousto-Optic Image Processing System..... 88

10.0 Detailed Analysis of the Parallel Acousto-Optic Image Processing System..... 93

10.1 Realization of zeroth order image processing..... 93

10.2 Realization of minus one order image processing..... 97

10.3 Results of the Parallel Acousto-Optic Image Processing System..... 100

11.0 Conclusion and Direction of Future Research.....109
11.1 General Discussion.....109
11.2 Summary of Original Contributions.....110
11.3 Future Research Direction and Goals.....110

12.0 References.....112

13.0 Vita.....118

List of Figures

Fig. 3.1-1: Typical Configuration for a piezoelectric transducers..... 11

Fig. 4.0-1: Geometric configuration for acousto-optic interaction..... 16

Fig. 6.1-1: Experimental Configuration to measure Peak Phase Delay, α.....28

Fig. 6.2-1: Plot of Cook-Klien Parameter, Q, versus Acoustic Wave Frequency, Λ....29

Fig. 6.3-1: Photographs of the original picture (a), and the images of the zeroth-order (left one) and the minus one order (right one) when (b) Q$(\Lambda) = 10,\ \alpha(S_1) = 0.65\pi$; (c) Q$(\Lambda) = 28,\ \alpha(S_2) = 0.65\pi;$ and $(d)$when Q$(\Lambda) = 28,\ \alpha = 0.3\pi$.....30

Fig. 6.3-2: Plot of transfer function for ζ=1, $Q = 10, \alpha = 0.65\pi, (a)$ 2-D transfer function, (b) 1-D transfer function.....31

Fig. 6.3-3: Plot of transfer function for ζ=1, $Q = 28, \alpha = 0.65\pi, (a)$ 2-D transfer function, (b) 1-D transfer function.....32

Fig. 6.3-4: Plot of transfer function for ζ=1, $Q = 28, \alpha = 0.3\pi, (a)$ 2-D transfer function, (b) 1-D transfer function.....33

Fig. $6.3 - 5$: Three dimensional graph of Acousto-Optic transfer function of the zeroth order for ζ=1, Q=28 and $L = 60mm$.....34

Fig. 7.1-1: Diagram of Acousto-Optic cell for Coordinate System Transformation.....47

Fig. 7.1-2: Coordinate system for the Acousto-Optic Cell, i.e. (x', y, z'), superimposed onto the coordinate system for the Zeroth Diffracted Order, i.e. (x,y,z)..... 48

Fig. 7.1-3: Coordinate system for the Acousto-Optic Cell, i.e. (x', y, z'), superimposed onto the coordinate system for the Input Image, i.e. (x''',y,z''').....49

Fig. 7.1-4: Coordinate system for the Acousto-Optic Cell, i.e. (x', y, z'), superimposed onto the coordinate system for the minus one Diffracted Order, i.e. (x'',y,z'').....50

Fig. 7.1-5: Coordinate system for the Zeroth Diffracted Order, i.e. (x, y, z), and minus one Diffracted Order, i.e. (x",y,z") superimposed onto the coordinate system for the AOC, i.e. (x',y,z')....51

Fig. 7.1-6: Parallel Acousto-Optic Image Processing System.... 52

Fig. 7.1-7: Coordinate system for the Acousto-Optic Cell, i.e. (x, y', z'), superimposed onto the coordinate system for the Input Image, i.e. (x,y"',z"')....53

Fig. 7.1-8: Coordinate system for the Acousto-Optic Cell, i.e. (x, y', z'), superimposed onto the coordinate system for the Zeroth Diffracted Order, i.e. (x,y,z).... 54

Fig. 7.1-9: Coordinate system for the Acousto-Optic Cell, i.e. (x, y', z'), superimposed onto the coordinate system for the minus one Diffracted Order, i.e. (x,y",z").....55

Fig. 7.1-10: Coordinate system for the Zeroth Diffracted Order, i.e. (x, y, z), and minus one Diffracted Order, i.e. (x,y",z") superimposed onto the coordinate system for the AOC, i.e. (x,y',z').... 56

Fig. 7.2-1: Diffraction by Acousto-Optic Modulator and Image formation by imaging lens 57

Fig. 8.1-1: Light path used in image processing experiment.... 69

Fig. 8.2-1: Single Cell Acousto-Optic Image Processing System....70

Fig. 8.3-1: Photos of the result of AOM image processing system using an AOM with an RF center frequency equal to $80MHz$: (a) image $1mm$ from transducers, (b) image $11\ mm$ from transducers, (c) image $21\ mm$ from transducers.... 71

Fig. 8.3-2: Color photos of an Acousto-Optic Modulator....72

Fig. 8.3-3: Photos of the result of AOM image processing system using an AOM with an RF center frequency equal to $80MHz$: (a) original image, (b) high pass filtered image.....73

Fig. 8.3-4: Photos of an image of a finger print using an AOM with an RF center frequency equal to $80MHz$ (a) original image, (b) low pass filtered image.....74

Fig. 8.3-5: Photos of an image of a 17 using an AOM with an RF center frequency equal to 40MHz, (a) original image, (b) high pass filtered image($left$) and low pass filtered image($right$).....75

Fig. 8.3-6: Photos of an images of a finger print using an AOM with an RF center frequency equal to 40MHz (a) original image, (b) low pass filtered image, (c) high pass filtered image.....76

Fig. 8.3-7: Photos of an image of amplitude grating using an AOM with an RF center frequency equal to 40MHz (a) original image, (b) low pass filtered image($left$) and high pass filtered image($right$).....77

Fig. 8.3-8: Results of a computer simulation using an AOM with RF center frequency equal to 40MHz (a) original image, (b) high pass processing of image through Bragg diffraction (the zeroth order).....78

Fig. 8.3-9: Results of a computer simulation using an AOM with RF center frequency equal to 40MHz (a) original image, (b) low pass processing of image through Bragg diffraction (the minus one order).....79

Fig. 8.3-10: Graph of the Acousto-Optic transfer function for the zeroth order (a) three dimensional (b) two dimensional when Q=58, $\alpha = 0.472\pi$ and $L = 60mm$.....80

Fig. 9.1-1: Series Acousto-Optic Image Processing System.....90

Fig. 9.3-1: Photos of a rectangular image processed using a series acousto-optic system (a) processed image after first AOM , (b) processed image after second AOM.....91

Fig. 9.3-2: Graph of the Acousto-Optic transfer function for the zeroth order for a series system (a) three dimensional and (b) two dimensional when AOM_1 has Q=58, $\alpha = 0.472\pi$, AOM_2 has Q=28, $\alpha = 0.65\pi$ and $L = 60mm$.....92

Fig. 10.1-1: Parallel Acousto-Optic Image Processing System.....102

Fig. 10.3-1: Photo of the parallel AOM image processing system.....103

Fig. 10.3-2: Photos of rectangular image using two AOMs with RF center frequency of $40MHz$ (a) 2-D low pass image, (b) 2-D high pass filtered image.....104

Fig. 10.3-3: Photos of edge detection using two AOMs with an RF center frequency of $40MHz$ (a) image of a 2 (b) image of a 5..... 105

Fig. 10.3-4: Photos of edge detection using two AOMs with an RF center frequency of $40MHz$ (a) image of a 17 (b) image of a 7..... 106

Fig. 10.3-5: Three dimensional graph of the Acousto-Optic transfer function for a parallel system (a) zeroth diffracted order and (b) minus one diffracted order when AOM_1 has Q=28, $\alpha = 0.65\pi$, AOM_2 has Q=28, $\alpha = 0.65\pi$ and $L = 60mm$..... 107

Fig. 10.3-6: Three dimensional graph of the Acousto-Optic transfer function for a parallel system (a) zeroth diffracted order and (b) minus one diffracted order when AOM_1 has Q=28, $\alpha = 0.65\pi$, AOM_2 has Q=58, $\alpha = 0.472\pi$ and $L = 60mm$..... 108

List of Tables

Table 6.1-1: Data to calculate the Peak Phase Delay,α for $F_{sound} = 50\,MHz$..... 35

Table 6.1-2: Data to calculate the Peak Phase Delay,α for $F_{sound} = 40\,MHz$..... 36

Table 6.1-3: Data to calculate the Peak Phase Delay,α for $F_{sound} = 28\,MHz$..... 37

Table 6.1-4: Data to calculate the Peak Phase Delay,α for $F_{sound} = 80\,MHz$..... 38

Table 6.1-5: Data to calculate the Peak Phase Delay,α for $F_{sound} = 80\,MHz$..... 39

Chapter 1.0 Introduction

Acousto-Optics, which is the diffraction of laser by ultrasonic waves, was first predicted independently by Brillouin[1] and Mandel'shtam[2] in 1921. The effect can be described qualitatively as follows: An ultrasonic wave propagating through a solid or liquid locally causes compression and rarefaction of the medium. This compression and rarefaction of the medium is known as a photoelastic effect. The photoelastic effect changes the refractive index of the medium. Periodically alternating layers with different refractive indices thus form in the medium, since the ultrasonic sound wave is sinusoidal in nature. These layers move at the velocity of sound and are separated by half the acoustic wavelength. When light is incident at a certain angle, called the Bragg angle, into the medium and propagates through the above mentioned periodic structure, it is Bragg- diffracted.

This dissertation will investigate an image processing technique based on the above mentioned acousto-optic effect. Images being amplitude modulated onto a laser beam will interact with acoustic waves inside a homogenous, isotropic, flint glass medium. The image enters the acousto-optic cell at the Bragg angle and the Bragg-scattered light will carry the processed images.

Several experimental setups will be considered. The heart of the setup will consist of a system that will contain one acousto-optic cell and a single imaging lens. Another experimental setup will consist of two acousto-optic cells placed in series with each other and two imaging lenses. While another system will consist of two acousto-optic cells placed perpendicular to each other and two imaging lenses. The first two systems will perform one dimensional image processing while the last system will perform 2-D image processing.

In all experimental setups, we will monitor the Bragg diffracted images to see if any image enhancement can be achieved.

Beside actual laboratory experiments, we have performed computer simulations of all the above mentioned acousto-optic image processing systems using a transfer function that will be derived analytically.

Chapter 2.0 Literature Review

In recent years, rapid new developments have been made in optical technology. These developments in infrared LED inside TV remotes, miniature semiconductors laser systems inside CD players, laser bar code scanners at supermarkets and complex optical fiber networks that transmit information. The use of lasers and optics is also wide spread in fields such as medicine, satellite communication, and manufacturing.

Many signal processing applications require the ability to analyze enormous amounts of information at very high speeds. Optical information processing techniques are capable of satisfying these requirements. One particular technique that is capable of meeting this demand is the diffraction of light by acousto-optic interaction.

Acoustic waves were studied extensively in the past century; surface acoustic waves were first described by Lord Rayleigh in 1885 as they pertained to earth quakes. As stated in chapter 1, acousto-optics developed from the original research of Brillouin[1]. His original theory predicted a phenomenon closely related to x-ray diffraction in crystals. In acousto-optic diffraction, plane waves of light striking acoustically induced planes of compression and rarefaction at a certain critical angle will be partially reflected. Unlike x-ray diffraction, however he stated that there would be only one critical angle (Bragg angle) because the spatial structure of acoustically induced density variations is

essentially sinusoidal and hence contains no space harmonic components. In addition, Brillouin predicted that reflected light would be Doppler shifted in frequency by an amount equal to the sound frequency because the reflecting grating moves with the sound velocity. Unfortunately, it was not experimentally possible, until ten years later, to confirm his predications due to the lack of optical sources of sufficiently high coherence.

Brillouin[3], in a second paper, suggested that the multiple orders only occurred with the application of high sound intensity (strong interaction), a condition for which his original weak interaction theory did not apply. He suggested that the multiple order effect might be interpreted as a rescattering of diffracted light. Although Brillouin did not solve the strong interaction problem in detail, he showed that it could be formulated in terms of the Mathieu equation (i.e., differential equations with time-varying coefficients). The solution of which would contain multiple orders of light scattered into the experimentally observed directions.

Debye and Sears[4] performed the first experiments that demonstrated the generation of many orders of refracted light. These experiments also indicated the presence of a range of critical angles. In their published papers, Debye and Sears suggested that this was due to the generation of higher harmonics of the sound. They also derived criteria for single and multiple order diffraction phenomena know as the Debye-Sears ratio.

Lucas and Biquard[5] was one of the first researchers to observe the presence of multiple diffraction orders experimentally. They, on the basis of calculated ray trajectories, showed that the ray distribution of light leaving the column of sound was periodic in space.

The presence of multiple diffraction orders was first explained in a series of classic papers by C.V. Raman and N. Nath[6] starting in 1935. Raman and Nath's analysis was based on some of the earlier work done by Lord Rayleigh[7]. They modeled the sound column as a two-dimensional thin phase grating moving in the direction perpendicular to the light. Their theory correctly predicted the Bessel function intensity variation of

various orders as a function of sound pressure. While in this first analysis the light beam was assumed to be incident perpendicular to the sound column, a second article[8] treated the case of oblique incidence. Their next publication[9] examined the frequency change in the diffracted light. In a fourth article[10], they formulated the problem in terms of a wave equation defining propagation of incident light in an acoustically perturbed medium. Raman and Nath went on to derive an infinite set of coupled differential equations which described the spatial behavior of various orders traversing the sound beam. In deriving these equations it was assumed that the light field was incident perpendicular to the sound column. There was no limitation on the interaction length. Raman and Nath showed that if the sound beam was sufficiently thin, the infinite set of equations led to the same solution as the phase grating model. Finally, in a fifth article[11], the authors extended their theory to include light incident at arbitrary angles.

Although the infinite set of differential equations was derived by Raman and Nath in a formal way by applying the wave equation to an acoustically perturbed medium, these equations may also be derived by an intuitive approach. This was shown by Van Cittert[12], who treated the thick sound column as an infinite set of infinitesimally thin parallel phase gratings. Repetitive diffraction of the initial few orders through successive gratings ultimately led to the generation of infinitely many orders and defined a set of recurrent differential equations identical to those of Raman and Nath. Hargrove[13] reformulated the successive diffraction theory of Van Cittert so that it is easier to implement it on a digital computer. Similar work in this area was carried out by Nomoto and Torikai[14].

Other researchers have used different methods to derive similar sets of equations. Bhatia and Noble[15] reformulated the successive diffraction problem using integral equation for the scattered field. Phariseau[16] further developed the Mathieu equation approach originally proposed by Brillouin. Extermann[17] used a method that involved the concepts used in the analysis of x-ray diffraction in crystals. Although most of these theories are considerably more complicated than the Raman-Nath and Van Cittert

formulation, they still arrive at the same results. It can be shown that an extension of Van Cittert's theory to include reflected orders produces results that are identical to those obtained by Phariseau. Generally, the intensity of the reflected orders is negligible and the Raman-Nath and Van Cittert equations adequately describe the problem. Many investigators[18,19,20] have derived specific solutions of these equations applying to various angles of incidence, interaction lengths, and sound pressures.

A more quantitative distinction between single and multiple order diffraction was derived by Klien and Cook, who supported their work with numerical computer simulation.[21,22] They derived the so called Q-parameter. It is interesting to note that Q-parameter is simply a constant multiple of the Debye-Sears ratio.

In 1965 a material figure of merit , M_2, was proposed by Smith and Korpel[23], who also introduced a dynamic measurement technique. Dixon and Cohen[24] later extended this to anisotropic materials.

The vast majority of the theories previously mentioned restrict themselves to a two-dimensional interaction model where the sound field consists of a single plane wave and the incident light field is taken to be an infinitely large plane wave. The emphasis of the previous mentioned theories is on the description of the rescattering process using the simplest model possible, rather than dealing with the weak interaction of more complex fields. A majority of the older theories did not include the physical effects of sound-light interaction as a Bragg angle scattering and rescattering of individual plane wave components.

A more current topic of research are the weak light-sound interaction formalisms. These formalisms rose out of the need to accurately describe such diverse phenomena as Brillouin scattering[25], beam parameter effects on Bragg diffraction[26,27] and Bragg diffraction imaging[28]. After introduction of the laser in the 1960s, quantum mechanical considerations regarding energy and momentum in photon-phonon collision processes

were incorporated into a simple theory[29,30,31]. As mention before, earlier theories were presented in terms of ultrasonic phase gratings.

Improvements in the sound column model were introduced by Leroy and Claeys[32] and by Pieper et al.[33], who assumed that the sound field had a constant but, arbitrary cross-section profile. The incident light field was still a plane wave and the sound field had plane-wave fronts. This model is only slightly more realistic than the uniform sound column model.

The use of a plane wave of light as the incident optical beam was replaced by Magdich and Molchanov[34] and by Chu, Kong, and Tamir.[35,36,37] with a two dimensional Gaussian beam. Chatterjee et al.[38,39] introduced a transfer function approach that was similar to the Magdich-Molchanov theory. The essential component of this approach was to convert the input Gaussian beam envelope into its angular plane wave spectrum by use of the exponential Fourier transform. Once in the spectral domain, a set of coupled differential equations representing acousto-optic interaction are solved. Their solution represents the transfer function for an acousto-optic modulator with an optical beam incident at the Bragg angle. Because the set of coupled differential equations applies strictly to an ultrasonic plane wave of sound, it is assumed that the input Gaussian beam is made up of many plane waves, each traveling in a direction slightly different than the ideal Bragg angle. By multiplying the input angular spectrum with the acousto-optic transfer function, it is possible to obtain the angular spectrum for each diffracted order. Note, however, that although the incident light field is arbitrary, the sound field is still a physically unrealistic uniform sound column.

A more general theory was developed by Korpel and Poon[40] in 1980, where both arbitrary light fields and arbitrary sound fields in two dimensions are assumed. Feynman-type diagrams are used to describe path integrals that represent the successive scattering or rescattering of the light field in the interaction region. By interpreting the path integrals in terms of complex quantum-mechanical probability amplitude densities, these paths

may be simulated by using a Monte Carlo simulation.[39] The disadvantages of this method are that it is restricted to two dimensions and many paths must be evaluated to produce accurate results.

Chapter 3.0 Fundamentals of Acousto-Optic Interaction

This chapter will consider two basic types of acousto-optic interaction, Raman-Nath and Bragg diffraction of light. We will see that in both cases a propagating ultrasonic sound wave acts as a diffraction grating. This phase grating can diffract and modulate an incident laser beam. The laser beam may diffract into only one diffracted order, Bragg diffraction, or many distinct diffracted orders, Raman-Nath diffraction. In the processes of describing the two types of acousto-optic diffraction, we will introduce again a few acousto-optic figures of merit that will be used in the later parts of this disseration to quantify the diffraction properties of the acousto-optic modulators.

3.1 Sound-Field Configuration and Plane-Wave interaction model

The interaction between the optical field, $\mathbf{E}_0(\boldsymbol{r},t)$, and sound field, $\mathbf{S}(\boldsymbol{r},t)$, can generally be described by Maxwell's equations. It is typically assumed that the interaction takes place in an optically inhomogeneous, nonmagnetic isotropic medium, characterized by a permeability μ_o and a permittivity $\epsilon(\boldsymbol{r},t)$. The time-varying permittivity is written as

$$\epsilon(\boldsymbol{r},t) = \epsilon + \epsilon'(\boldsymbol{r},t) \qquad (3.1-1)$$

where $\epsilon'(\boldsymbol{r},t)$=$\epsilon$CS$(\boldsymbol{r},t)$. That is $\epsilon'(\boldsymbol{r},t)$ is proportional to the sound field amplitude

$S(\boldsymbol{r}, t)$ and C, which is the proportionality constant that depends on the material. Hence $\epsilon'(\boldsymbol{r}, t)$ represents the action of the sound field.

Equation 3.1-1 indicates that the acousto-optic effect is produced by a propagating ultrasonic wave in an optically transparent media. As stated earlier, the sound wave propagates through the optical material, it causes periodic variation of the refractive index. This is caused by what is known as a photoelastic effect, i.e. the media under goes compression and refraction. This compression and refraction follows the sinusoidal nature of the ultrasonic acoustic wave.

The acoustic wave is normally launched into the optical medium by use of piezoelectric transducers, illustrated in figure $3.1-1$[41]. When a voltage is applied to the transducers, the piezoelectric material is deformed which causes an internal strain. This induced strain is used to convert the electrical signal into an acoustic strain wave that causes the photoelastic effect in the acousto-optic medium.

In the sections that follows, I will describe the particular difference between Raman-Nath diffraction and Bragg diffraction.

3.2 Raman-Nath Diffraction

As mentioned before, Raman-Nath diffraction is characterized by the simultaneous generation of many scattered orders. Raman-Nath diffraction is also characterized by the operation of the acousto-optic cell with the angle of the incident laser light beam nearly equal to zeroth and choosing the Cook-Klien parameter to be much less than one, i.e., $Q \ll 1$. The Cook-Klien parameter relates the wavelength of the incident light beam to the wavelength of sound. This condition ensures that the acoustic column is thin enough to neglect multiple optical diffraction effects within the sound field. In other words, the assumption is made that the acoustic column is weak enough to neglect the bending of the optical rays as they passes through the interaction length. This also implies

that the interaction length, L, must be short enough such that the accumulated degree of phase mismatch between the particular order of interest, ψ_{m}, and its neighboring orders is a minimum.

As a side note, Uchida and Niizeki[42] have suggested in a journal article that for operation in Raman-Nath regime, a more pactical figure of merit for the Cook-Klien parameter is $Q \leq 0.3$.

3.3 Bragg Diffraction

As pointed out earlier, Bragg diffraction is characterized by the generation of two scattered orders. In terms of the Cook-Klien parameter, Q should be far greater one for operation in the Bragg regime. The zeroth order can only couple optical power into the plus or minus first order. That is, there is phase matching between the zeroth and plus or minus first order. Laser beam light cannot be transferred into the second or higher orders because there is no phase matching between these orders.

Bragg diffraction can be model using a thick phase grating. This phase grating can be visualized as a series of parallel, partially reflective planes. The phase grating can be considered to be stationary during the interaction process, because the velocity of the acoustic wave is much less than the velocity of light. Multiple diffraction occurs at every cross section plane throughout the interaction length of the sound column. So, only the single order that is phase matched will emerge as a diffracted beam of light; the other orders will be canceled by destructive interference within the acousto-optic modulator. Another point that should be made about Bragg diffraction is that the interaction length, L, should be made large so that nearly all of the incident laser beam light is diffracted into a single order.

Here too, Uchida and Niizeki[42] have suggested that for operation in the Bragg regime, a more practical figure of merit for the Cook-Klien parameter is that $Q \geq 4\pi$. An

additional comment is needed here. Most commercial acousto-optic devices operate in the Bragg regime except for some low-frequency processors. In certain cases, however the condition that $Q \geq 4\pi$ does not hold for acousto-optic devices. It is often possible to ignore the intensities of higher diffraction orders in comparison with the minus one and zeroth order, and therefore still assume that the acousto-optic device is operating in the Bragg regime.

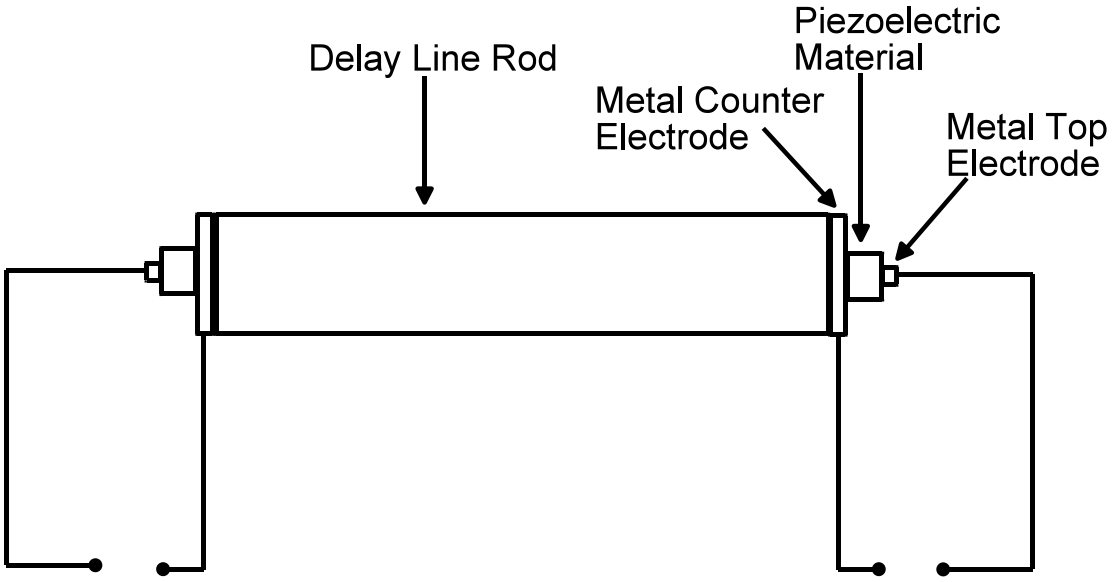

Figure 3.1-1[41]: Typical Configuration for a piezoelectric transducers

Chapter 4.0 The Scalar Wave Equation and its Application to Acousto-Optic Interaction

As a starting point, I will used the scalar wave equation to mathematically model strong acousto-optic interaction in three dimensions:

$$\nabla^2\psi(\boldsymbol{r},t) - \mu\epsilon_o\frac{\partial^2\psi(\boldsymbol{r},t)}{\partial t^2} = \mu\epsilon'(\boldsymbol{r},t)\frac{\partial^2\psi(\boldsymbol{r},t)}{\partial t^2}, \qquad (4.0-1)$$

where $\psi(\boldsymbol{r},t)$ refers to an arbitrary polarization component, μ is the permeability of the medium and ϵ_o is the permittivity of the medium.

Now, using the scalar wave equation in $(4.0-1)$, let us define ϵ' as follows:

$$\epsilon'(\boldsymbol{r},t) = \epsilon_o C Re[S_e(\boldsymbol{r})exp[j\Omega t - Kx]], \qquad (4.0-2)$$

where $S_e(\boldsymbol{r})$ is the complex sound field envelop, C is a material constant, Ω is the temporal sound frequency, and K is the propagation constant for sound. $\psi(\boldsymbol{r},t)$ is assumed to be time harmonic and is defined as

$$\psi(\boldsymbol{r},t) = \sum_{m=-n}^{n} Re[\psi_{em}(\boldsymbol{r}) \times exp[j\{(w+m\Omega)t - k_{mx}x - k_{mz}z\}]], \qquad (4.0-3)$$

where m is a particular order of diffracted laser light, w is the temporal light frequency, k_{mx} and k_{mz} are the propagation constants for the m^{th} order light field, ψ_{em} is the complex envelope of the m^{th} order light field at frequency $w + m\Omega$, and n is equal to ∞. The propagation constants, k_{mx} and k_{mz} which are defined mathematically by equation $4.0-5$, can be visualised by reviewing figure $4.0-1$. As stated earlier, the laser light travels in the nominal $z-$direction at an angle ϕ_B with respect to the $z-$axis. This means the propagation vector is made up of two components, k_x, and k_z, defined as follows:

$$k_x = k_o sin(\phi_B) \qquad (4.0-4)$$
$$k_z = k_o cos(\phi_B).$$

Applying this concept to figure $4.0-1$, allows us to express the propagation constants for each diffracted order in a form similar to that in $(4.0-4)$. Looking at figure $4.0-1$, notice that the laser beam is incident at an angle equal to $+\phi_B$ thereby allowing for downshifted interaction. The incident order emerges from the acousto-optic interaction as the zeroth diffracted order with propagation constants equal to those in equation $(4.0-4)$. From the discussions in chapter 3, we know that the minus one diffracted order is deflected in a direction that is $2\phi_B$ less than that of the zeroth order. This effectively leads to propagation in the $-\phi_B$ direction. Due to the finite interaction region, higher orders are produced in directions $2\phi_B$ away from the zeroth and minus one diffracted orders, respectively. Hence, $\psi_{e(1)}$ and $\psi_{e(-2)}$ both travel in directions $\pm 3\phi_B$ with respect to the z-axis. Looking at again at figure $4.0-1$, clearly there is a pattern to the angle of the diffracted orders such that each diffracted order appears at every odd multiple of ϕ_B, i.e. $\phi_{\text{m}} = (2m+1)\phi_B$. Consequently, the propagation constants, k_{mx} and k_{mz} can be represented by:

$$k_{mx} = k_o sin[(2m+1)\phi_B] \qquad (4.0-5)$$
$$k_{mz} = k_o cos[(2m+1)\phi_B]$$

Substituting $(4.0-2)$ and $(4.0-3)$ into $(4.0-1)$ yields the m^{th} order set of coupled differential equations for acousto-optic interaction.

$$\frac{\partial^2 \psi_{e(m)}}{\partial x^2} + \frac{\partial^2 \psi_{e(m)}}{\partial y^2} - 2j\left[k_{mx}\frac{\partial \psi_{e(m)}}{\partial x} + k_{mz}\frac{\partial \psi_{e(m)}}{\partial z}\right] \qquad (4.0-6)$$
$$+ \frac{1}{2}k_o^2 CS_e(\boldsymbol{r})\psi_{e(m-1)} + \frac{1}{2}k_o^2 CS_e^*(\boldsymbol{r})\psi_{e(m+1)} = 0$$

The physics behind equation $(4.0-6)$ implies that the m^{th} order scattered light in z direction depends on the interactions between adjacent orders $(m\pm 1)$ with sound field and the effect of propagational diffraction. Therefore, re-arranging for the term $\frac{\partial \psi_{e(m)}}{\partial z}$ in

equation $(4.0-6)$ we get:

$$\frac{\partial \psi_{e(m)}}{\partial z} = -\frac{j}{2k_{mz}}\left[\frac{\partial^2 \psi_{e(m)}}{\partial x^2}+\frac{\partial^2 \psi_{e(m)}}{\partial y^2}\right]-\frac{k_{mx}}{k_{mz}}\frac{\partial \psi_{e(m)}}{\partial x} \qquad (4.0-7)$$
$$-\frac{jk_o^2 C}{4k_{mz}}\left[S_e(\boldsymbol{r})\psi_{e(m-1)}+S_e^*(\boldsymbol{r})\psi_{e(m+1)}\right]$$

Next, we normalize z-variable using $\zeta=\frac{z}{L}$, and introduce the peak phase delay, $\alpha=\frac{k_o C|S|L}{2}$, and equation $(4.0-5)$, we get

$$\frac{\partial \psi_{e(m)}}{\partial \zeta} = -\frac{jL}{2k_o cos[(2m+1)\phi_B]}\left[\frac{\partial^2 \psi_{e(m)}}{\partial x^2}+\frac{\partial^2 \psi_{e(m)}}{\partial y^2}\right] \qquad (4.0-8)$$
$$-Ltan[(2m+1)\phi_B]\frac{\partial \psi_{e(m)}}{\partial x}$$
$$-\frac{j\alpha}{2cos[(2m+1)\phi_B]}\left[S_e(\boldsymbol{r})\psi_{e(m-1)}+S_e^*(\boldsymbol{r})\psi_{e(m+1)}\right]$$

Restricting the coupled system of equations in $4.0-8$ to four diffracted orders, m = -2, $m=-1,\ m=0$, and $m=1$ leads to:

$$\frac{\partial \psi_{e(-1)}}{\partial \zeta} = -\frac{jL}{2k_o cos(-\phi_B)}\left[\frac{\partial^2 \psi_{e(-1)}}{\partial x^2}+\frac{\partial^2 \psi_{e(-1)}}{\partial y^2}\right] \qquad (4.0-9a)$$
$$-L\,tan(-\phi_B)\frac{\partial \psi_{e(-1)}}{\partial x}$$
$$-\frac{j\alpha}{2cos(-\phi_B)}\left[S_e(x,y,z)\psi_{e(-2)}+S_e^*(x,y,z)\psi_{e(0)}\right]$$

$$\frac{\partial \psi_{e(0)}}{\partial \zeta} = -\frac{jL}{2k_o cos(\phi_B)}\left[\frac{\partial^2 \psi_{e(0)}}{\partial x^2}+\frac{\partial^2 \psi_{e(0)}}{\partial y^2}\right] \qquad (4.0-9b)$$
$$-L\,tan(\phi_B)\frac{\partial \psi_{e(0)}}{\partial x}$$
$$-\frac{j\alpha}{2cos(\phi_B)}\left[S_e(x,y,z)\psi_{e(-1)}+S_e^*(x,y,z)\psi_{e(1)}\right]$$

$$\frac{\partial \psi_{e(1)}}{\partial \zeta} = -\frac{jL}{2k_o cos(3\phi_B)}\left[\frac{\partial^2 \psi_{e(1)}}{\partial x^2} + \frac{\partial^2 \psi_{e(1)}}{\partial y^2}\right] - L\,tan(3\phi_B)\frac{\partial \psi_{e(1)}}{\partial x} - \frac{j\alpha}{2cos(3\phi_B)} S_e(x,y,z)\psi_{e(0)} \qquad (4.0-9c)$$

$$\frac{\partial \psi_{e(-2)}}{\partial \zeta} = -\frac{jL}{2k_o cos(-3\phi_B)}\left[\frac{\partial^2 \psi_{e(-2)}}{\partial x^2} + \frac{\partial^2 \psi_{e(-2)}}{\partial y^2}\right] - L\,tan(-3\phi_B)\frac{\partial \psi_{e(-2)}}{\partial x} - \frac{j\alpha}{2cos(-3\phi_B)} S_e(x,y,z)\psi_{e(-1)} \qquad (4.0-9d)$$

where $\alpha = \frac{k_o C|S|L}{2}$ and we assume that $S_e(x,y,z)$ has a maximum amplitude of unity.

The focus of the following chapter will be to solve the coupled acousto-optic differential equations using a transfer function approach. The mathematical tools used to accomplish this goal will include the Fourier and Laplace transform techniques. These transfer functions will become part of the foundation for the result of the work presented in this dissertation.

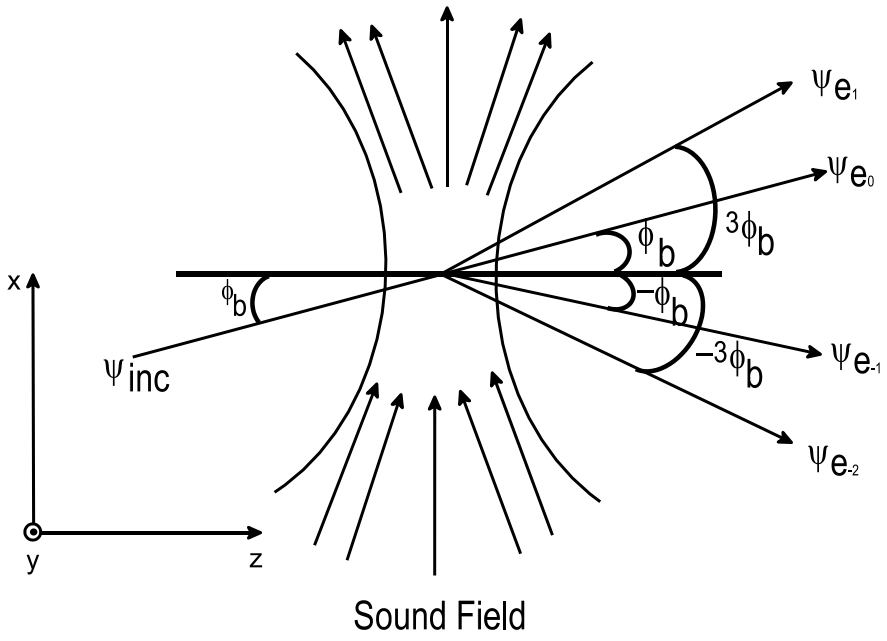

Figure $4.0-1$: Geometric configuration for acousto-optic interaction

Chapter 5.0 Analytical Solutions to the Acousto-Optic interaction Problem

The primary focus of this chapter is to solve the coupled acousto-optic differential equation, derived in chapter four, using a transfer function approach. The mathematical tools used to accomplish this goal will include the Fourier and Laplace transform techniques. The first section of this chapter will present acousto-optic transfer functions that exist in two spatial dimensions and one space dimension, i.e., $H_{(m)}(k_x,k_y,\zeta)$. The second section of this chapter will take this result and using a Fourier transform table to write the transfer function in three spatial dimensions, i.e., $H_{(m)}(k_x,k_y,k_z)$. These transfer functions will become part of the foundation for the result of the work presented in this dissertation.

5.1 2-D Solution of Acousto-Optic Interaction Equations

In the following section, I will attempt to solve the coupled partial differential equation that govern acousto-optic interaction inside a homogenous, isotropic medium for two diffracted orders. During my first attempt to solve the coupled partial differential equations for acousto-optic interaction, I will use some trigonometric simplification and assume that some of the diffracted order are equal to zero.

Next, I find the solution to the coupled partial differential equations for acousto-optic interaction using only the assumption that some of the diffracted order are equal to zero. Finally, after deriving the solutions for acousto-optic interaction under these two situation, I will compare and contrast the solutions.

5.1.1 Using Exponential Fourier Transform Theory

Using equation $4.0-9$ as a starting point with $\psi_{e(1)} \doteq 0$ and $\psi_{e(-2)} \doteq 0$, we have

$$\frac{\partial \psi_{e(-1)}}{\partial \zeta} = -\frac{jL}{2k_o cos(-\phi_B)}\left[\frac{\partial^2 \psi_{e(-1)}}{\partial x^2} + \frac{\partial^2 \psi_{e(-1)}}{\partial y^2}\right] - L\,tan(-\phi_B)\frac{\partial \psi_{e(-1)}}{\partial x} - \frac{j\alpha}{2cos(-\phi_B)} S_e^*(x,y,z)\psi_{e(0)} \qquad (5.1.1-1)$$

$$\frac{\partial \psi_{e(0)}}{\partial \zeta} = -\frac{jL}{2k_o cos(\phi_B)}\left[\frac{\partial^2 \psi_{e(0)}}{\partial x^2} + \frac{\partial^2 \psi_{e(0)}}{\partial y^2}\right] - L\,tan(\phi_B)\frac{\partial \psi_{e(0)}}{\partial x} - \frac{j\alpha}{2cos(\phi_B)} S_e(x,y,z)\psi_{e(-1)} \qquad (5.1.1-2)$$

where $\psi_{e(0)}(x,y,\zeta)$ and $\psi_{e(-1)}(x,y,\zeta)$ are the complex envelopes of the zeroth and minus one diffracted orders. $S_e(x,y,z)$ is the sound field envelope inside the acousto-optic cell, AOC, which has a maximum amplitude of unity. L is the length of the AOC, k_o is propagation constant for the laser light inside the AOC, $\alpha = \frac{k_o C|S|L}{2}$ is called the peak-phase delay, and $\zeta = \frac{z}{L}$. If we assume that the sound field envelope is planar in nature, i.e. $S_e^*(x,y,z) = S_e(x,y,z) = 1$, then equation $5.1.1-1$ and $5.1.1-2$ become

$$\frac{\partial \psi_{e(-1)}}{\partial \zeta} = -\frac{jL}{2k_o cos(-\phi_B)}\left[\frac{\partial^2 \psi_{e(-1)}}{\partial x^2} + \frac{\partial^2 \psi_{e(-1)}}{\partial y^2}\right] - L\,tan(-\phi_B)\frac{\partial \psi_{e(-1)}}{\partial x} - \frac{j\alpha}{2cos(-\phi_B)} \psi_{e(0)} \qquad (5.1.1-3)$$

$$\frac{\partial \psi_{e(0)}}{\partial \zeta} = -\frac{jL}{2k_o cos(\phi_B)}\left[\frac{\partial^2 \psi_{e(0)}}{\partial x^2} + \frac{\partial^2 \psi_{e(0)}}{\partial y^2}\right] - L\,tan(\phi_B)\frac{\partial \psi_{e(0)}}{\partial x} - \frac{j\alpha}{2cos(\phi_B)}\psi_{e(-1)} \tag{5.1.1-4}$$

Taking the Fourier transform of equation $5.1.1-3$ and $5.1.1-4$ w.r.t x and y gives the following result

$$\frac{\partial \Psi_{e(-1)}}{\partial \zeta} = \frac{jL}{2k_o cos(-\phi_B)} \times \left[k_x^2 + k_y^2 - 2k_o sin(-\phi_B)k_x\right]\Psi_{e(-1)} - \frac{j\alpha}{2cos(-\phi_B)}\Psi_{e(0)} \tag{5.1.1-5}$$

$$\frac{\partial \Psi_{e(0)}}{\partial \zeta} = \frac{jL}{2k_o cos(\phi_B)} \times \left[k_x^2 + k_y^2 - 2k_o sin(\phi_B)k_x\right]\Psi_{e(0)} - \frac{j\alpha}{2cos(\phi_B)}\Psi_{e(-1)} \tag{5.1.1-6}$$

In an attempt to simplify equations $5.1.1-5$ to $5.1.1-6$, let $\gamma_{-1} = \frac{\alpha}{2cos(-\phi_B)}$, $\gamma_0 = \frac{\alpha}{2cos(\phi_B)}$, $\beta_{-1} = \frac{L}{2k_o cos(-\phi_B)}\left[k_x^2 + k_y^2 - 2k_o sin(-\phi_B)k_x\right]$ and $\beta_0 = \frac{L}{2k_o cos(\phi_B)}\left[k_x^2 + k_y^2 - 2k_o sin(\phi_B)k_x\right]$. Doing this, we arrive at the following simplified acousto-optic interaction equations:

$$\frac{\partial \Psi_{e(-1)}}{\partial \zeta} = j\beta_{-1}\Psi_{e(-1)} - j\gamma_{-1}\Psi_{e(0)} \tag{5.1.1-7}$$

$$\frac{\partial \Psi_{e(0)}}{\partial \zeta} = j\beta_0\Psi_{e(0)} - j\gamma_0\Psi_{e(-1)} \tag{5.1.1-8}$$

Now, applying the Laplace transform to equations $5.1.1-7$ and $5.1.1-8$ and performing some algebraic manipulations, we obtain the following results

$$\Psi^{\varsigma}_{e(-1)}(k_x,k_y,s)=\frac{\Psi_{e(-1)}(k_x,k_y,\zeta=0)}{s-j\beta_{-1}} - j\gamma_{-1}\frac{\Psi^{\varsigma}_{e(0)}(k_x,k_y,s)}{s-j\beta_{-1}} \qquad (5.1.1-9)$$

$$\Psi^{\varsigma}_{e(0)}(k_x,k_y,s)=\frac{\Psi_{e(0)}(k_x,k_y,\zeta=0)}{s-j\beta_{0}} - j\gamma_{0}\frac{\Psi^{\varsigma}_{e(-1)}(k_x,k_y,s)}{s-j\beta_{0}}, \qquad (5.1.1-10)$$

where $\Psi^{\varsigma}_{e(0)}=\Psi_{e(0)}(k_x,k_y,s)$, $\Psi^{\varsigma}_{e(-1)}=\Psi_{e(-1)}(k_x,k_y,s)$ and $\Psi_{e(0)}(k_x,k_y,\zeta=0)$ or $\Psi_{e(-1)}(k_x,k_y,\zeta=0)$ is the appropriate boundary condition. After taking the inverse Laplace Transform and using some linear system theory, we arrive at the following acousto-optic transfer function for the minus one and zeroth diffracted orders:

$$H_{(-1)}(k_x,k_y;\zeta)= - j\gamma_{-1}exp\left[j\left(\frac{\beta_0+\beta_{-1}}{2}\right)\zeta\right]\frac{sin\left[\sqrt{\eta}\zeta\right]}{\sqrt{\eta}} \qquad (5.1.1-11)$$

$$H_{(0)}(k_x,k_y;\zeta)=exp\left[j\left(\frac{\beta_0+\beta_{-1}}{2}\right)\zeta\right]\left\{cos\left[\sqrt{\eta}\zeta\right] + j\left(\frac{\beta_0-\beta_{-1}}{2}\right)\frac{sin\left[\sqrt{\eta}\zeta\right]}{\sqrt{\eta}}\right\}, \qquad (5.1.1-12)$$

where $\eta=\frac{(\beta_0+\beta_{-1})^2-4(\beta_0\beta_{-1}-\gamma_0\gamma_{-1})}{4}$, $\gamma_{-1}=\frac{\alpha}{2cos(-\phi_B)}$, $\gamma_0=\frac{\alpha}{2cos(\phi_B)}$, $\beta_{-1}=\frac{L}{2k_ocos(-\phi_B)}\left[k_x^2+k_y^2-2k_osin(-\phi_B)k_x\right]$ and $\beta_0=\frac{L}{2k_ocos(\phi_B)}\left[k_x^2+k_y^2-2k_osin(\phi_B)k_x\right]$.

5.2 3-D Solution of Acousto-Optic Interaction Equations

5.2.1 Using Exponential Fourier Transform Theory

Our next task is to find the 3-D spatial acousto-optic transfer function for the minus one and zeroth diffracted order. This can be done by taking equations $5.1.1-11$ and $5.1.1-12$ which are the 2-D spatial acousto-optic transfer function with a space parameter, i.e., $H_{(-1)}(k_x,k_y;\zeta)$ and $H_{(0)}(k_x,k_y;\zeta)$, and apply the appropriate Fourier transform[67] $w.r.t.$ the ζ variable. We then have the Acousto-Optic transfers functions in three spatial dimension for the zeroth and minus one diffracted orders, i.e., $H_{(-1)}(k_x,k_y,k_z)$ and $H_{(0)}(k_x,k_y,k_z)$. Therefore, if we do this we arrive at the following results:

$$H_{(-1)}(k_x,k_y,k_z)=\frac{-j\gamma_{-1}}{2\sqrt{\eta}}\frac{1-exp\big[j\big\{\big(\frac{\beta_0+\beta_{-1}}{2}\big)+\sqrt{\eta}+k_z\big\}\big]}{k_z}+\frac{j\gamma_{-1}}{2\sqrt{\eta}}\frac{1-exp\big[j\big\{\big(\frac{\beta_0+\beta_{-1}}{2}\big)-\sqrt{\eta}+k_z\big\}\big]}{k_z} \quad (5.2.1-1)$$

$$\begin{aligned}H_{(0)}(k_x,k_y,k_z)=&\frac{j}{2}\frac{1-exp\big[j\big\{\big(\frac{\beta_0+\beta_{-1}}{2}\big)+\sqrt{\eta}+k_z\big\}\big]}{k_z}+\frac{j}{2}\frac{1-exp\big[j\big\{\big(\frac{\beta_0+\beta_{-1}}{2}\big)-\sqrt{\eta}+k_z\big\}\big]}{k_z}\\&+j\left[\frac{\beta_0-\beta_{-1}}{4\sqrt{\eta}}\right]\frac{1-exp\big[j\big\{\big(\frac{\beta_0+\beta_{-1}}{2}\big)+\sqrt{\eta}+k_z\big\}\big]}{k_z}\\&-j\left[\frac{\beta_0-\beta_{-1}}{4\sqrt{\eta}}\right]\frac{1-exp\big[j\big\{\big(\frac{\beta_0+\beta_{-1}}{2}\big)-\sqrt{\eta}+k_z\big\}\big]}{k_z}\end{aligned} \quad (5.2.1-2)$$

After considerable algebraic manipulations, equations $5.2.1-1$ and $5.2.1-2$ can be simplified to the following

$$H_{(-1)}(k_x,k_y,k_z)=\frac{-\gamma_{-1}}{\sqrt{\eta}k_z}exp\left[j\left(\frac{\beta_0+\beta_{-1}}{2}+k_z\right)\right]\times sin\left(\sqrt{\eta}\right) \qquad (5.2.1-3)$$

$$H_{(0)}(k_x,k_y,k_z)=\frac{j}{k_z}\left\{1-exp\left[j\left(\frac{\beta_0+\beta_{-1}}{2}+k_z\right)\right]\times cos\left(\sqrt{\eta}\right)\right\}+\left(\frac{\beta_0-\beta_{-1}}{2\sqrt{\eta}k_z}\right)\times exp\left[j\left(\frac{\beta_0+\beta_{-1}}{2}+k_z\right)\right]sin\left(\sqrt{\eta}\right) \qquad (5.2.1-4)$$

where $\eta=\frac{(\beta_0+\beta_{-1})^2-4(\beta_0\beta_{-1}-\gamma_0\gamma_{-1})}{4}$, $\gamma_{-1}=\frac{\alpha}{2cos(-\phi_B)}$, $\gamma_0=\frac{\alpha}{2cos(\phi_B)}$, $\beta_{-1}=\frac{L}{2k_ocos(-\phi_B)}\left[k_x^2+k_y^2-2k_osin(-\phi_B)k_x\right]$ and $\beta_0=\frac{L}{2k_ocos(\phi_B)}\left[k_x^2+k_y^2-2k_osin(\phi_B)k_x\right]$. The only restriction on equations $5.2.1-3$ and $5.2.1-4$ is that $0<\zeta<1$.

The acousto-optic transfer functions that we derived in this chapter will be used to model the effect that the acousto-optic cell, AOC, has on laser light that is incident into the AOC at the Bragg angle. Therefore, these transfer functions form the conerstone of this research.

Chapter 6.0 The Function of the Sound Wave in an Acousto-Optic Image Processing System

The ultrasonic sound wave in an acousto-optic cell, AOC, plays an important role in the ability of the AOC to perform image enhancements. The following sections describe the important parameters that allow one to control the AOC image processing abilities. The following sections also give a detailed analysis of the effect of these parameters on the acousto-optic cell image processing abilities.

6.1 Calculation of the Peak Phased Delay

The peak phase delay, α, can be determined experimentally by using the following relation:

$$tan^2\left(\frac{\alpha}{2}\right) = \frac{I_{-1}}{I_0}, \qquad (6.1-1)$$

where I_{-1} and I_0 are the minus one and zeroth order intensities, respectively. Solving equation $(6.1-1)$ for α we arrive at the following result

$$\alpha = 2tan^{-1}\left(\sqrt{\frac{I_{-1}}{I_0}}\right). \qquad (6.1-2)$$

The minus one and zeroth order intensities can be obtained by using a photodetector to measure the intensities I_0 and I_{-1} (see figure $6.1-1$). The photodetector produces a voltage that is directly proportional to the magnitude of each diffracted orders light intensities. Therefore, equation $(6.1-2)$ can be modified to the following

$$\alpha = 2tan^{-1}\left(\sqrt{\frac{V_{-1}}{V_0}}\right), \qquad (6.1-3)$$

where $V_1 \sim I_{-1}$and $V_0 \sim I_0$. Tables $6.1-1$ to $6.1-3$ list the calculated peak phase delay, α, using IntraAction ADM-40, serial number 1932, acousto-optic modulator connected to a IntraAction DE-40M, serial number 2238, voltage controlled oscillator. The data contained in tables $6.1-4$ and $6.1-5$ was obtained using a IntraAction AOM-802 acousto-optic modulator connected to a IntraAction DE-80 voltage controlled oscillator.

6.2 Calculation of the Cook-Klien Parameter

The acousto-optic cells that are simulated in this paper are an AOM-40 and AOM-80 from the IntraAction Corp.. The RF center frequency of operation for the AOM-40 is 40MHz with a usable RF frequency range from 30 MHz to 50MHz. The RF center frequency for the AOM-80 is 80 MHz with a usable RF frequency range from 65 MHz to 95MHz. Therefore, the lower and upper limits for the Cook-Klein parameter for each AOM cell is approximately 8 to 22 for the AOM-40 and approximately 38 to 82 for the AOM-80. The velocity of the ultrasonic sound wave inside the acousto-optic cells is $3960\frac{meters}{second}$. The acousto-optic cells are made of flint glass. Bounded to the acousto-optic cell are Lithium Niobate piezoelectric transducers which generate the RF ultrasonic acoustic wave. The height of the sound field or active aperture is approximately $2\ mm$. The index of refraction for both the AOM-80 and AOM-40 is approximately $n = 1.689$. The equation that connects the Cook-Klien parameter, Q, to the frequency of the sound wave is the following equation:

$$Q = \frac{2\pi\lambda L}{n\Lambda^2} = \frac{2\pi\lambda L F_{sound}^2}{nV_{sound}^2} \qquad (6.2-1)$$

where L is the length of the acousto-optic modulator, n is the index of refraction, λ is the wavelength of light in free-space, F_{sound} is the frequency of the sound wave, V_{sound} is the

velocity of the sound wave, Λ is the wavelength of sound inside the modulator. A plot of the Cook-Klein parameter versus the RF acoustic wave frequency, using equation $6.2-1,$ is shown in figure $6.2-1$. To obtain this plot, the following constants were used: λ=0.632μm, $L = 60mm$.

6.3 Effect of the Peak Phase Delay Parameter and the Cook-Klien Parameter on the AO transfer function

By using experimental image processing results and the acousto-optic spatial transfer function developed in chapter five, we can make some conclusions about the effect of the ultrasonic sound wave on the abilities of an acousto-optic system to perform image enhancements. Looking at the experimental results shown in figure 6.3-1: (a) is the photograph of the original picture to be processed; figure $6.3-1$(b) through figure $6.3-1$(d) are the photographs of the experimental results of the zeroth order and the minus one order from an acousto-optic system that contains one AOM and one imaging lens when (b) $Q(\Lambda)$=10, $\alpha(S) = 0.65\pi$, when (c) $Q(\Lambda)$=28, $\alpha(S) = 0.65\pi$, and when (d) $Q(\Lambda)$=28, $\alpha(S) = 0.3\pi$, respectively. The effect of the edge enhancement in figure 6.3-1(c) is clearly stronger than that in figure 6.3-1(b) and (d) since the curves of $H_0(k_x, k_y; \zeta = 1)$ when $Q(\Lambda)$=28, $\alpha(S) = 0.65\pi$ are sharper than when $Q(\Lambda)$=10, $\alpha(S) = 0.3\pi$ and $Q(\Lambda)$=28, $\alpha(S) = 0.3\pi$ see figure $6.3-2$ through 6.3-4.

The physical meaning of a large Q and α can be seen from equations $6.2-1$ and $\alpha = \frac{k_o C|S|L}{2}$. Looking at equation $6.2-1$, the Cook-Klien parameter, Q, is proportional to the square of the frequency of the ultrasonic sound wave. Therefore, to increase Q means that physically the frequency of the ultrasonic sound wave is increased. Next, look at the equation $\alpha = \frac{k_o C|S|L}{2}$, the peak phase delay , α, is proportional to the amplitude of the ultrasonic sound wave given that all other parameters are fixed. So, to increase the peak phase delay means physically that the amplitude of the ultrasonic sound wave is

increased or more specifically the voltage applied to the transducers bound the acousto-optic modulator is increased.

Plots of the two dimensional and one dimensional transfer functions for the zeroth order, given the values of Q and α above, are plotted in figures $6.3-2$ to $6.3-4$. The experimental results and plots show that the parameters of the sound wave in the acousto-optic image processing system plays an important role. Also, it is possible to obtain better image enhancement results by changing the parameters, Q and α. Next, let us examine in more detailed the cases where 1) α is zero and all other parameters are fixed and 2) Q is zero and all other parameters are fixed.

The case when the peak phase delay, α, was equal to zero has been mentioned in a previous chapter. But, in this section we will examine this case in more detail. The physically meaning of α being equal to zero is that the amplitude of the ultrasonic sound wave is equal to zero. Therefore, since it is the propagation of the ultrasonic sound wave through the acousto-optic modulator that causes the incident light to diffract. When $\alpha = 0$, no diffracted orders are produced by the modulator. This fact can be confirmed by letting α be equal to zeroth in the acousto-optic transfer function from chapter five. Doing this gives the following result:

$$H_0(k_x, k_y; \zeta = 1) = exp[-jk_xLtan(\phi_B)] \{cos\sqrt{k_x^2L^2tan^2(\phi_B)} - jk_xLtan(\phi_B)sinc\sqrt{k_x^2L^2tan^2(\phi_B)}\} \quad (6.3-1)$$

$$H_{-1}(k_x, k_y; \zeta = 1) = 0 \quad (6.3-2)$$

As you can see from equation $6.3-2$, the minus one order is not produced when $\alpha = 0$. Looking at figure $6.3-5$, the magnitude of equation $6.3-1$ is unity when $\alpha = 0$, which means physically the incident light field propagates through the modulator undiffracted.

Next, we examine the case when the Cook-Klien parameter, Q, is equal to zero. The physical meaning of Q being equal to zero is that the frequency of the ultrasonic sound wave is equal to zero or conversely the wavelength of the sound wave is infinite. Basically, what the former statement is saying is that a DC voltage is being applied to the transducers bonded to the acousto-optic modulator. Therefore, the acousto-optic medium is not under going any compression or refraction since this stress is caused by the sinusoidal nature of the sound wave. So, as in the previous case where the peak phase delay was equal to zero, we would expected the magnitude of the transfer function for the zeroth order to be equal to unity, while the magnitude of the transfer function for the minus one order is zero. So, substituting $Q = 0$ in the acousto-optic transfer function derived in chapter five we have

$$\left|H_0(k_x, k_y; \zeta = 1)\right| = 1 \qquad (6.3-3)$$

$$\left|H_{-1}(k_x, k_y; \zeta = 1)\right| = 0 \qquad (6.3-4)$$

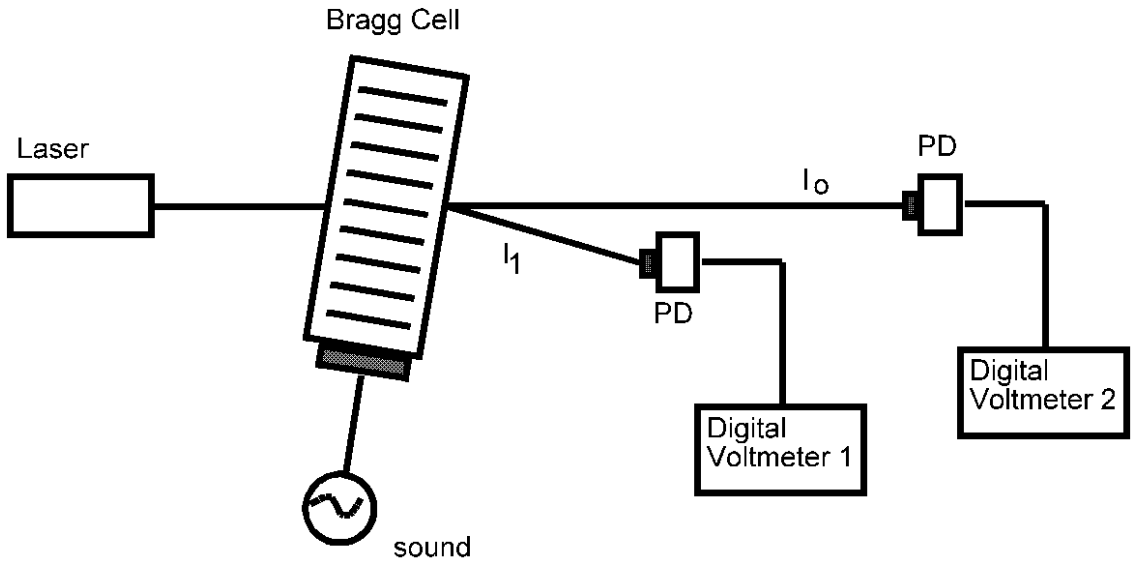

Figure $6.1-1$: Experimental Configuration to measure Peak Phase Delay, α.

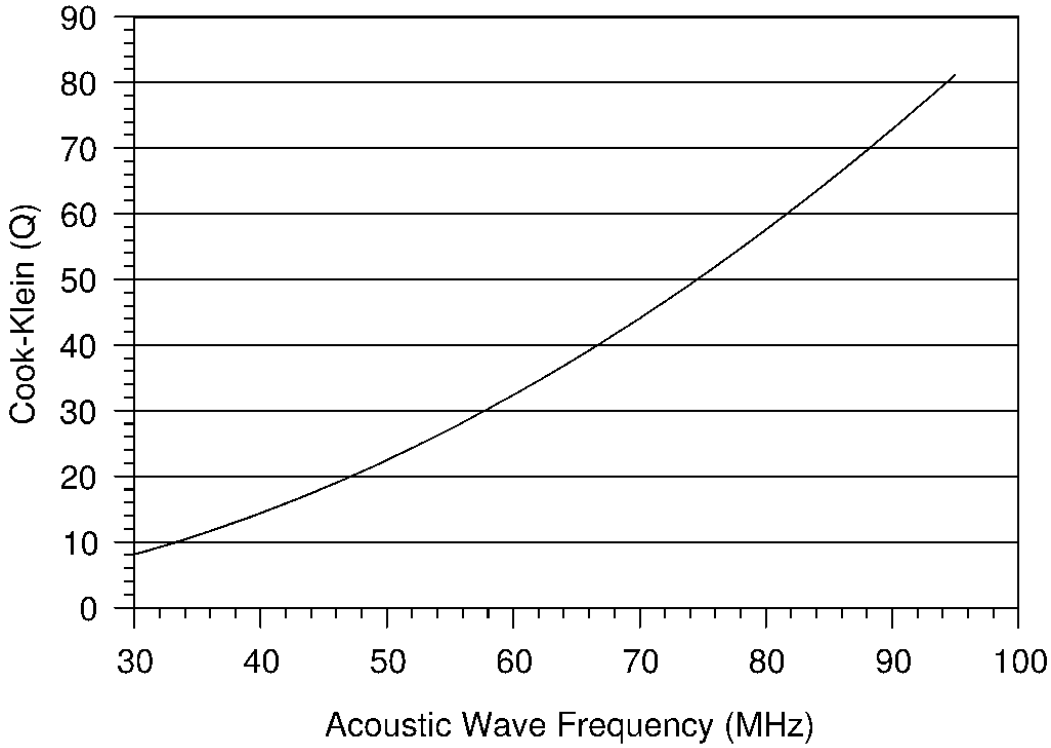

Figure 6.2-1: Plot of Cook-Klien Parameter, Q, versus Acoustic Wave Frequency, Λ.

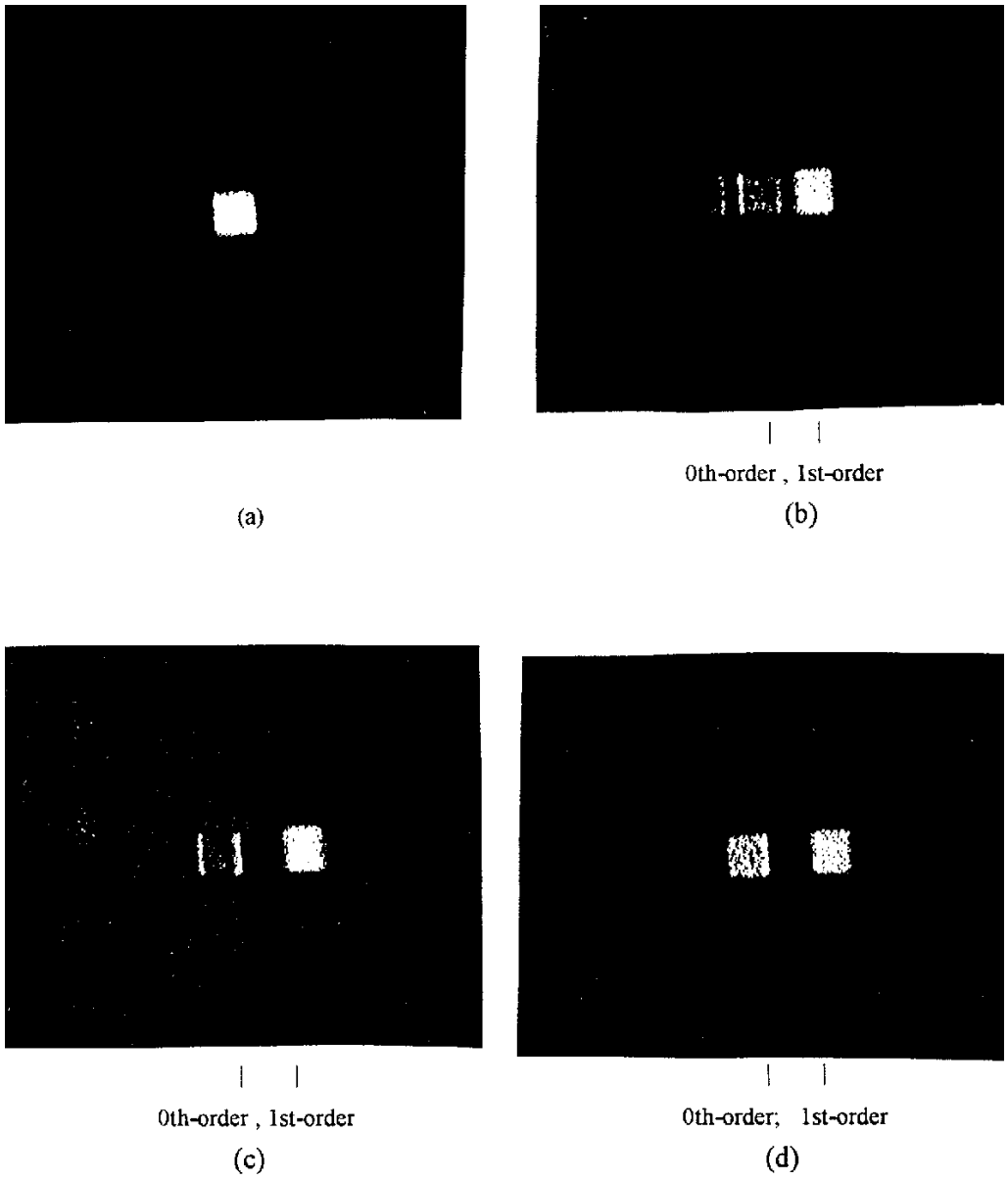

Figure 6.3-1: Photographs of the original picture (a), and the images of the zeroth-order (left one) and the minus one order (right one) when (b) $\mathrm{Q}(\Lambda) = 10$, $\alpha(S_1) = 0.65\pi$; (c) $\mathrm{Q}(\Lambda) = 28$, $\alpha(S_2) = 0.65\pi$; and $(d)$when $\mathrm{Q}(\Lambda) = 28$, $\alpha = 0.3\pi$

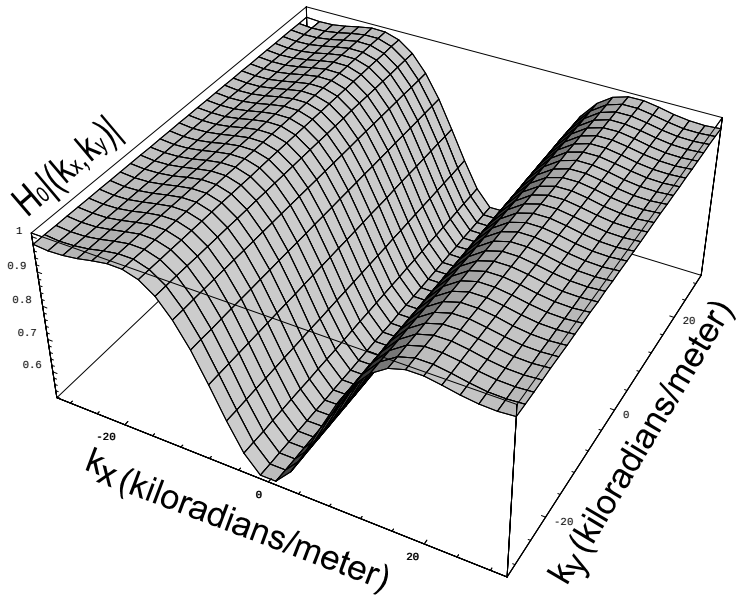

(a)

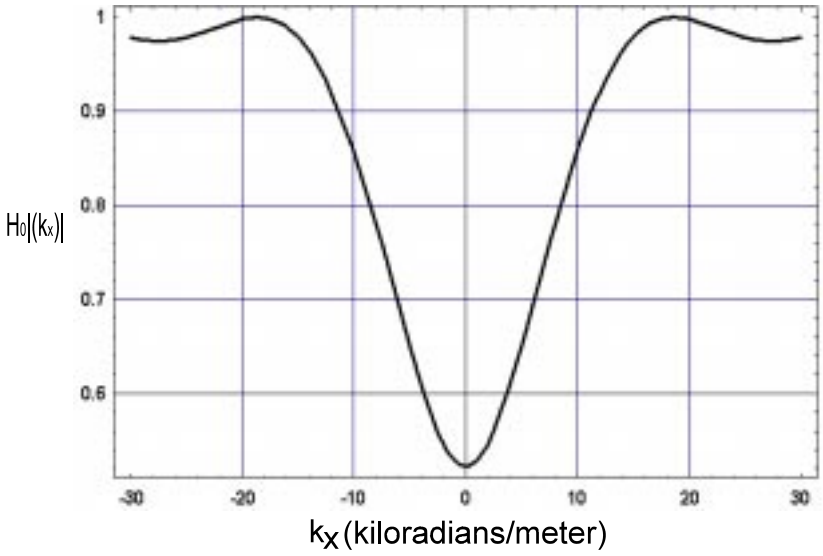

(b)

Figure 6.3-2: Plot of transfer function for ζ=1, $Q = 10, \alpha = 0.65\pi, (a)$ 2-D transfer function, (b) 1-D transfer function

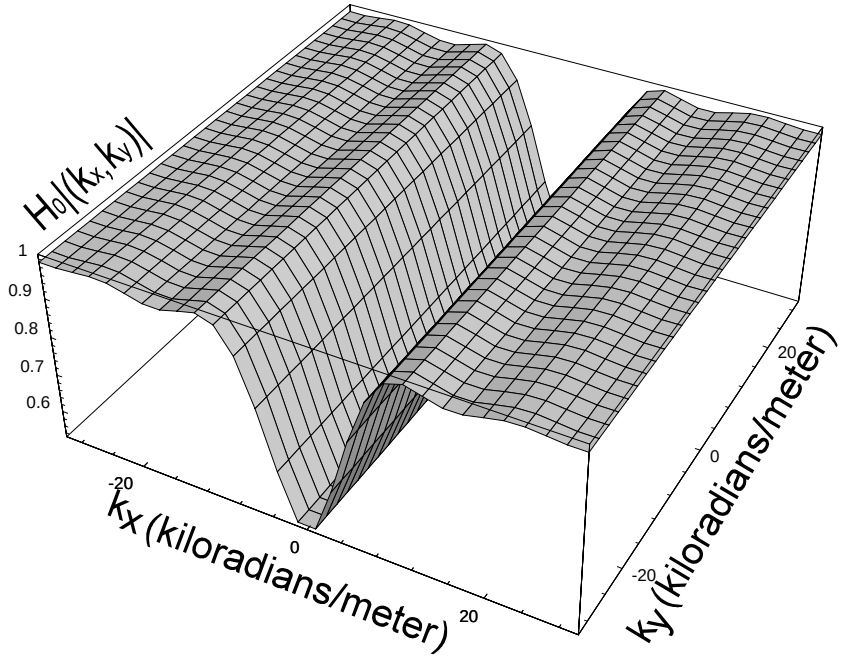

(a)

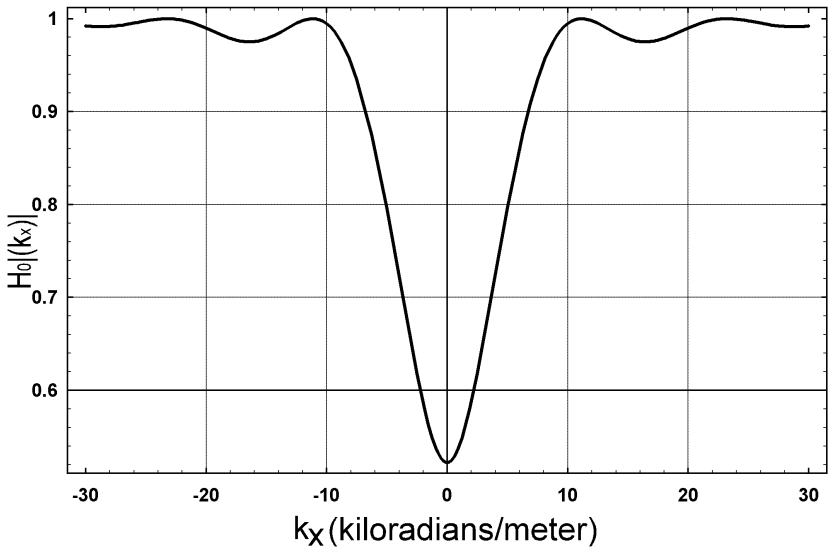

(b)

Figure 6.3-3: Plot of transfer function for ζ=1, $Q = 28, \alpha = 0.65\pi, (a)$ 2-D transfer function, (b) 1-D transfer function

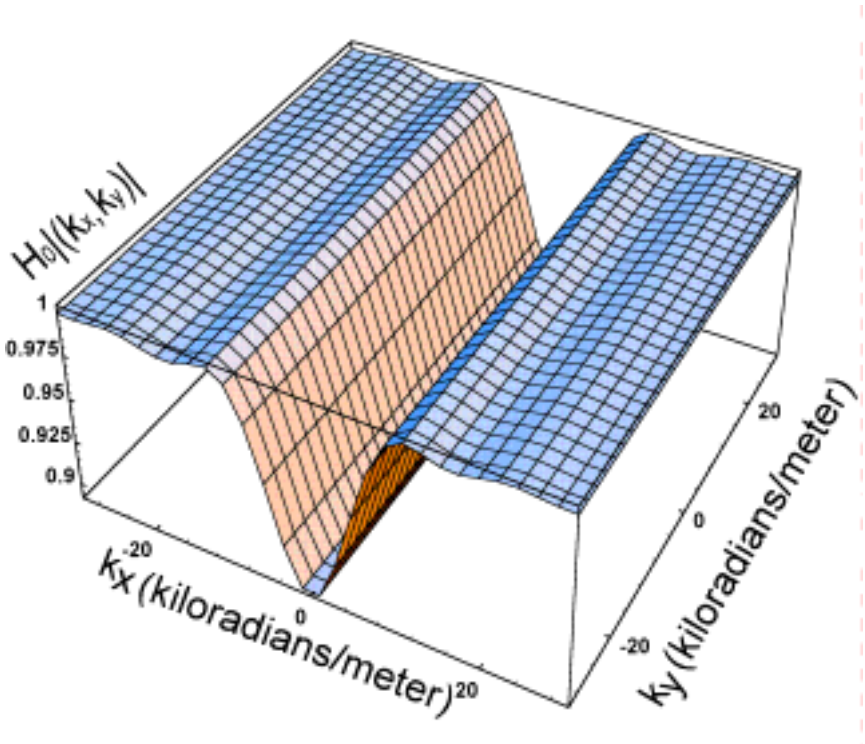

(a)

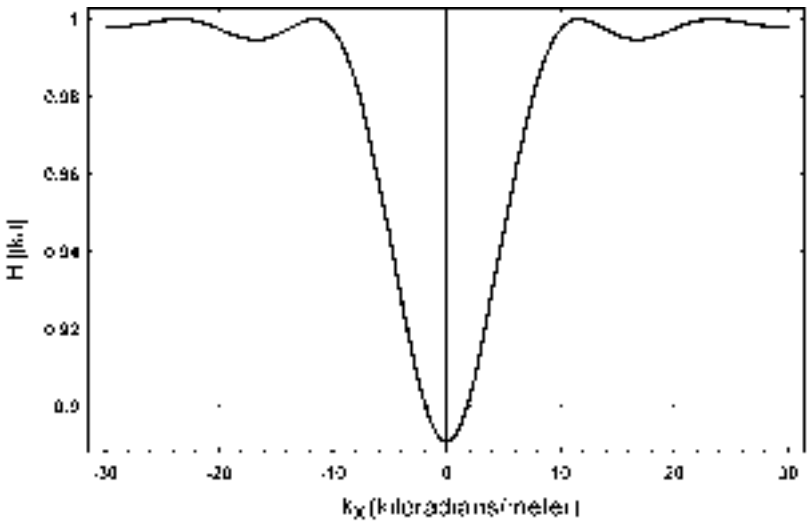

(b)

Figure 6.3-4: Plot of transfer function for ζ=1, $Q = 28, \alpha = 0.3\pi$, (a) 2-D transfer function, (b) 1-D transfer function

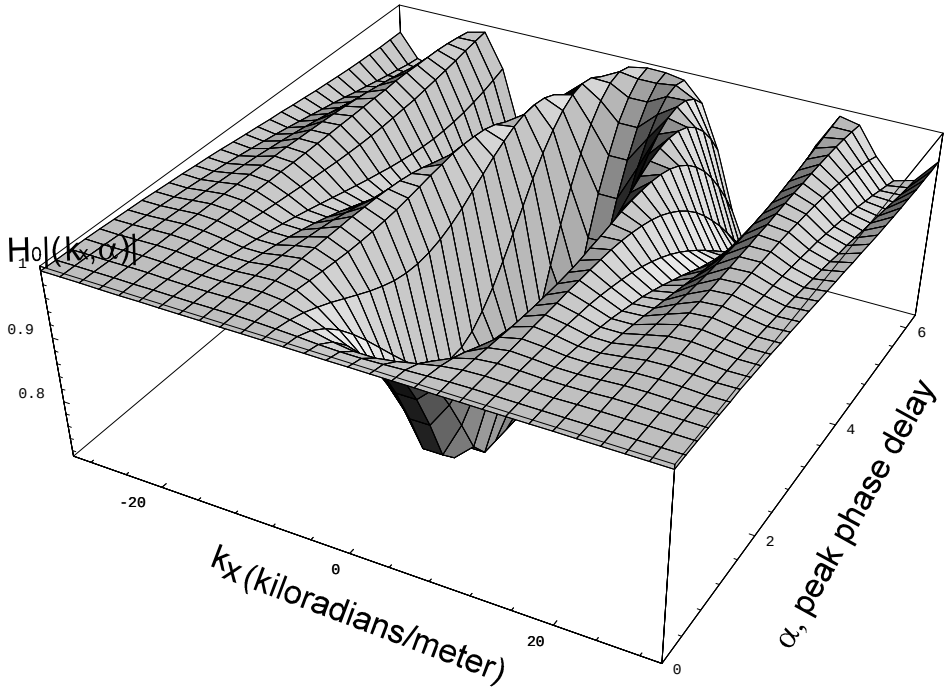

Figure $6.3-5$: Three dimensional graph of Acousto-Optic transfer function of the zeroth order for ζ=1, Q=28 and $L = 60mm$

Table 6.1-1: Measured Data to Calculate the Peak Phase Delay, α.

Sound Frequency=50 MHz							
Trial No.	VCO dial	|S|(vpp)	$I_o(volts)$	$I_{-1}(volts)$	$\text{Tan}\left(\frac{\alpha}{2}\right)$	$\alpha(degrees)$	$\alpha(radians)$
1	10	128.8	1.98	5.68	1.69	118.80	0.6600π
2	9	128	2.02	5.77	1.68	118.70	0.6594π
3	8	112	2.25	5.56	1.57	115.07	0.6393π
4	7	96	2.93	4.9	1.29	104.57	0.5809π
5	6	84	3.92	3.92	1.00	90.00	0.5000π
6	5	64	4.9	2.96	0.77	75.70	0.4206π
7	4	52	5.91	1.98	0.57	60.12	0.3340π
8	3	40	6.91	1.1	0.39	43.50	0.2417π
9	2	25.2	7.52	0.55	0.26	30.21	0.1678π
10	1	10.4	7.93	0.14	0.13	15.31	0.0851π

Table 6.1-2: Measured Data to Calculate the Peak Phase Delay, α.

Sound Frequency=40 MHz							
Trial No.	VCO dial	|S|(vpp)	$I_o(volts)$	$I_{-1}(volts)$	$\text{Tan}\left(\frac{\alpha}{2}\right)$	$\alpha(degrees)$	$\alpha(radians)$
1	10	128	3.08	5.22	1.3	104.94	0.5830π
2	9	121.6	2.82	5.58	1.41	109.18	0.6066π
3	8	118.4	2.25	6.5	1.7	119.05	0.6614π
4	7	97.6	2.42	6.4	1.63	116.82	0.6490π
5	6	80.8	3.18	5.55	1.32	105.75	0.5875π
6	5	68	4.48	4.54	1.01	90.38	0.5021π
7	4	52	5.9	3.58	0.78	75.83	0.4213π
8	3	36	7.15	1.90	0.52	54.54	0.3030π
9	2	24	8.09	1.05	0.36	39.62	0.2201π
10	1	11.04	8.70	0.45	0.23	25.57	0.1421π

Table 6.1-3: Measured Data to Calculate the Peak Phase Delay, α.

Sound Frequency=28 MHz							
Trial No.	VCO dial	|S|(vpp)	$I_o(volts)$	$I_{-1}(volts)$	$\text{Tan}\left(\frac{\alpha}{2}\right)$	$\alpha(degrees)$	$\alpha(radians)$
1	10	126	3.02	4.66	1.22	101.1	0.5617π
2	9	121.2	2.84	4.88	1.31	105.3	0.5850π
3	8	104	2.28	5.8	1.6	115.84	0.6436π
4	7	92	2.45	5.75	1.53	113.73	0.6318π
5	6	76	3.1	5.28	1.31	105.08	0.5838π
6	5	60	4.15	4.16	1.01	90.06	0.5003π
7	4	45	5.51	2.89	0.72	71.83	0.3991π
8	3	35	6.8	1.84	0.52	54.97	0.3054π
9	2	24	7.72	0.98	0.34	37.31	0.2073π
10	1	9.4	8.44	0.28	0.18	20.65	0.1147π

Table 6.1-4: Measured Data to Calculate the Peak Phase Delay, α

Sound Frequency=80 MHz							
Trial No.	VCO dial	|S|(vpp)	$I_o(volts)$	$I_{-1}(mvolts)$	$\text{Tan}\left(\frac{\alpha}{2}\right)$	$\alpha(degrees)$	$\alpha(radians)$
1	10	104	0.292	7.2	0.1570	17.848	0.0991π
2	9	96	0.453	7.4	0.1278	14.567	0.0809π
3	8	80	0.831	6.7	0.0897	10.261	0.0570π
4	7	72	1.2	5.9	0.0701	8.022	0.0446π
5	6	52	1.5	4.9	0.0571	6.542	0.0363π
6	5	48	1.8	3.7	0.0453	5.192	0.0288π
7	4	38	2.14	2.9	0.3681	4.216	0.0234π
8	3	28	2.3	2.2	0.0309	3.543	0.0196π
9	2	16	2.69	1.8	0.0258	2.963	0.0164π
10	1	7.2	2.60	1.6	0.0248	2.842	0.0157π

Table 6.1-5: Measured Data to Calculate the Peak Phase Delay, α

Sound Frequency $= 80$ MHz connected to PA-4 InterAction Amplifier							
Trial No.	VCO dial	|S|(vpp)	$\mathrm{I}_o(volts)$	$\mathrm{I}_{-1}(volts)$	$\mathrm{Tan}\left(\frac{\alpha}{2}\right)$	$\alpha(degrees)$	$\alpha(radians)$
1	10	44	7.44	6.25	0.916	85.03	0.472π
2	9	44	7.18	6.11	0.922	85.38	0.474π
3	8	36	7.49	5.18	0.831	79.49	0.442π
4	7	36	7.66	4.37	0.755	74.12	0.412π
5	6	28	7.89	2.96	0.613	62.98	0.349π
6	5	22	8.21	1.971	0.489	52.21	0.290π
7	4	18	8.30	1.288	0.393	43.00	0.238π
8	3	12.96	8.43	0.718	0.292	32.54	0.181π
9	2	7.4	8.61	0.281	0.181	20.48	0.114π
10	1	3.4	8.56	0.0108	0.035	4.068	0.0226π

Chapter 7.0 Coordinate System Transformations and Image Separation

This chapter will present a detailed mathematical formalism for each of the proposed acousto-optic image processing systems. The analysis will model the effect of the systems on images as they propagate through the systems. The first section in the chapter will derive coordinate transformations needed for the development of the formalisms.

7.1 Coordinate System Transformations

Looking at figure $7.1-1$, you will notice that the light field, $\psi_{inc}(x'''\text{,}y)$, incident onto the acousto-optic cell (AOC) is not in the same coordinate system as the AOC. In fact the coordinate system that the incident light field is in is rotated by an amount $+\phi_{inc} = (1+\delta)\phi_b$ with respect to the defined AOC coordinate system. The diffracted light field, minus one order, is rotated by an amount $-\phi_b$ with respect to the AOC and rotated by an amount $-2\phi_b$ with respect to the zeroth order. The undiffracted light, zeroth order, coordinate system is rotated by an angle $+\phi_b$ with respect to the AOC.

These observations will be taken into account when I derive analytical formalisms for the various acousto-optic image processing systems in the next sections. But, as a practical matter it is not really necssary for me to include these coordinate system changes due to the fact that the incident angle, ϕ_{inc}, is very small such that you can approximate $cos(\phi_{inc})$ as one and the $sin(\phi_{inc})$ as zero. But, I will include the effect coordinates system changes in an effort to maintain a certain level of mathematical rigour.

It is assumed that the acousto-optic modulator is parallel to the $x-z$ plane with the acoustic wave, $S_e(x',y,z')$, propagating in the positive $x'-$ direction. The light field, $\psi(x''',y,z''')$, propagates in the positive $z'''-$ direction. With this configuration in mind, let us derive coordinate system transformation that will allows us to map the input image coordinate system, $(x,y,z),$ to the coordinate system of the acousto-optic cell, (x',y,z'). Looking at figure $7.1-2$, the correct coordinate transformation to accomplish this goal is:

$$x = cos(\phi_b)x' - sin(\phi_b)z' \qquad (7.1-1a)$$

$$z = sin(\phi_b)x' + cos(\phi_b)z' \qquad (7.1-1b)$$

Next, let us derive the coordinate system transformation that will allows one to map the acousto-optic cell coordinate system, $(x',y,z'),$ to the coordinate system of the zeroth order, (x,y,z). Looking at figure $7.1-2$ again, the correct coordinate transformation to accomplish this goal is:

$$x' = cos(\phi_b)x + sin(\phi_b)z \qquad (7.1-2a)$$

$$z' = -sin(\phi_b)x + cos(\phi_b)z \qquad (7.1-2b)$$

Next, let us derive the coordinate system transformation that will allows one to map the acousto-optic cell coordinate system, $(x',y,z'),$ to the coordinate system of the zeroth order, (x''',y,z'''). Looking at figure $7.1-3$, the correct coordinate transformation to accomplish this goal is:

$$x''' = cos(\phi_{inc})x' - sin(\phi_{inc})z' \qquad (7.1-3a)$$

$$z''' = sin(\phi_{inc})x' + cos(\phi_{inc})z' \qquad (7.1-3b)$$

Now, let us derive the coordinate system transformation that will allows one to map the minus one order coordinate system, (x'',y,z''), to the coordinate system of the acousto-optic cell, (x',y,z'). Looking at figure $7.1-4$, the correct coordinate transformation to accomplish this goal is:

$$x\text{”} = cos(\phi_b)x\text{’} + sin(\phi_b)z\text{’} \qquad (7.1-4a)$$

$$z\text{”} = -sin(\phi_b)x\text{’} + cos(\phi_b)z\text{’} \qquad (7.1-4b)$$

Now, let us derive the coordinate system transformation that will allows one to map the zeroth order coordinate system, $(x, y, z),$ to the coordinate system of the minus one order, $(x\text{”}, y, z\text{”})$. Looking at figure $7.1-5$, the correct coordinate transformation to accomplish this goal is:

$$x = cos(2\phi_b)x\text{”} - sin(2\phi_b)z\text{”} \qquad (7.1-5a)$$

$$z = sin(2\phi_b)x\text{”} + cos(2\phi_b)z\text{”} \qquad (7.1-5b)$$

Let us derive the coordinate system transformation that will allows one to map the minus one order coordinate system, $(x\text{”}, y, z\text{”}),$ to the coordinate system of the zeroth order, (x, y, z). Again, looking at figure $7.1-5$, the correct coordinate transformation to accomplish this goal is:

$$x\text{”} = cos(2\phi_b)x + sin(2\phi_b)z \qquad (7.1-6a)$$

$$z\text{”} = -sin(2\phi_b)x + cos(2\phi_b)z \qquad (7.1-6b)$$

In the Parallel Acousto-Optic image processing system, figure 7.1-6, AOM_1 is parallel to the $x-z$ plane. But, AOM_2 is parallel to the $y-z$ plane. Because, AOM_2 is oriented differently. The coordinate system transformation must be modified to account for this factor. Lets first derive the coordinate system transformation that will allows me to map the input image coordinate system, $(x, y\text{”’}, z\text{”’}),$ to the coordinate system of the acousto-optic cell, $(x, y\text{’}, z\text{’})$. Looking at figure $7.1-7$, the correct coordinate transformation to accomplish this goal is:

$$y\text{”’} = cos(\phi_{inc})y\text{’} - sin(\phi_{inc})z\text{’} \qquad (7.1-7a)$$

$$z\text{”’} = sin(\phi_{inc})y\text{’} + cos(\phi_{inc})z\text{’} \qquad (7.1-7b)$$

Next, let us derive the coordinate system transformation that will allows one to map the zeroth order coordinate system, (x, y, z), to the coordinate system of the acousto-optic cell, (x, y', z'). Looking at figure $7.1-8$, the correct coordinate transformation to accomplish this goal is:

$$y = cos(\phi_b)y' - sin(\phi_b)z' \qquad (7.1-8a)$$

$$z = sin(\phi_b)y' + cos(\phi_b)z' \qquad (7.1-8b)$$

Now, lets derive the coordinate system transformation that will allows one to map the acousto-optic cell coordinate system, (x, y', z'), to the coordinate system of the zeroth order, (x, y, z). Looking at figure $7.1-8$, the correct coordinate transformation to accomplish this goal is:

$$y' = cos(\phi_b)y + sin(\phi_b)z \qquad (7.1-9a)$$

$$z' = -sin(\phi_b)y + cos(\phi_b)z \qquad (7.1-9b)$$

Again, lets derive the coordinate system transformation that will allows one to map the minus one order coordinate system, (x, y'', z''), to the coordinate system of the acousto-optic cell, (x, y', z'). Looking at figure $7.1-9$, the correct coordinate transformation to accomplish this goal is:

$$y'' = cos(\phi_b)y' + sin(\phi_b)z' \qquad (7.1-10a)$$

$$z'' = -sin(\phi_b)y' + cos(\phi_b)z' \qquad (7.1-10b)$$

One more, lets derive the coordinate system transformation that will allows one to map the zeroth order coordinate system, (x, y, z), to the coordinate system of the minus one order, (x, y'', z''). Looking at figure $7.1-10$, the correct coordinate transformation to accomplish this goal is:

$$y = cos(2\phi_b)y'' - sin(2\phi_b)z'' \qquad (7.1-11a)$$

$$z = sin(2\phi_b)y'' + cos(2\phi_b)z'' \qquad (7.1-11b)$$

Next, lets derive the coordinate system transformation that will allows one to map the minus one order coordinate system, $(x, y", z")$, to the coordinate system of the zeroth order, (x, y, z). Looking again at figure $7.1-10$, the correct coordinate transformation to accomplish this goal is:

$$y" = cos(2\phi_b)y + sin(2\phi_b)z \qquad (7.1-12a)$$

$$z" = -sin(2\phi_b)y + cos(2\phi_b)z \qquad (7.1-12b)$$

7.2 Image Separation

For a better explanation of the experimental arrangement , we derive the separation of the two images corresponding to the zeroth order and the minus one order on the output imaging plane 1. According to Snell refraction law[29], the distance between AOM and the virtual image, O', formed by the two parallel planes of the AOM, see Figure $7.2-1$, can be written as

$$d = b_1 - \left(1 - \frac{1}{n}\right)L. \qquad (7.2-1)$$

on the basis of lens imaging formula and referring to Figure $8.4-1$, we have

$$\frac{1}{d_1} - \frac{1}{S} = \frac{1}{f'}, \qquad (7.2-2)$$

where

$$S = d + L + c_1. \qquad (7.2-3)$$

Using equation $7.2-1$, S becomes

$$S = b_1 + \frac{L}{n} + c_1. \qquad (7.2-4)$$

Employing equation $7.2-2$ and equation $7.2-4$, we can determine the quantities b_1 and c_1 once we have chosen the desired separation distance between the zeroth order and the minus one order images on the output plane.

Assuming the width of the object along the $x-$direction is l, the frequency and the velocity of the plane wave of sound passing through the Acousto-Optic Modulator, also in the $x-$direction, to be f and v. The diffraction angle of light, ϕ_{b}(Bragg angle), can be described according to Bragg diffraction equation[45]

$$\phi_{\mathrm{b}} = \frac{\lambda f}{2v}. \qquad (7.2-5)$$

Considering the secondary refraction due to the two surface planes of the AOM, which the light field passes through, the separation AA'between two centers of the O' and O" corresponding to the zeroth order and the minus one order images is (see Figure $7.2-1$)

$$AA' = 2n(\phi_{\mathrm{b}})d \qquad (7.2-6)$$

Now, the separation BB' between two centers of the zeroth order and the minus one order images, if we express the magnification of the lens as M, is

$$BB' = M \cdot AA' = \frac{d_1}{S}(2n\phi_{\mathrm{b}})d. \qquad (7.2-7)$$

Substituting for d, S and ϕ_{b}, and using equations $7.2-1, 7.2-4$ and $7.2-5$, the separation BB' may be written as

$$BB' = \left(\frac{n\lambda f}{v}\right)\left(\frac{b_1 - \left(1-\frac{1}{n}\right)L}{b_1 + \frac{L}{n} + c_1}\right)d_1. \qquad (7.2-8)$$

From equation $7.2-8$, methods for increasing the separation BB' of two images corresponding to the zeroth order and the minus one order are: 1) increasing the frequency of sound wave through the AOM; 2) increasing the distance $b_1$and decreasing c_1 if other quantities in equation $7.2-8$ are fixed. When $c_1 = 0$, the separation BB' attains a maximum since b_1 takes on its maximum value.

In addition, the two images of the zeroth order and the minus one order diffracted by the AOM are separated or "resolved" when the following condition is satisfied

$$BB' > l \cdot \frac{d_1}{S} \qquad (7.2-9a)$$

or

$$BB' > \frac{l\, d_1}{b_1 + \frac{L}{n} + c_1}. \qquad (7.2-9b)$$

In fact, in order to obtain a clear image separation, one should choose the focal length of the imaging lens and the location of the object to be processed carefully.

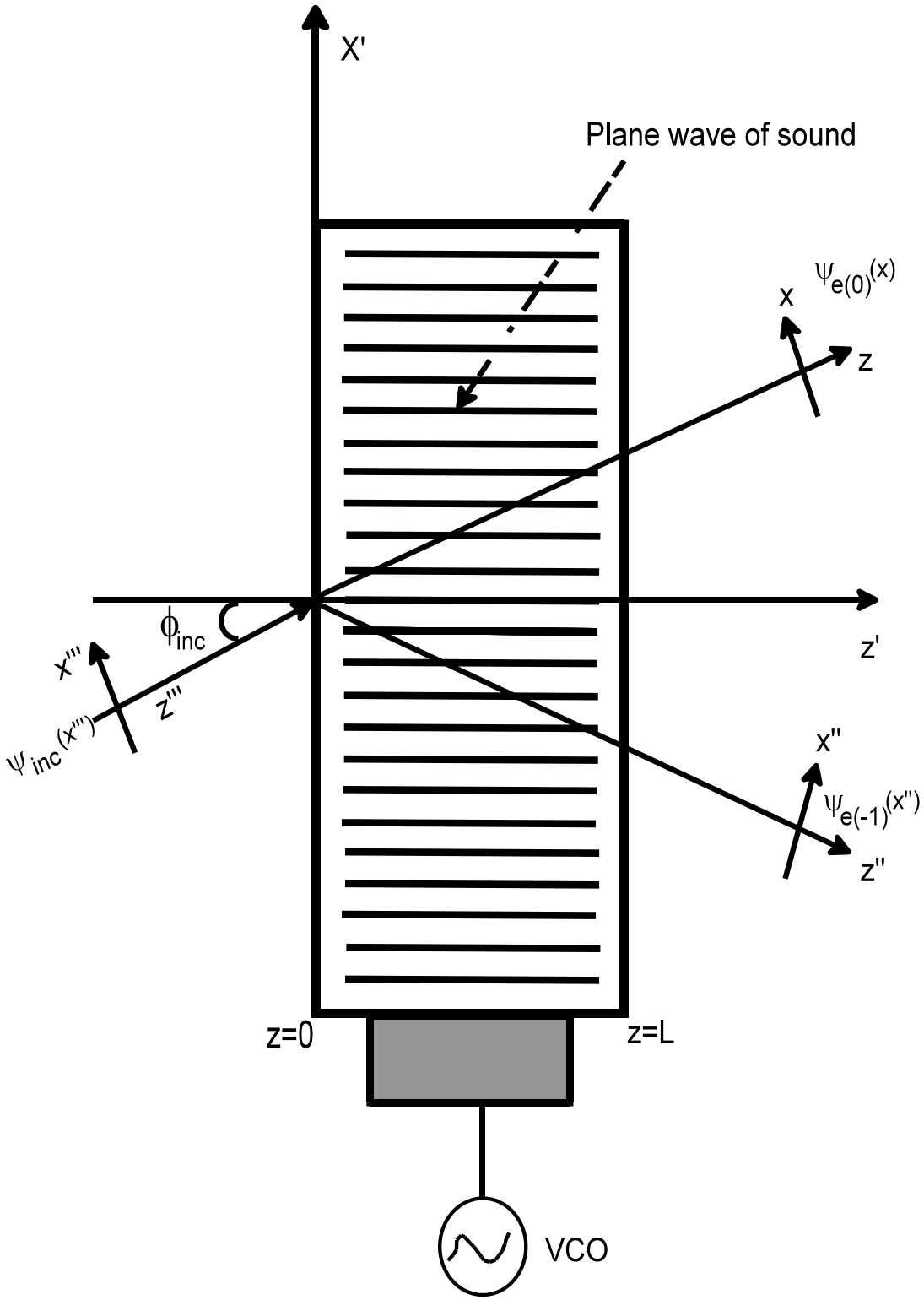

Figure 7.1-1: Diagram of Acousto-Optic cell for Coordinate System Transformation

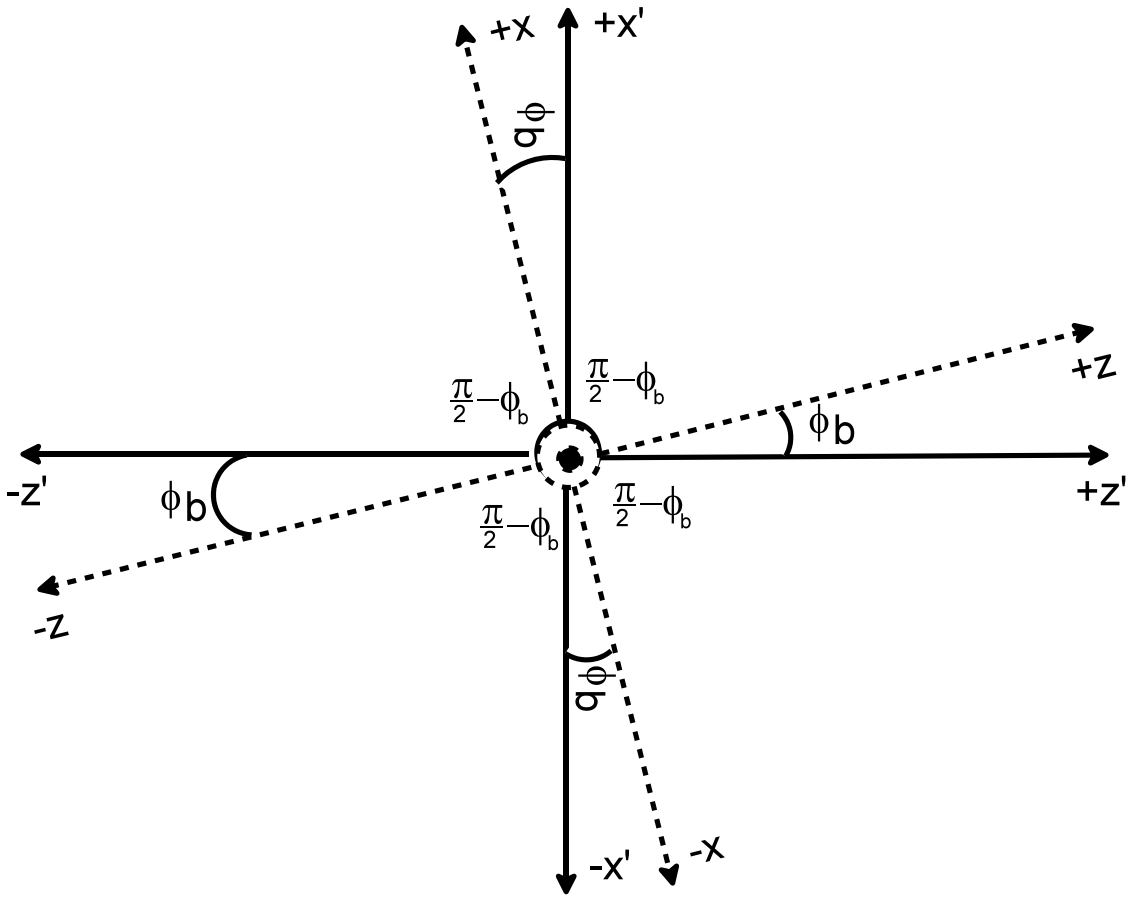

Figure 7.1-2: Coordinate system for the Acousto-Optic Cell, i.e. (x', y, z'), superimposed onto the coordinate system for the Zeroth Diffracted Order, i.e. (x,y,z).

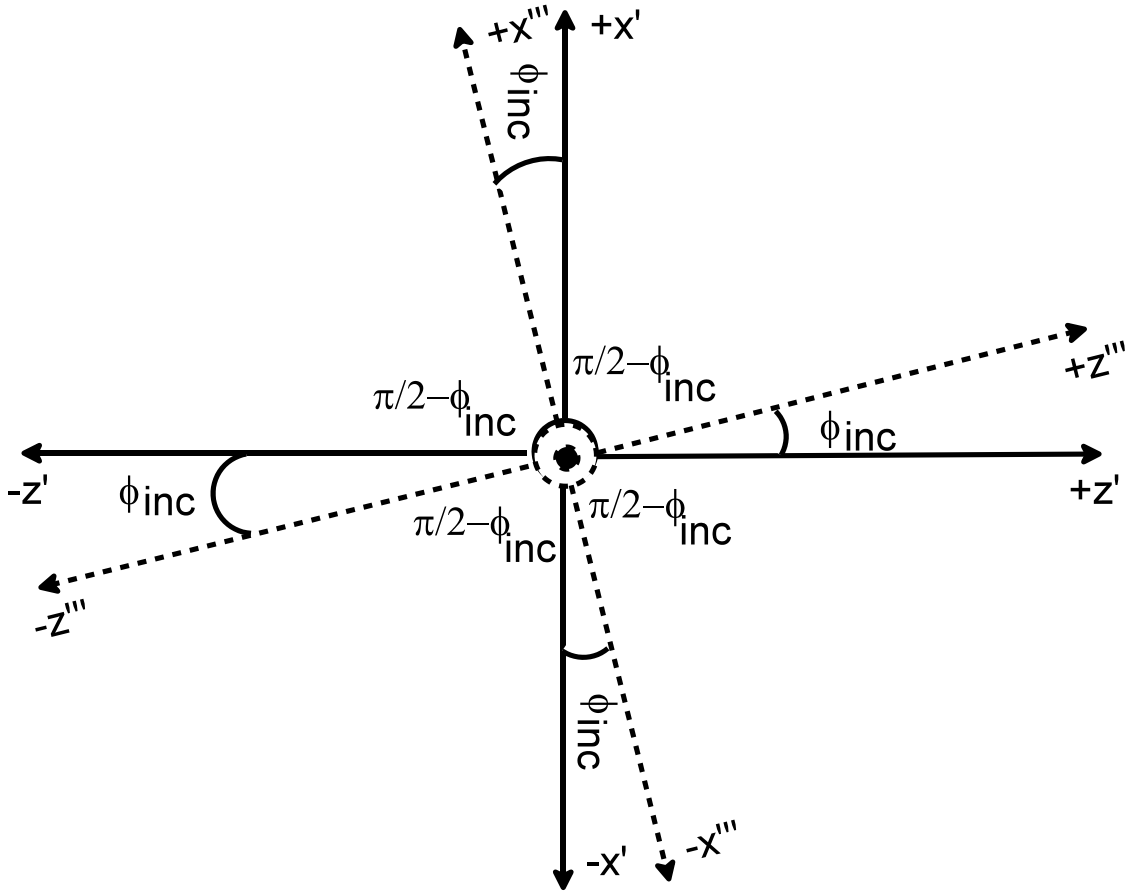

Figure 7.1-3: Coordinate system for the Acousto-Optic Cell, i.e. (x', y, z'), superimposed onto the coordinate system for the Input Image, i.e. (x''',y,z''').

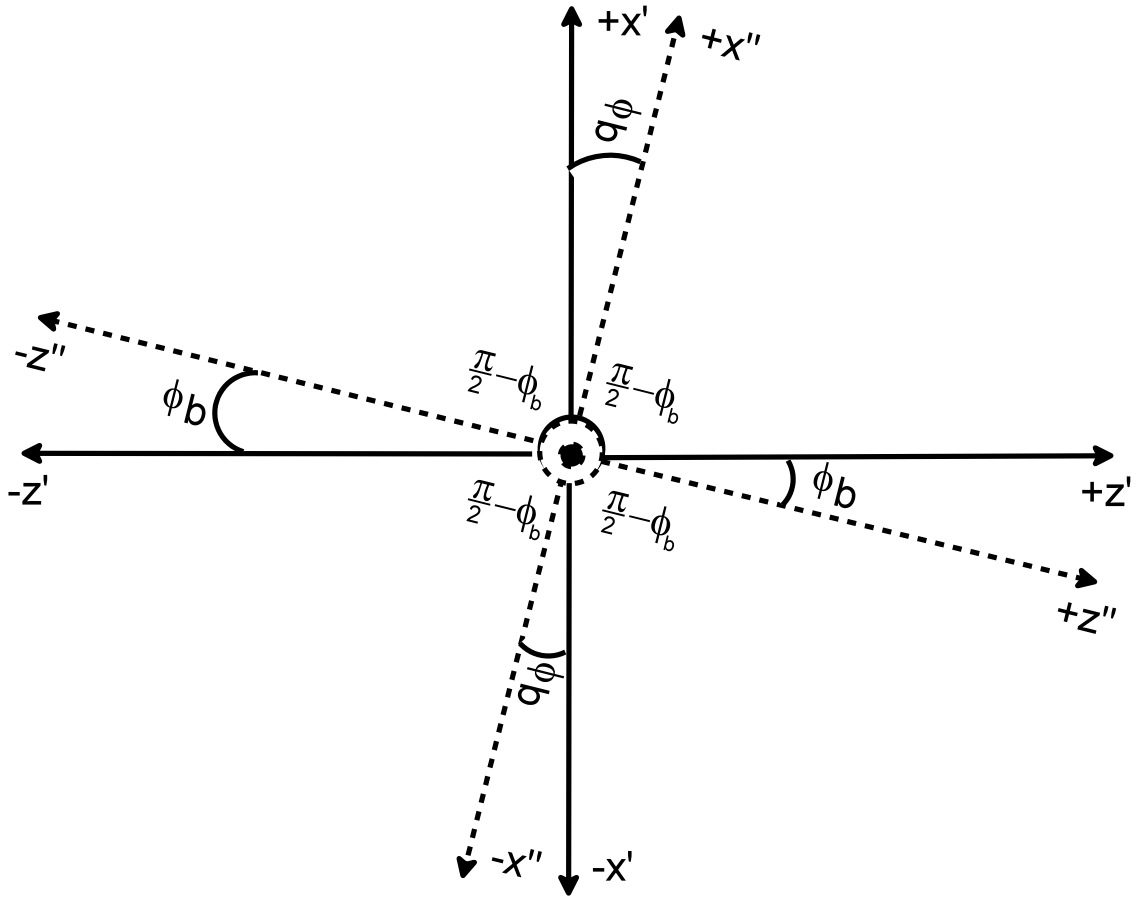

Figure 7.1-4: Coordinate system for the Acousto-Optic Cell, i.e. (x', y, z'), superimposed onto the coordinate system for the minus one Diffracted Order, i.e. (x'',y,z'').

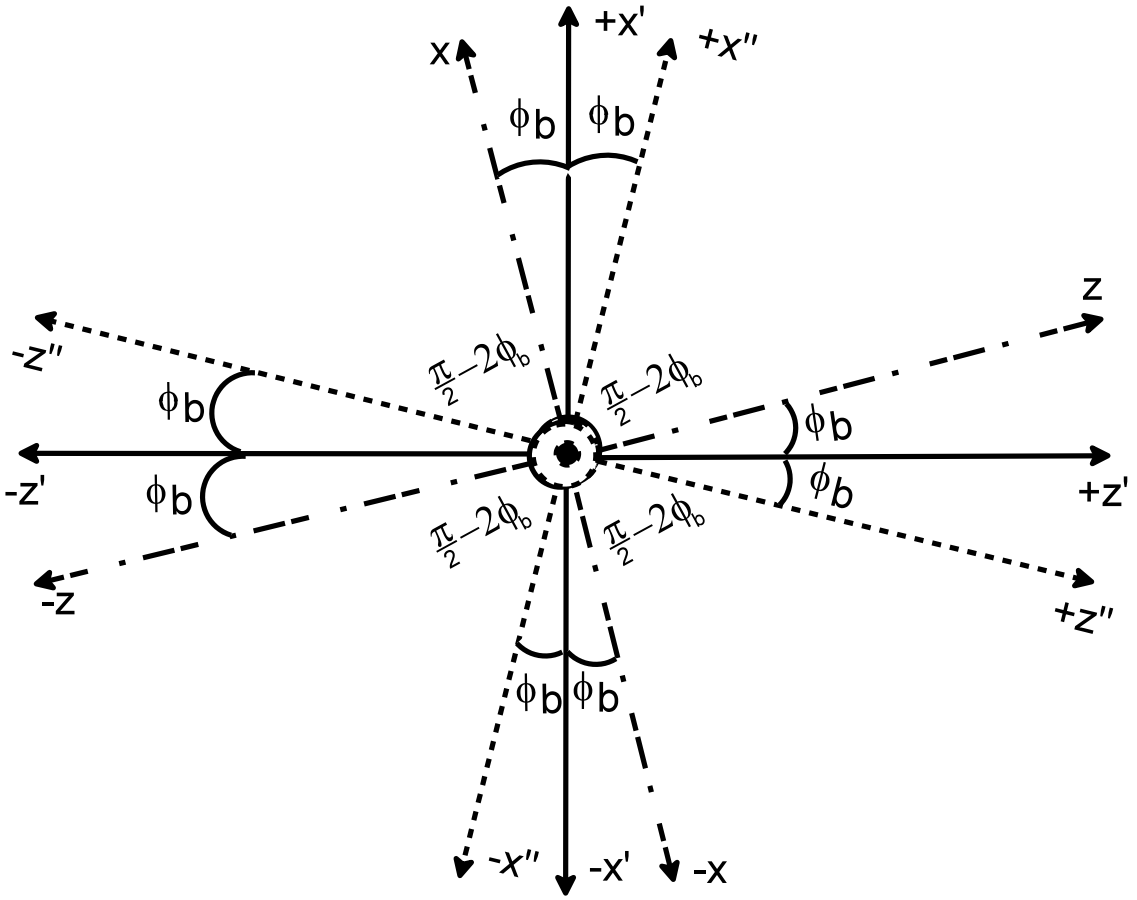

Figure 7.1-5: Coordinate system for the Zeroth Diffracted Order, i.e. (x, y, z), and minus one Diffracted Order, i.e. (x",y,z") superimposed onto the coordinate system for the AOC, i.e. (x',y,z').

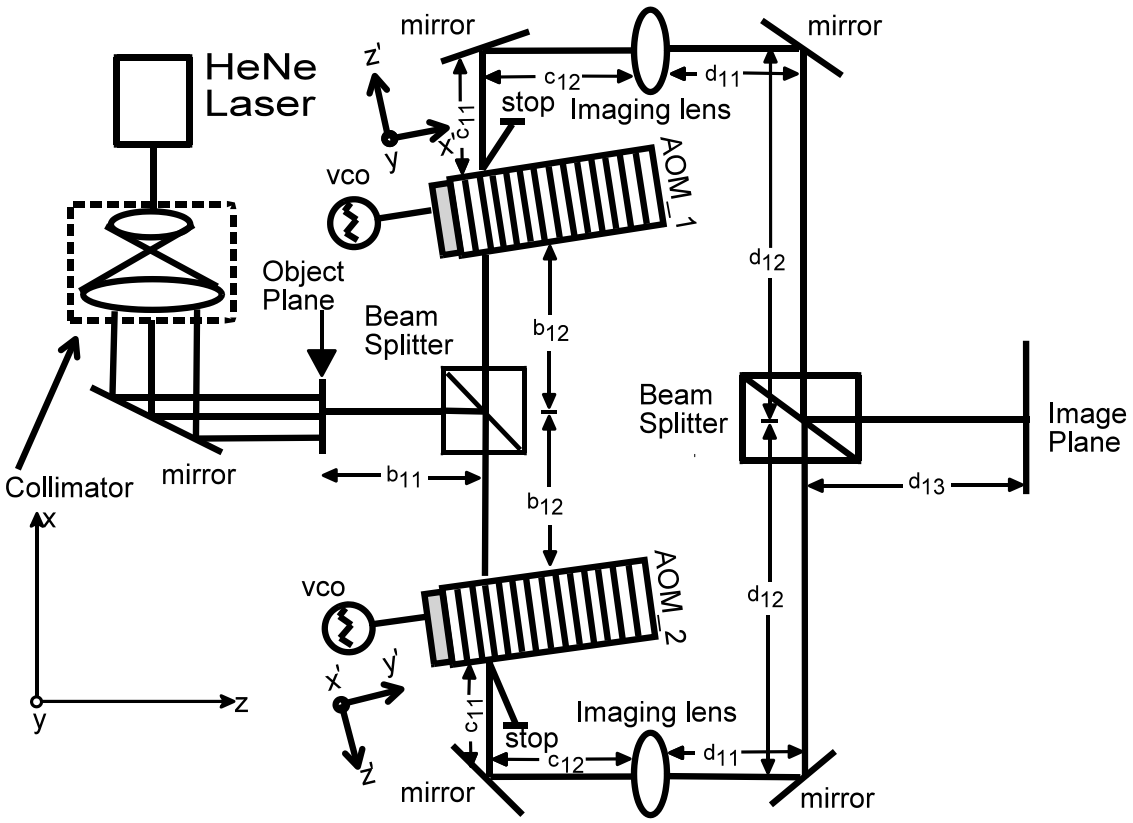

Figure 7.1-6: Parallel Acousto-Optic Image Processing System

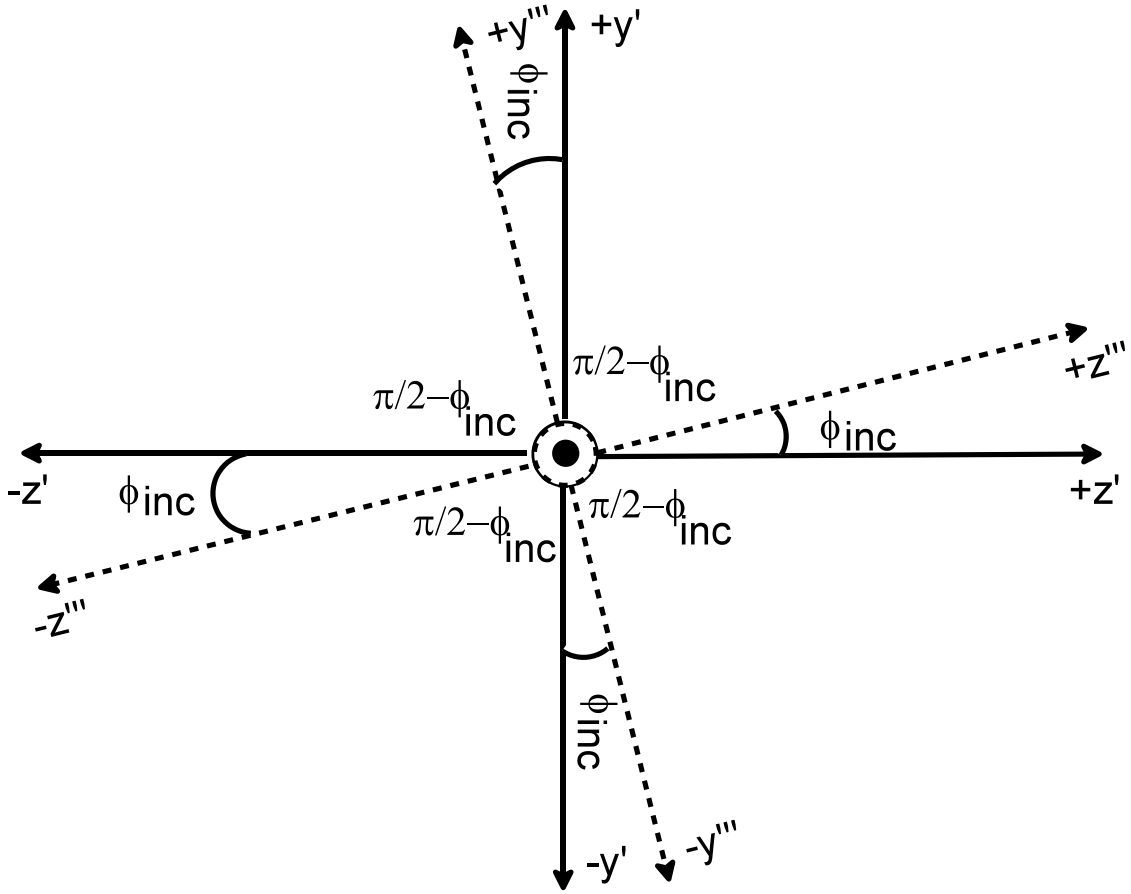

Figure 7.1-7: Coordinate system for the Acousto-Optic Cell, i.e. (x, y', z'), superimposed onto the coordinate system for the Input Image, i.e. (x,y''',z''').

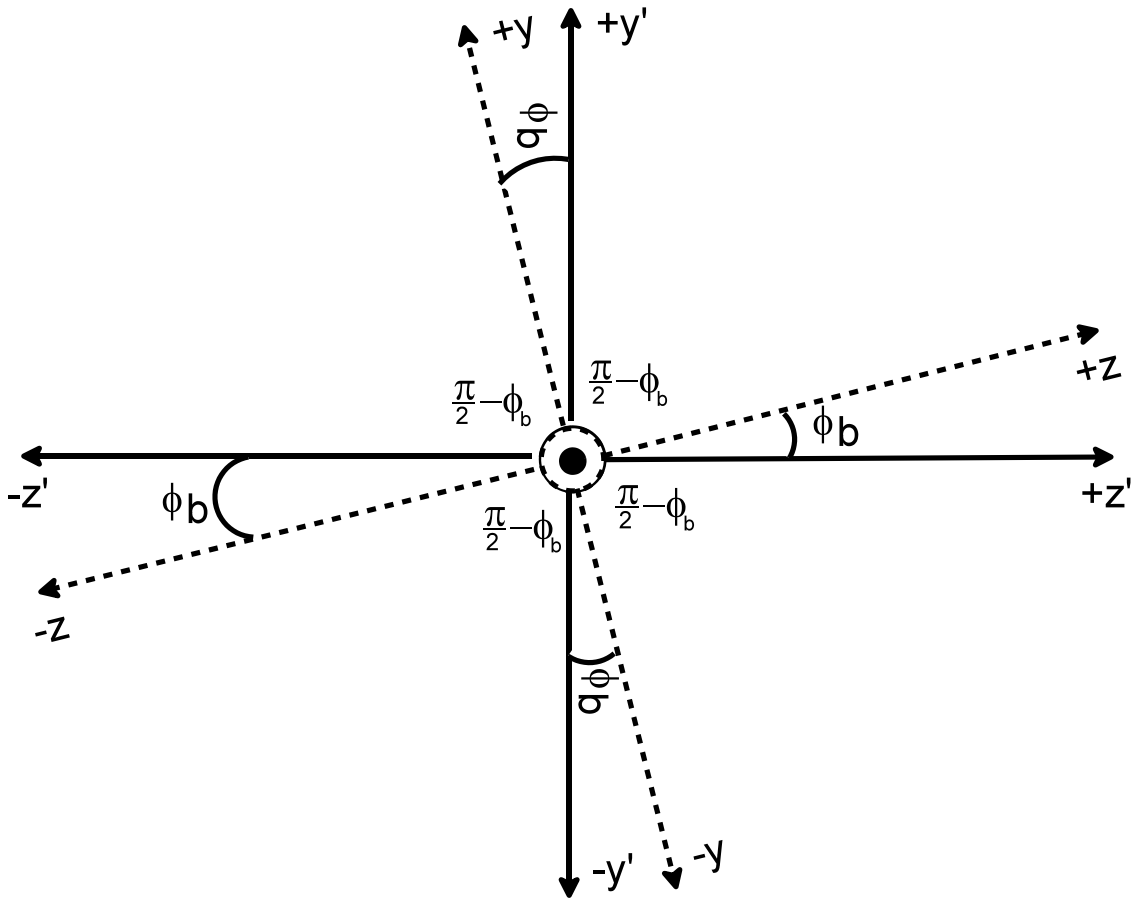

Figure 7.1-8: Coordinate system for the Acousto-Optic Cell, i.e. (x, y', z'), superimposed onto the coordinate system for the Zeroth Diffracted Order, i.e. (x,y,z).

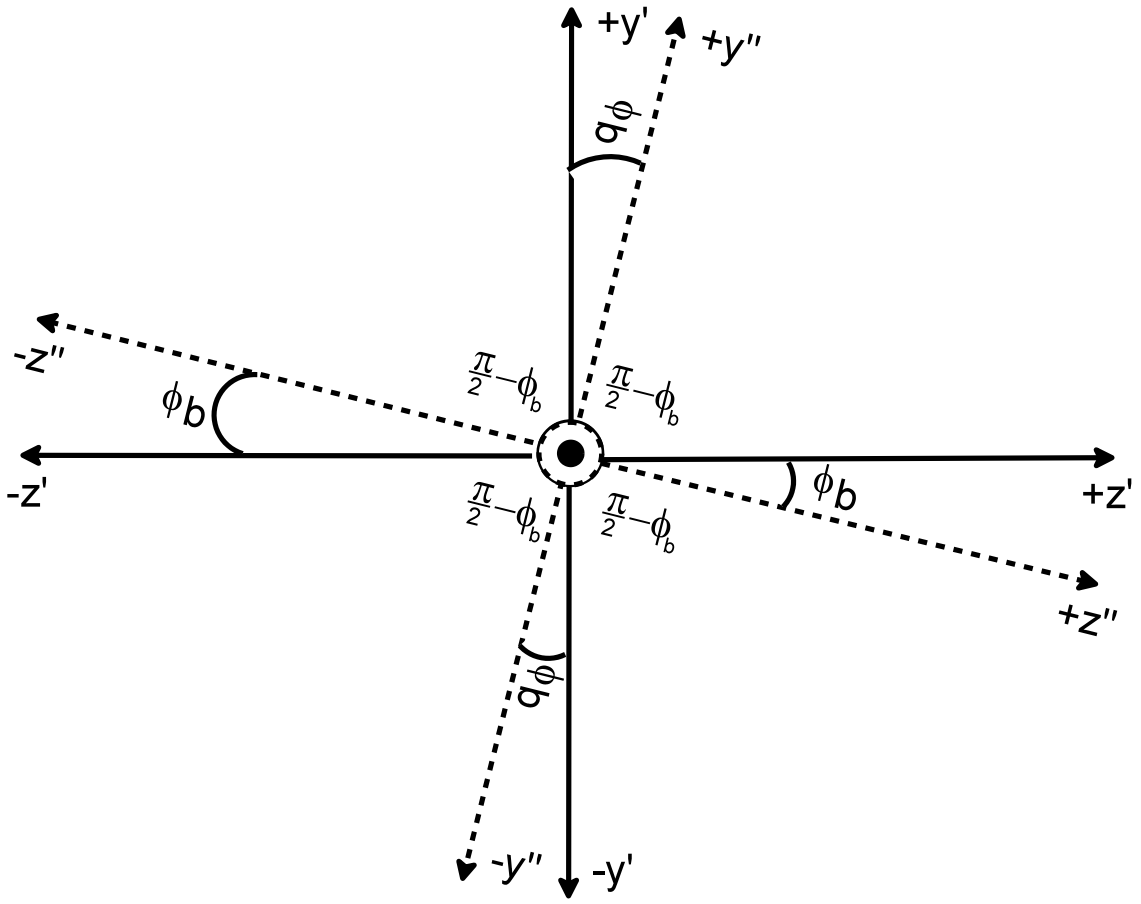

Figure 7.1-9: Coordinate system for the Acousto-Optic Cell, i.e. (x, y', z'), superimposed onto the coordinate system for the minus one Diffracted Order, i.e. (x,y",z").

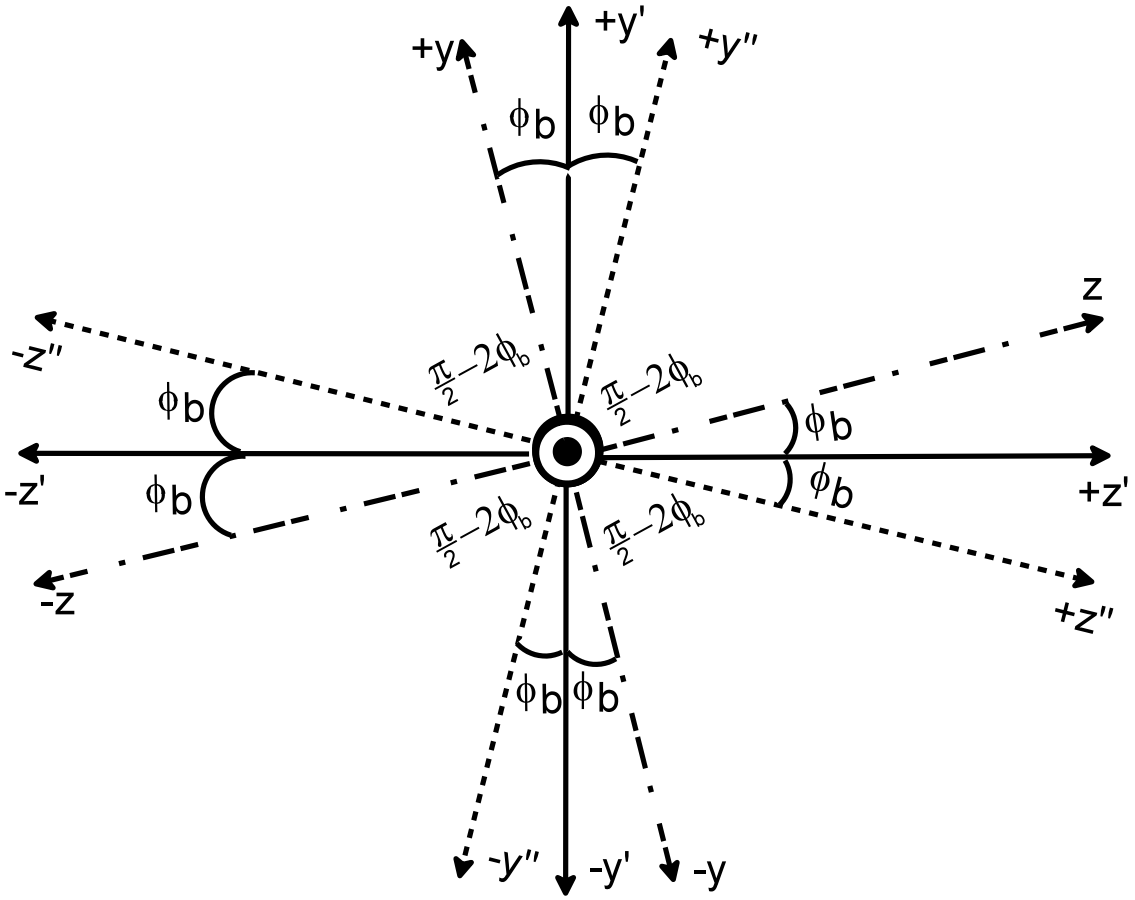

Figure 7.1-10: Coordinate system for the Zeroth Diffracted Order, i.e. (x, y, z), and minus one Diffracted Order, i.e. (x,y",z") superimposed onto the coordinate system for the AOC, i.e. (x,y',z').

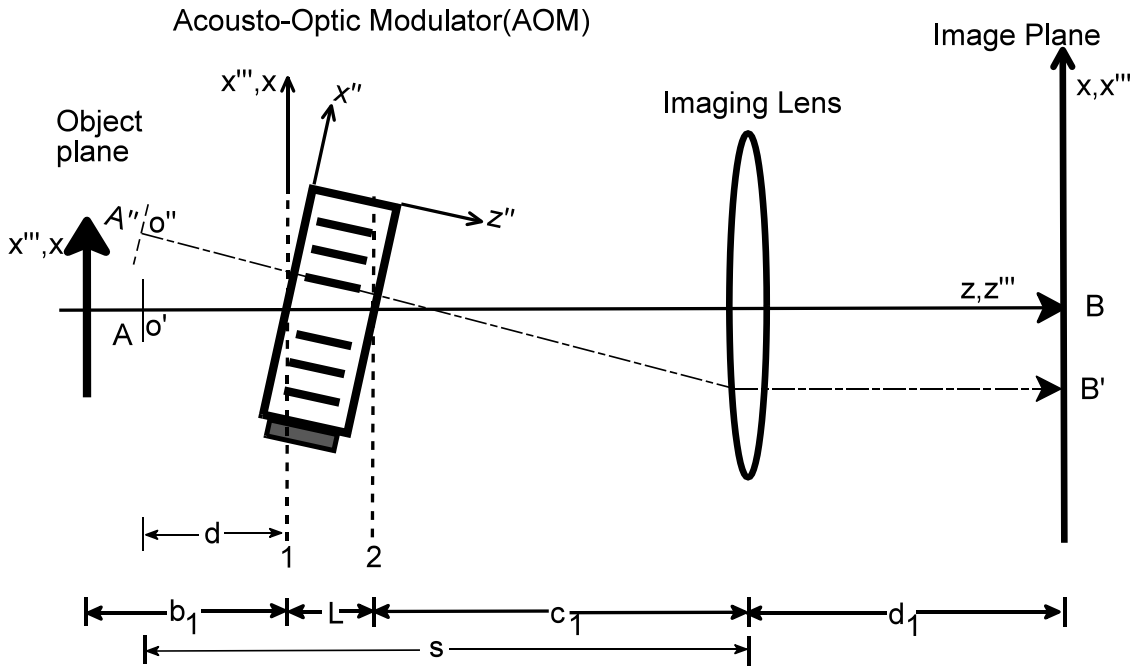

Figure 7.2 – 1 : Diffraction by Acousto-Optic Modulator and Image formation by imaging lens

Chapter 8.0 Detailed Analysis of Single Acousto-Optic Image Processing System

This chapter will present a detailed mathematical formalism for each of the proposed acousto-optic image processing systems. The analysis will model the effect of the systems on images as they propagate through the systems.

8.1 Realization of image processing using the zeroth diffracted order

Figure $8.1-1$ represents the experiment setup for image edge enhancement using the zeroth diffracted order. The object (a transparency), $i(x''', y)$, is placed on the input plane and the Acousto-Optic Modulator, AOM, is located between the object and an imaging lens. Note that the AOM has been rotated in the x-z plane counterclockwise by ϕ_{inc}. During the rotation of axes, we keep the x-z plane fixed. The distances from the object to the AOM, and from the AOM to the imaging lens are b_1 and c_1, respectively. The length of the AOM is denote by L. The distance between the image lens and the output plane (image plane) is d_1.

Assuming the light field distribution on input plane to be $i(x''', y)$ (amplitude distribution of the transparent picture), the light field distribution at plane 1 after propagating the distance b_1 is described as

$$\psi_1(x''', y; z = b_1) = i(x''', y) * h_v(x''', y; z = b_1), \qquad (8.1-1)$$

where $*$ denotes convolution operation and $h_v(x''', y; z = b_1) = \frac{k_v}{j2\pi b_1} e^{-j\frac{k_v}{2b_1}\left[(x''')^2 + y^2\right]}$ is the free-space impulse response function with k_v denoting the propagation constant in free space. So the spatial frequency spectrum distribution of $\psi_1(x'''; z = b_1)$ is

$$\begin{aligned} \Psi_1(k_{x'''}, k_y; z = b_1) &= \mathcal{F}\{\psi_1(x''', y; z = b_1)\} \\ &= \mathcal{F}\{i(x''', y) * h_v(x''', y; z = b_1)\} \\ &= I(k_{x'''}, k_y) H_v(k_{x'''}, k_y; z = b_1) \end{aligned} \qquad (8.1-2)$$

where $H_v(k_{x'''},k_y; z = b_1) = exp\left[\frac{j\left[(kx''')^2+ky^2\right]z}{2k_v}\right]$. Before applying the result in equation $8.1-2$ to the AOM, one must use a coordinate transformation so that Ψ_1 is in the same coordinate system as the AOM. Using the coordinate transformation in equation $7.1-1a$ with z'=0, equation $8.1-1$ becomes

$$\psi_1(x', y; z = b_1) = i(cos(\phi_{inc})x', y) * h_v(cos(\phi_{inc})x', y; z = b_1). \quad (8.1-3)$$

Therefore, the spatial frequency spectrum distribution of $\psi_1(x', y; z = b_1)$ is

$$\begin{aligned}\Psi_1(k_{x'}, k_y; z = b_1) &= \mathcal{F}\{\psi_1(x', y; z = b_1)\} = \mathcal{F}\{i(cos(\phi_{inc})x', y) \\ &\quad * h_v(cos(\phi_{inc})x', y; z = b_1)\} \\ &= \left[\frac{I\left(\frac{k_{x'}}{cos(\phi_{inc})}, k_y\right)}{|cos(\phi_{inc})|}\right] \\ &\quad \times \left[\frac{H_v\left(\frac{k_{x'}}{cos(\phi_{inc})}, k_y; z = b_1\right)}{|cos(\phi_{inc})|}\right]. \quad (8.1-2)\end{aligned}$$

Using a transfer function, equation $5.1.1-12$, to model the effect of the AOM on the incident light field. The light field distribution of the zeroth order on plane 2 can be written as

$$\begin{aligned}\psi_2^{(0)}(x', y) &= \mathcal{F}^{-1}\{\Psi_1(k_{x'}, k_y; z = b_1) \times H_0(k_{x'}, k_y; z = L)\} \quad (8.1-3) \\ &= i(cos(\phi_{inc})x', y) \\ &\quad * h_v(cos(\phi_{inc})x', y; z = b_1) * h_0(x', y; z = L),\end{aligned}$$

where $h_{(0)}(x', y; z = L) = \mathcal{F}^{-1}\{H_{(0)}(k_{x'}, k_x; z = L)\}$, is called the spatial impulse response function of the zeroth diffracted order of the AOM; the subscript (0) corresponds to the zeroth order light. As the light exits the AOM, it must be mapped to the coordinate system of the zeroth diffracted order. Therefore, the result in equation $8.1-3$ must be mapped to the coordinate system of the zeroth order. This can be done using the coordinate transformation in equation $7.1-2a$ with $z = 0$. Therefore equation

$8.1-3$ becomes

$$\begin{aligned}\psi_2^{(0)}(x,y) &= \mathcal{F}^{-1}\{\Psi_1(k_{x'},k_y;z=b_1)\cdot H_{(0)}(k_{x'},k_y;z=L)\} \\ &= i(cos(\phi_{inc})cos(\phi_{\mathrm{b}})x,y) \\ &*h_v(cos(\phi_{inc})cos(\phi_{\mathrm{b}})x,y;z=\ b_1) \\ &*h_{(0)}(cos(\phi_{\mathrm{b}})x,y;z=L).\end{aligned} \tag{8.1-4}$$

The spatial frequency spectrum distribution of $\psi_2^{(0)}(x,y)$ is

$$\begin{aligned}\Psi_2^{(0)}(k_x,k_y) &= \Psi_1(k_{x'},k_y;z=b_1)\times H_{(0)}(k_{x'},k_y;z=L) \\ &= \frac{I\left(\frac{k_x}{cos(\phi_{inc})cos(\phi_{\mathrm{b}})},k_y\right)}{|cos(\phi_{inc})cos(\phi_{\mathrm{b}})|} \\ &\times \frac{H_v\left(\frac{k_x}{cos(\phi_{inc})cos(\phi_{\mathrm{b}})},k_y;z=\ b_1\right)}{|cos(\phi_{inc})cos(\phi_{\mathrm{b}})|} \\ &\times \frac{H_{(0)}\left(\frac{k_x}{cos(\phi_{\mathrm{b}})},k_y;z=\ L\right)}{|cos(\phi_{\mathrm{b}})|}.\end{aligned} \tag{8.1-5}$$

The light field distribution at the input plane of the imaging lens is

$$\begin{aligned}\psi_2^{(0)}(x,y;z=\ c_1) &= \mathcal{F}^{-1}\left\{\Psi_2^{(0)}(k_x,k_y)H_v(k_x,k_y;z=\ c_1)\right\} \\ &= i(cos(\phi_{inc})cos(\phi_{\mathrm{b}})x,y) \\ &*h_v(cos(\phi_{inc})cos(\phi_{\mathrm{b}})x,y;z=\ b_1) \\ &*h_{(0)}(cos(\phi_{\mathrm{b}})x,y;z=L)*h_v(x,y;z=\ c_1),\end{aligned} \tag{8.1-6}$$

where as the light field distribution at the output plane of the imaging lens is

$$\begin{aligned}\psi_{\mathrm{im}}^{(0)}(x,y) &= \mathcal{F}^{-1}\left\{\Psi_2^{(0)}(k_x,k_y)H_v(k_x,k_y;z=\ c_1)\right\}e^{\left(j\frac{k_0}{2f'}[x^2+y^2]\right)} \\ &= \{i(cos(\phi_{inc})cos(\phi_{\mathrm{b}})x,y) \\ &*h_v(cos(\phi_{inc})cos(\phi_{\mathrm{b}})x,y;z=\ b_1) \\ &*h_{(0)}(cos(\phi_{\mathrm{b}})x,y;z=L)*h_v(x,y;z=\ c_1)\}e^{\left(j\frac{k_0}{2f'}[x^2+y^2]\right)}\end{aligned} \tag{8.1-7}$$

The term $e^{\left(j\frac{k_0}{2f'}[x^2+y^2]\right)}$ expresses the phase change when the light field passes through the imaging lens; where f' is the focal length of the imaging lens. Finally, the light field

distribution at the output plane is given by the following formalism

$$\psi^{(0)}_{\text{output plane 1}}(x,y) = \mathcal{F}^{-1}\Big\{\Psi^{(0)}_2(k_x,k_y)H_v(k_x,k_y;z=\ c_1)\Big\} \qquad (8.1-8)$$
$$e^{\left(j\frac{k_0}{2f'}\left[x^2+y^2\right]\right)} * \mathcal{F}^{-1}\{H_v(k_x,k_y;z=\ d_1)\}$$
$$= \Big\{\{i(cos(\phi_{inc})cos(\phi_{\text{b}})x,y)$$
$$* h_v(cos(\phi_{inc})cos(\phi_{\text{b}})x,y;z=\ b_1)$$
$$* h_{(0)}(cos(\phi_{\text{b}})x,y;z=L) * h_v(x,y;z=\ c_1)\}$$
$$exp\left(j\frac{k_0}{2f'}\left[x^2+y^2\right]\right)\Big\} * h_v(x,y;z=\ d_1).$$

The spatial frequency spectrum distribution of $\psi^{(0)}_{\text{output plane 1}}(x,y)$ is

$$\Psi^{(0)}_{\text{output plane 1}}(k_x,k_y) = \Big\{\Big\{\Psi^{(0)}_2(k_x,k_y)H_v(k_x,k_y;z=\ c_1)\Big\} \qquad (8.1-9)$$
$$* \frac{2jf'\pi}{k_o} e^{\left(j\frac{k_o}{2f'}\left[x^2+y^2\right]\right)}\Big\} H_v(k_x,k_y;z=\ d_1)$$
$$= \Big\{\{\frac{I\left(\frac{k_x}{cos(\phi_{inc})cos(\phi_{\text{b}})},k_y\right)}{|cos(\phi_{inc})cos(\phi_{\text{b}})|}$$
$$\times \frac{H_v\left(\frac{k_x}{cos(\phi_{inc})cos(\phi_{\text{b}})},k_y;z=\ b_1\right)}{|cos(\phi_{inc})cos(\phi_{\text{b}})|}$$
$$\times \frac{H_{(0)}\left(\frac{k_x}{cos(\phi_{\text{b}})},k_y;z=\ L\right)}{|cos(\phi_{\text{b}})|} H_v(k_x,k_y;z=\ c_1)\}$$
$$* \frac{2jf'\pi}{k_o} exp\left(j\frac{k_0}{2f'}\left[k_x^2+k_y^2\right]\right)\Big\} H_v(k_x,k_y;z=\ d_1).$$

8.2 Realization of image processing using the minus one diffracted order

Figure $8.2-1$ represents the experimental setup for high frequency noise reduction using the minus one diffracted order. The object (a transparency), $i(x''',y)$, is placed on the input plane and the acousto-optic Modulator, AOM, is located between the object and an imaging lens. Note that the AOM has been rotated in the x-z plane counterclockwise by ϕ_{inc}. During the rotation of axes, we keep the x-z plane fixed. The distances from the object to the AOM, and from the AOM to the imaging lens are b_1 and c_1, respectively.

The length of the AOM is denote by L. The distance between the image lens and the output plane (image plane) is d_1.

Assuming the light field distribution on input plane to be $i(x''', y)$ (amplitude distribution of the transparent picture), the light field distribution at plane 1 after propagating the distance b_1 is described as

$$\psi_1(x''', y; z = b_1) = i(x''', y) * h_v(x''', y; z = b_1), \qquad (8.2-1)$$

where $*$ denotes convolution operation and $h_v(x''', y; z = b_1) = \frac{k_v}{j2\pi b_1} e^{-j\frac{k_v}{2b_1}\left[(x''')^2 + y^2\right]}$ is the free-space impulse response function with k_v denoting the propagation constant in free space. So the spatial frequency spectrum distribution of $\psi_1(x''', z = b_1)$ is

$$\begin{aligned} \Psi_1(k_{x'''}, k_y; z = b_1) &= \mathcal{F}\{\psi_1(x''', y; z = b_1)\} \\ &= \mathcal{F}\{i(x''', y) * h_v(x''', y; z = b_1)\} \\ &= I(k_{x'''}, k_y) H_v(k_{x'''}, k_y; z = b_1), \end{aligned} \qquad (8.2-2)$$

where $H_v(k_{x'''}, k_y; z = b_1) = exp\left[\frac{j\left[(kx''')^2 + ky^2\right]z}{2k_v}\right]$. Before applying the result in equation 8.2-2 to the AOM, one must use a coordinate transformation, so that Ψ_1 is in the same coordinate system as the AOM. Using the coordinate transformation in equation $7.1-1a$ with z'=0, equation $8.2-1$ becomes

$$\begin{aligned} \psi_1(x', y; z = b_1) &= i(cos(\phi_{inc})x', y) \\ &\quad * h_v(cos(\phi_{inc})x', y; z = b_1). \end{aligned} \qquad (8.2-3)$$

So the spatial frequency spectrum distribution of $\psi_1(x', y; z = b_1)$ is

$$\begin{aligned} \Psi_1(k_{x'}, k_y; z = b_1) &= \mathcal{F}\{\psi_1(x', y; z = b_1)\} \\ &= \mathcal{F}\{i(cos(\phi_{inc})x', y) \\ &\quad * h_v(cos(\phi_{inc})x', y; z = b_1)\} \\ &= \left[\frac{I\left(\frac{k_{x'}}{cos(\phi_{inc})}, k_y\right)}{|cos(\phi_{inc})|}\right] \\ &\quad \times \left[\frac{H_v\left(\frac{k_{x'}}{cos(\phi_{inc})}, k_y; z = b_1\right)}{|cos(\phi_{inc})|}\right]. \end{aligned} \qquad (8.2-4)$$

Using a transfer function, equation $5.2.1-11$, to model the AOM, the light field distribution of the minus one order at plane 2 is written as

$$\begin{aligned}\psi_2^{(1)}(x',y) &= \mathcal{F}^{-1}\{\Psi_1(k_{x'},k_y;z=b_1)\times H_{(-1)}(k_{x'},k_y;z=L)\} \\ &= i(cos(\phi_{inc})x',y) \\ &*h_v(cos(\phi_{inc})x',y;z=b_1)*h_{(-1)}(x',y;z=L),\end{aligned} \tag{8.2-5}$$

where $h_{(-1)}(x',y;z=L)=\mathcal{F}^{-1}\{H_{(-1)}(k_{x'},k_x;z=L)\}$, is called the spatial impulse response function of the AOM; the subscript (-1) corresponds to the minus one order diffracted light. The result in equation $8.2-5$ must be mapped to the coordinate system of the zeroth order. This can be done using the coordinate transformation in equation $7.1-2a$ with $z=0$. Therefore equation $8.2-5$ becomes

$$\begin{aligned}\psi_2^{(-1)}(x,y) &= \mathcal{F}^{-1}\{\Psi_1(k_{x'},k_y;z=b_1)\times H_{(-1)}(k_{x'},k_y;z=L)\} \\ &= i(cos(\phi_{inc})cos(\phi_b)x,y) \\ &*h_v(cos(\phi_{inc})cos(\phi_b)x,y;z=b_1) \\ &*h_{(-1)}(cos(\phi_b)x,y;z=L).\end{aligned} \tag{8.2-6}$$

The spatial frequency spectrum distribution of $\psi_2^{(-1)}(x,y)$ is

$$\begin{aligned}\Psi_2^{(-1)}(k_x,k_y) &= \Psi_1(k_{x'},k_y;z=b_1)\times H_{(-1)}(k_{x'},k_y;z=L) \\ &= \frac{I\left(\frac{k_x}{cos(\phi_{inc})cos(\phi_b)},k_y\right)}{|cos(\phi_{inc})cos(\phi_b)|} \\ &\times \frac{H_v\left(\frac{k_x}{cos(\phi_{inc})cos(\phi_b)},k_y;z=b_1\right)}{|cos(\phi_{inc})cos(\phi_b)|} \\ &\times \frac{H_{(-1)}\left(\frac{k_x}{cos(\phi_b)},k_y;z=L\right)}{|cos(\phi_b)|}.\end{aligned} \tag{8.2-7}$$

The light field distribution at the input plane of the imaging lens is

$$\begin{aligned}\psi_2^{(-1)}(x,y;z=c_1) &= \mathcal{F}^{-1}\left\{\Psi_2^{(-1)}(k_x,k_y)H_v(k_x,k_y;z=c_1)\right\} \\ &= i(cos(\phi_{inc})cos(\phi_b)x,y) \\ &*h_v(cos(\phi_{inc})cos(\phi_b)x,y;z=b_1) \\ &*h_{(-1)}(cos(\phi_b)x,y;z=L)*h_v(x,y;z=c_1),\end{aligned} \tag{8.2-8}$$

Where as the light field distribution at the output plane of the imaging lens is

$$\begin{aligned}\psi_{\text{im}}^{(-1)}(x,y) &= \mathcal{F}^{-1}\Big\{\Psi_2^{(-1)}(k_x,k_y)H_v(k_x,k_y;z=\ c_1)\Big\}e^{\left(j\frac{k_0}{2f'}\left[x^2+y^2\right]\right)} \\ &= \{i(cos(\phi_{inc})cos(\phi_{\text{b}})x,y) \\ &*h_v(cos(\phi_{inc})cos(\phi_{\text{b}})x,y;z=\ b_1) \\ &*h_{(-1)}(cos(\phi_{\text{b}})x,y;z=L)*h_v(x,y;z=\ c_1)\}e^{\left(j\frac{k_0}{2f'}\left[x^2+y^2\right]\right)}.\end{aligned} \tag{8.2-9}$$

The term $e^{\left(j\frac{k_0}{2f'}\left[x^2+y^2\right]\right)}$ expresses the phase change when the light field passes through the imaging lens; where f' is the focal length of the imaging lens. Finally, the light field distribution at the output plane is given by the following formalism

$$\begin{aligned}\psi_{\text{output plane 1}}^{(-1)}(x,y) &= \mathcal{F}^{-1}\Big\{\Psi_2^{(-1)}(k_x,k_y)H_v(k_x,k_y;z=\ c_1)\Big\} \\ & e^{\left(j\frac{k_0}{2f'}\left[x^2+y^2\right]\right)}*\mathcal{F}^{-1}\{H_v(k_x,k_y;z=\ d_1)\} \\ & = \Big\{\{i(cos(\phi_{inc})cos(\phi_{\text{b}})x,y) \\ & *h_v(cos(\phi_{inc})cos(\phi_{\text{b}})x,y;z=\ b_1) \\ & *h_{(-1)}(cos(\phi_{\text{b}})x,y;z=L)*h_v(x,y;z=\ c_1)\} \\ & exp\left(j\frac{k_0}{2f'}\left[x^2+y^2\right]\right)\Big\}*h_v(x,y;z=\ d_1).\end{aligned} \tag{8.2-10}$$

The spatial frequency spectrum distribution of $\psi_{\text{output plane 1}}^{(-1)}(x,y)$ is

$$\begin{aligned}\Psi_{\text{output plane 1}}^{(-1)}(k_x,k_y) &= \Big\{\Big\{\Psi_2^{(-1)}(k_x,k_y)H_v(k_x,k_y;z=\ c_1)\Big\} \\ & *\frac{2jf'\pi}{k_o}e^{\left(j\frac{k_0}{2f'}\left[x^2+y^2\right]\right)}\Big\}H_v(k_x,k_y;z=\ d_1) \\ & = \Big\{\{\frac{I\left(\frac{k_x}{cos(\phi_{inc})cos(\phi_{\text{b}})},k_y\right)}{|cos(\phi_{inc})cos(\phi_{\text{b}})|} \\ & \times \frac{H_v\left(\frac{k_x}{cos(\phi_{inc})cos(\phi_{\text{b}})},k_y;z=\ b_1\right)}{|cos(\phi_{inc})cos(\phi_{\text{b}})|} \\ & \times \frac{H_{(-1)}\left(\frac{k_x}{cos(\phi_{\text{b}})},k_y;z=\ L\right)}{|cos(\phi_{\text{b}})|}H_v(k_x,k_y;z=\ c_1)\} \\ & *\frac{2jf'\pi}{k_o}exp\left(j\frac{k_0}{2f'}\left[k_x^2+k_y^2\right]\right)\Big\}H_v(k_x,k_y;z=\ d_1).\end{aligned} \tag{8.2-11}$$

8.3 Results from Single Acousto-Optic Image Processing System

Our first experimental results are from a single cell acousto-optic image processing system shown in figure $8.2-1$. This experimental setup will use an AOM with a RF center frequency of $80 MHz$ connected to an InterAction Corp. PA-4 amplifier. The distances in figure 8.2-1 are set to the following values: b_1=$9.1 cm$, $L = 6$ cm, $c_1 = 3.5\, cm$. Now using the lens formula, equation $8.4-2$, we can determine d_1. The focal length of the imaging lens used in this particular experimental setup is equal to $15.5\, cm$, therefore d_1 is approximately equal to $93\, cm$. The value of the peak phase delay, α, was measured to be equal to 0.472π, see table 6.1-5.

The first image that is processed using the above mention system is a rectangle. Figure $8.3-1$ shows the result of high pass filtering of the rectangular image. The result shown in figure $8.3-1$a was obtained when the laser beam is position approximately $1 mm$ from the piezoelectric transducers that create the ultrasonic wave in the AOM. Taking a moment to look at figure $8.3-2$a, the piezoelectric transducer are contained in the four black rectangular squares at the rear of the acousto-optic modulator. Figure $8.3-1$b is again a rectangular image that has under gone the high pass filtering operation, but the position of the laser beam from the transducers in this case is 11 mm. Lastly, figure $8.3-1$c is again the result of high pass filtering of the same rectangular image, but the laser beam is position approximately 21 mm from the transducers. The ability to obtained the similar image processing results, although the laser be is positioned at different distances from the transducers, indicates that the diffraction of the sound beam envelope, using this particular case, does not have an adverse impact on the image processing abilities of the AOM when using one with an RF center frequency of 80 MHz. Previous research has assumed that as the position of the laser beam moves further and further from the AOM transducers that the diffraction of the sound wave would have an detrimental effect on the ability of the AOM to perform image processing.

Another interesting result is, the images in figure $8.3-1$a,b,c were measured at approximately 10 mm apart which is a whole multiple of the wavelength of sound. In fact, these processed images were spaced at approximately 202Λ, where Λ is the wavelength of the ultrasonic sound wave.

Figure $8.3-3$a shows the original image of a finger print, while figure $8.3-3$b shows the high pass filtered result. In figure $8.3-3$b, most of the low frequency noise, which in this image are the smudges, has been removed and the finger print ridges are clearly enhanced. Real-time processing of images like these would be useful to law-in-forcement officials. Also, banks which now require a person who is not a customer to give thumb prints when cashing bank checks could find some usefulness with a system similar to the ones presented in this thesis.

The above mentioned processed images were obtained using the zeroth diffracted order of the acousto-optic modulator. The following results were obtained using the minus one order of the AOM. Figure $8.3-4$a shows the original image of another finger print and figure $8.3-4$b shows the result of image processing using the minus one order. Recall that the minus one order acts as a low pass filter on the incident image for the range of Q and α under consideration here. Therefore, all the ridges that are visible in figure $8.3-4$a have been smudge over in figure $8.3-4$b.

All the processed images discussed in the previous paragraphs were obtained using a optical image processing system that contained a single AOM with a RF center frequency of $80\,MHz$. The results that are discussed in the following paragraphs were obtained using an AOM with a RF center frequency of $40MHz$.

Figure $8.3-5$a shows the original image of a 17 that we will process using an optical system that will contain a single acousto-optic modulator. Figure $8.3-5$b shows both the high pass and low pass result of the image processing operation. The image on the left of figure $8.3-5$b contains the edges of the 17, while the image on the left is a blurry image of the seventeen which indicates that it has undergone a low pass filter operation. Figure

$8.3-6$a is the original image of another finger print. Figure $8.3-6$b is the low pass filtering result using the minus one diffracted order of the acousto-optic modulator. Figure $8.3-6$c, shows the image that is contained in the zeroth order which has been edge enhanced. Again the images presented in figure $8.3-6$ were obtain using a AOM with a center frequency of $40MHz$.

Figure $8.3-7$a is the original image of an amplitude grating. Figure $8.3-7$b are the results of processing using a single cell acousto-optic image processing system. The image on the left is the zeroth order processed image, while the image on the right is the minus one order image. You can see that in the minus one order the fringes had been completely removed due to the low pass filtering nature of the minus one diffracted order. Figure $8.3-8$a is the original image of a 17. Figure is $8.3-8$b is the processed image of the 17 using the zeroth order of a single cell acousto-optic system like in figure $8.2-1$. Looking at the processed image, one can see that edge detection was achieved. This result compares well with the experimental image processing result discussed in section 9.1.1. Another analytical result shown in figure $8.3-9$, uses the minus one order to process a "constructed" amplitude grating. Figure $8.3-9$a is the original image. Figure $8.3-9$b is the low pass filter result. If the black bands, in figure $8.3-9$a, represent high frequency noise then figure $8.3-9$b the noise is removed.

Comparing figure $8.3-1$ to figure $6.3-1$c, it appears that the edge enhancement in figure $6.3-1c$ is more pronounced than in figure $8.3-1$. In an effort to clarify this situation, let us use the acousto-optic transfer functions derived in chapter five. The value of Q and α used in the experiment to obtained the result in figure 6.3-1 was 28 and 0.65π, respectively. The value of Q and α used in the experiment to obtained the results in figure $8.3-1$ was 58 and 0.472π respectively. The image processing results in figure $8.3-1$ we obtained using an AOM with an RF center frequency of $80MHz$. The results in figure 6.3-1 were obtained using an AOM with an RF center frequency of 40 MHz.

A plot of the zero order of acousto-optic transfer function that corresponds to the Q and α for the results in figure 6.3-1 is shown in figure 6.3-3. Figure $8.3-1$, shows the zeroth order acousto-optic transfer function for the Q and α that corresponds to figure $8.3-1$. The above mentioned graphs of the acousto-optic transfer function confirm the experimental data in figures 6.3-1c and $8.3-1$. The graph in figure 6.3.-3b has a sharper transition region, from the pass band to stop band, than the graph in figure $8.3-1$. A sharper transition region means that the edges from the high pass filtering operation will be thinner. So, this is why edges in figure 6.3-1c is thinner than those in figure $8.3-1$.

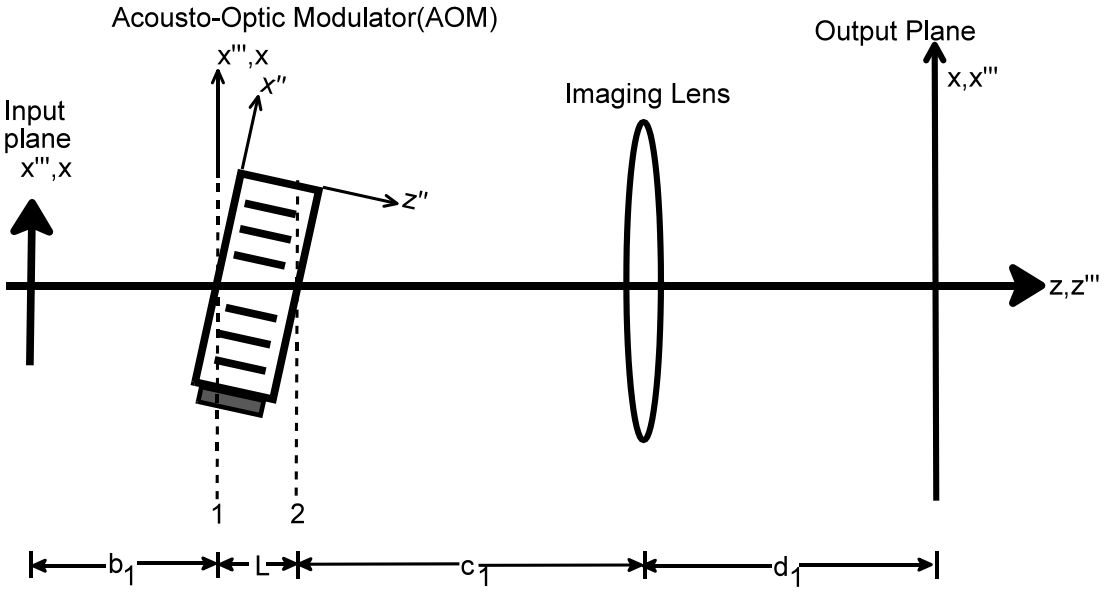

Figure 8.1-1: Light path used in image processing experiment

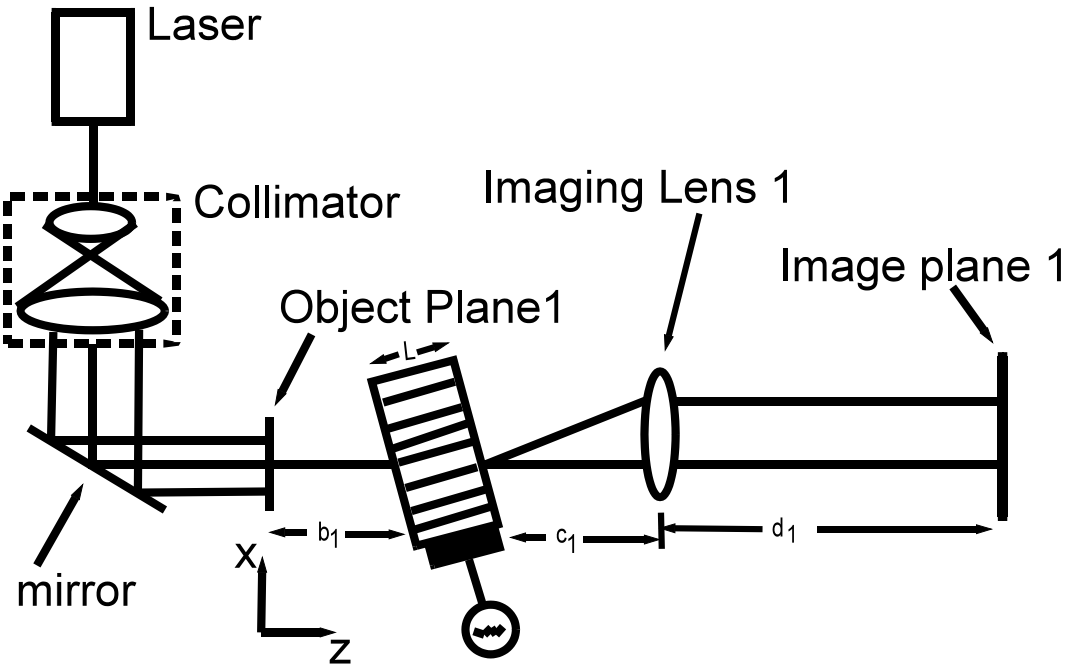

Figure 8.2 – 1 : Single Cell Acousto-Optic Image Processing System

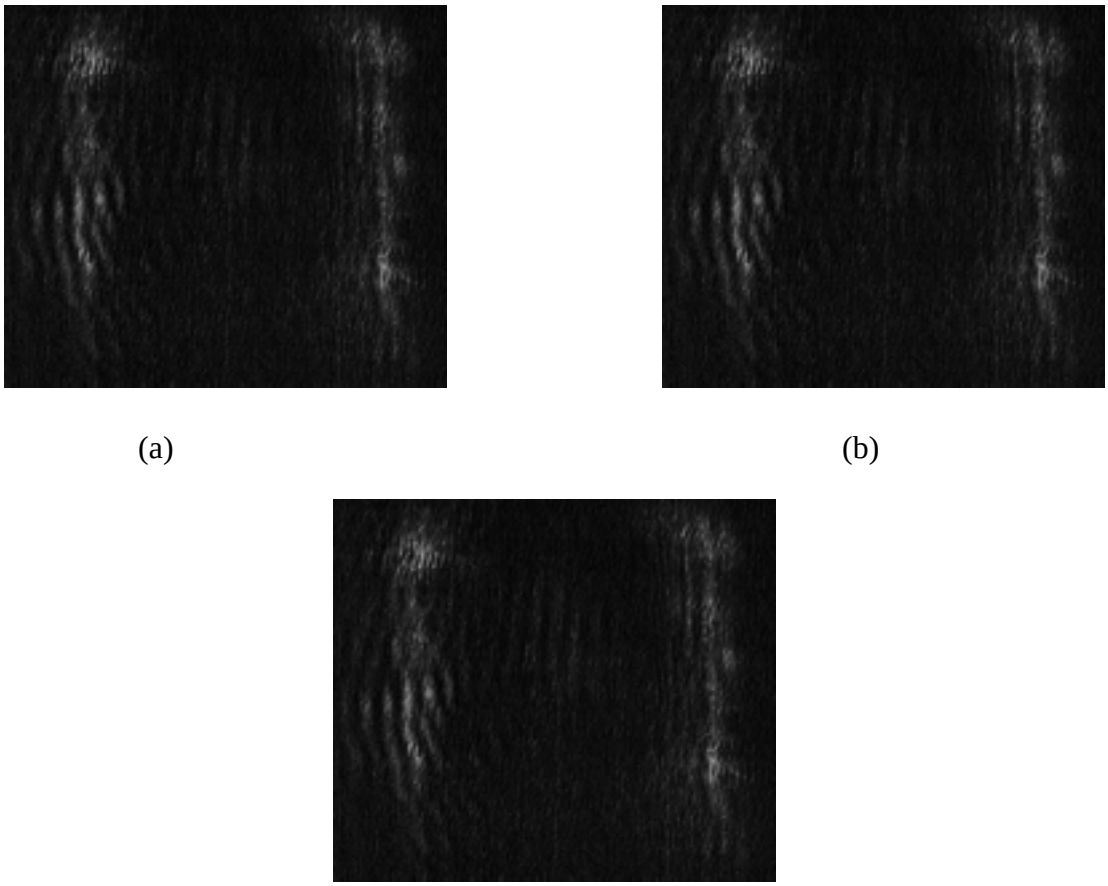

(a) (b)

(c)

Figure 8.3-1: Photos of the result of AOM image processing system using an AOM with an RF center frequency equal to 80MHz: (a) image 1mm from transducers, (b) image 11 mm from transducers, (c) image 21 mm from transducers

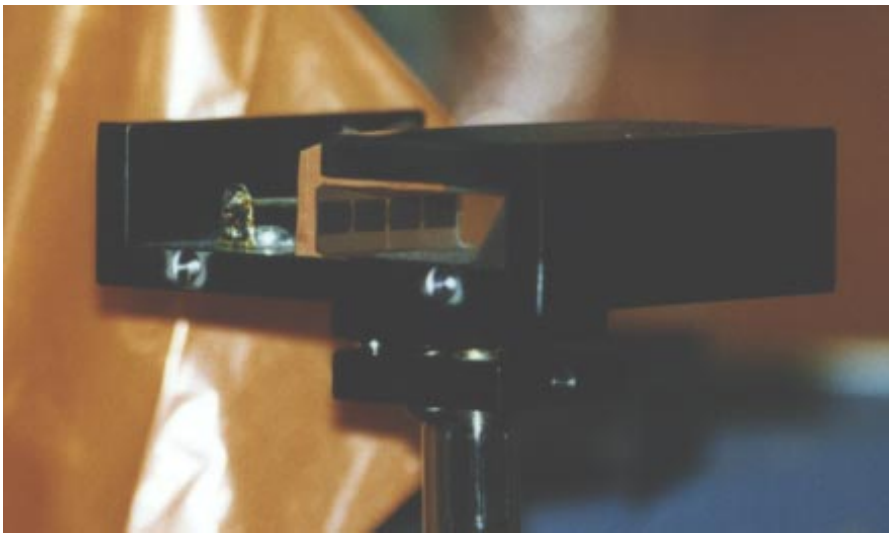

(a)

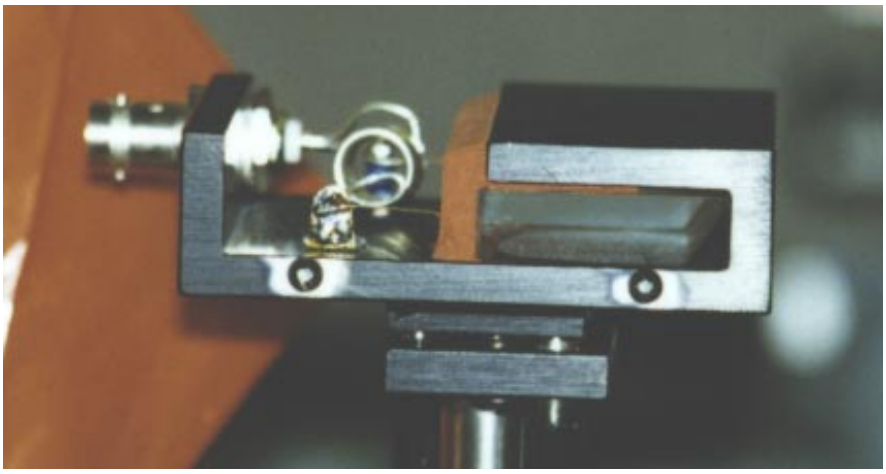

(b)

Figure 8.3-2: Color photos of an Acousto-Optic Modulator

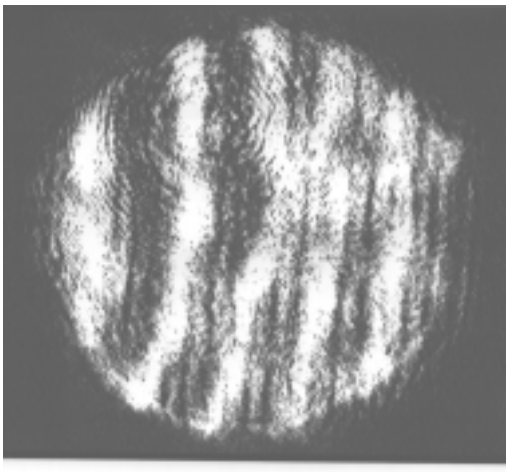

(a)

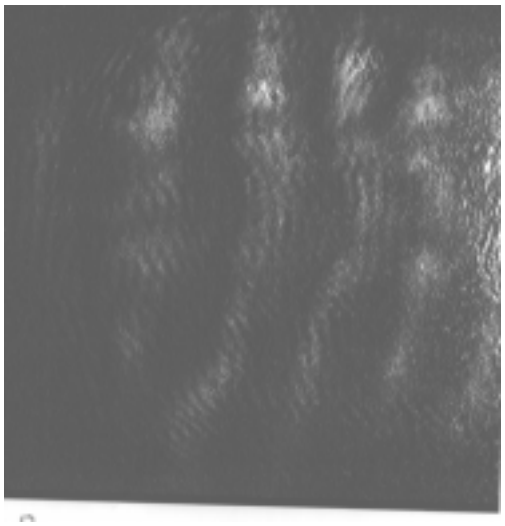

(b)

Figure $8.3-3$: Photos of the result of AOM image processing system using an AOM with an RF center frequency equal to $80 MHz$: (a) original image, (b) high pass filtered image

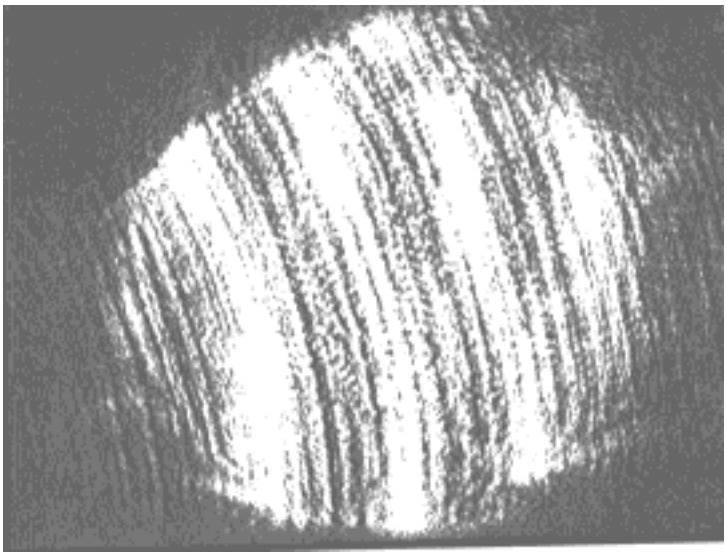

(a)

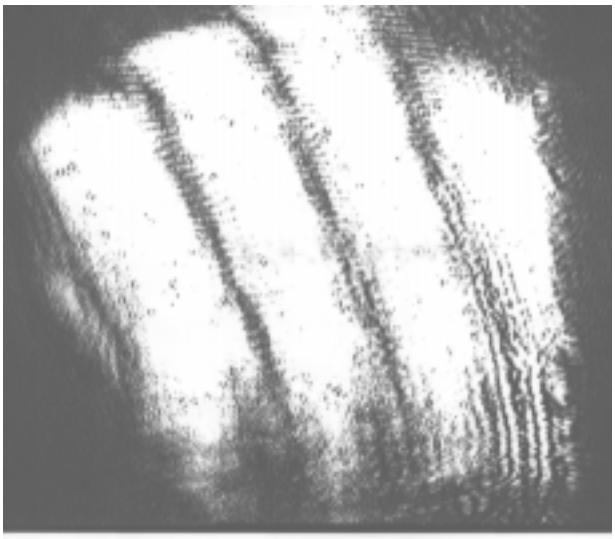

(b)

Figure $8.3-4$: Photos of an image of a finger print using an AOM with an RF center frequency equal to $80MHz$ (a) original image, (b) low pass filtered image

(a)

(b)

Figure $8.3-5$: Photos of an image of a 17 using an AOM with an RF center frequency equal to $40MHz$, (a) original image, (b) high pass filtered image($left$) and low pass filtered image($right$)

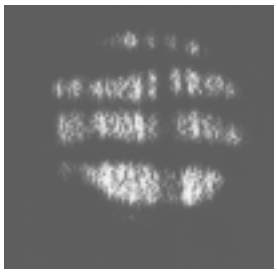

(a)

(b)

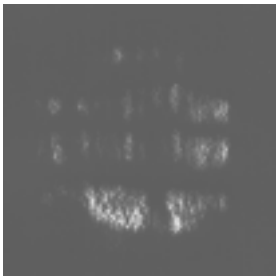

(c)

Figure $8.3-6$: Photos of an images of a finger print using an AOM with an RF center frequency equal to $40MHz$ (a) original image, (b) low pass filtered image, (c) high pass filtered image

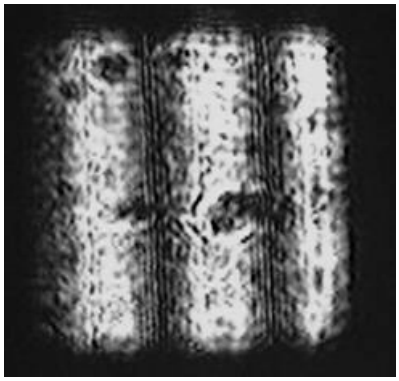

(a)

(b)

Figure $8.3-7$: Photos of an image of amplitude grating using an AOM with an RF center frequency equal to $40MHz$ (a) original image, (b) low pass filtered image($left$) and high pass filtered image($right$)

(a)

(b)

Figure $8.3-8$: Results of a computer simulation using an AOM with RF center frequency equal to $40MHz$ (a) original image, (b) high pass processing of image through Bragg diffraction (the zeroth order).

(a)

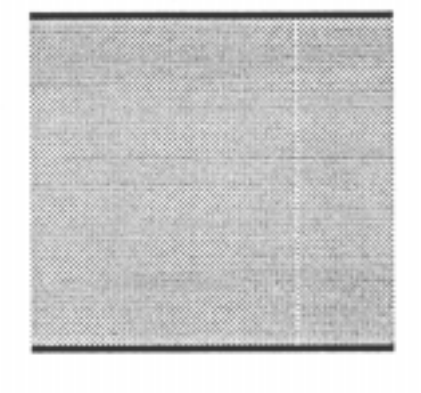

(b)

Figure $8.3-9$: Results of a computer simulation using an AOM with RF center frequency equal to $40 MHz$ (a) original image, (b) low pass processing of image through Bragg diffraction (the minus one order).

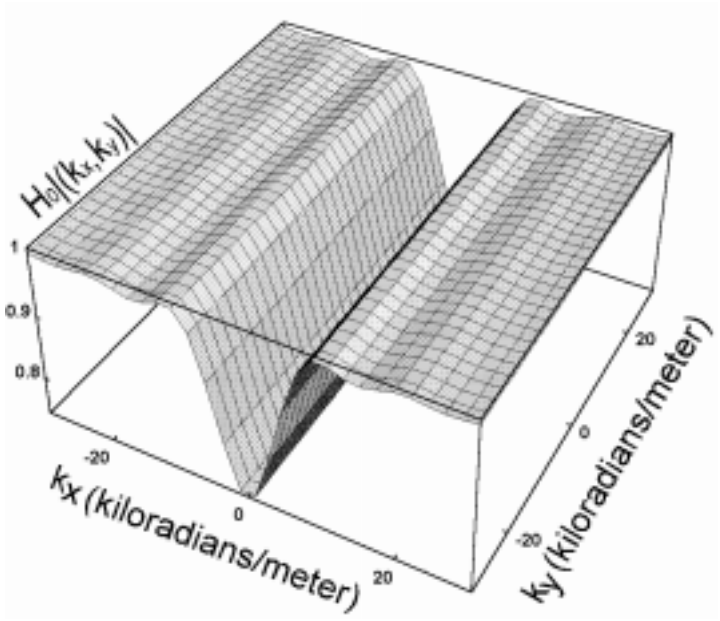

(a)

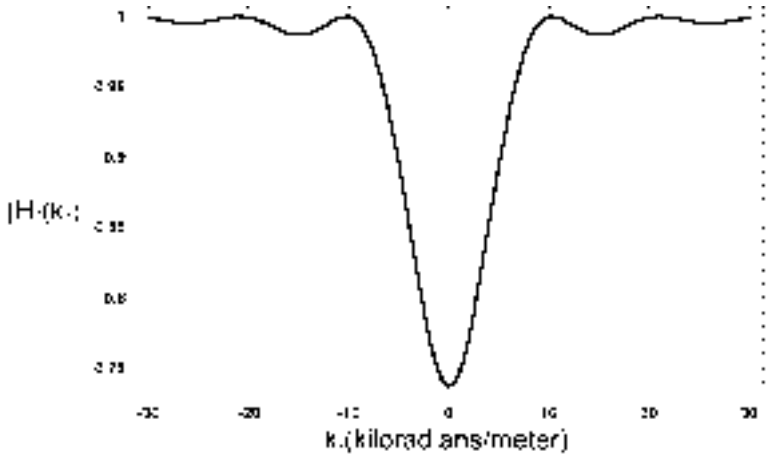

(b)

Figure $8.3-10$: Graph of the Acousto-Optic transfer function for the zeroth order (a) three dimensional (b) two dimensional when Q=58, $\alpha = 0.472\pi$ and $L = 60mm$

Chapter 9.0 Detailed Analysis of Series Acousto-Optic Cells Image Processing System

9.1 Realization of zeroth order image processing

Figure $9.1-1$ represents the experiment setup for image edge enhancement using the zeroth diffracted order from two acousto-optic cells placed in series. The part of the image processing system from object plane 1 to image plane 1 has already been analyzed in section 8.1. Therefore the only thing that is left to be done is to analyze the system from object plane 2 through image plane 2. This can be done by first assuming that image located at image plane 1 is the same as at object plane 2. So the result in equation $8.1-9$ will be the image , $\psi^{(0)}_{\text{input plane 2}}(x''', y)$, at input plane 2. The acousto-optic Modulator, AOM, is located between the object and an imaging lens. As stated earlier, the AOM has been rotated in the x-z plane counter clockwise by ϕ_{inc}. During the rotation of axes, we keep the x-z plane fixed. The distances from the object to the AOM, and from the AOM to the imaging lens are b_2 and c_2, respectively. The length of the AOM is denote by L. The distance between the imaging lens and the output plane (image plane) is d_2.

Assuming the light field distribution on input plane 2 to be $\psi^{(0)}_{\text{input plane 2}}(x''', y)$ (amplitude distribution of the transparent picture), the light field distribution as the image enters the AOM after propagating the distance b_2 is described as

$$\psi_1^2(x''', y; z = b_2) = \psi^{(0)}_{\text{input plane 2}}(x''', y) * h_v(x''', y; z = b_2), \qquad (9.1-1)$$

where $*$ denotes convolution operation and $h_v(x''',y;z=b_2) = \frac{k_v}{j2\pi b_2} e^{-j\frac{k_v}{2b_1}\left[(x''')^2+y^2\right]}$ is the free-space impulse response function with k_v denoting the propagation constant in free

space. So the spatial frequency spectrum distribution of $\psi_1^2(x''', y; z = b_2)$ is

$$\begin{aligned}\Psi_1^2(k_{x'''}, k_y; z = b_2) &= \mathcal{F}\{\psi_1^2(x''', y; z = b_2)\} \\ &= \mathcal{F}\{\psi^{(0)}_{\text{input plane 2}}(x''', y) * h_v(x''', y; z = b_2)\} \\ &= \Psi^{(0)}_{\text{input plane 2}}(k_{x'''}, k_y) H_v(k_{x'''}, k_y; z = b_2),\end{aligned} \tag{9.1 - 2}$$

where $H_v(k_{x'''}, k_y; z = b_1) = exp\left[\frac{j\left[(kx''')^2 + ky^2\right]z}{2k_v}\right]$. Before applying the result in equation $9.1 - 2$ to the AOM, one must use a coordinate transformation, so that Ψ_1^2 is in the same coordinate system as the AOM. Using the coordinate transformation in equation $7.1 - 1a$ with z'=0, equation $9.1 - 1$ becomes

$$\begin{aligned}\psi_1^2(x', y; z = b_2) = \psi^{(0)}_{\text{input plane 2}}&(cos(\phi_{inc})x', y) \\ &* h_v(cos(\phi_{inc})x', y; z = b_2).\end{aligned} \tag{9.1 - 3}$$

So the spatial frequency spectrum distribution of $\psi_1^2(x', y; z = b_2)$ is

$$\begin{aligned}\Psi_1^2(k_{x'}, k_y; z = b_2) &= \mathcal{F}\{\psi_1^2(x', y; z = b_2)\} \\ &= \mathcal{F}\{\psi^{(0)}_{\text{input plane 2}}(cos(\phi_{inc})x', y) \\ &* h_v(cos(\phi_{inc})x', y; z = b_2)\} \\ &= \left[\frac{\Psi^{(0)}_{\text{input plane 2}}\left(\frac{k_{x'}}{cos(\phi_{inc})}, k_y\right)}{|cos(\phi_{inc})|}\right] \\ &\times \left[\frac{H_v\left(\frac{k_{x'}}{cos(\phi_{inc})}, k_y; z = b_2\right)}{|cos(\phi_{inc})|}\right].\end{aligned} \tag{9.1 - 4}$$

Using a transfer function, equation $(5.1.1 - 12)$, to model the AOM, the light field distribution of the zeroth order as the light field exits the AOM is written as

$$\begin{aligned}\psi_2^{2(0)}(x', y) &= \mathcal{F}^{-1}\left\{\Psi_1^2(k_{x'}, k_y; z = b_2) \times H_0(k_{x'}, k_y; z = L)\right\} \\ &= \psi^{(0)}_{\text{input plane 2}}(cos(\phi_{inc})x', y) \\ &* h_v(cos(\phi_{inc})x', y; z = b_2) * h_0(x', y; z = L),\end{aligned} \tag{9.1 - 5}$$

where $h_0(x', y; z = L) = \mathcal{F}^{-1}\{H_0(k_{x'}, k_x; z = L)\}$, is called the spatial impulse response function of the AOM; the superscript or subscript (0) corresponds to the zeroth order

diffracted light. Next, the result in equation $9.1-5$ must be mapped to the coordinate system of the zeroth order. This can be done using the coordinate transformation in equation $7.1-2a$ with $z=0$. Therefore equation $9.1-5$ becomes

$$\begin{aligned}\psi_2^{2(0)}(x,y) &= \mathcal{F}^{-1}\{\Psi_1^2(k_{x'},k_y;z=b_2)\cdot H_{(0)}(k_{x'},k_y;z=L)\} \\ &= \psi^{(0)}_{\text{input plane 2}}(cos(\phi_{inc})cos(\phi_{\text{b}})x,y) \\ &*h_v(cos(\phi_{inc})cos(\phi_{\text{b}})x,y;z=\ b_2) \\ &*h_{(0)}(cos(\phi_{\text{b}})x,y;z=L).\end{aligned} \tag{9.1-6}$$

The spatial frequency spectrum distribution of $\psi_2^{2(0)}(x,y)$ is

$$\begin{aligned}\Psi_2^{2(0)}(k_x,k_y) &= \Psi_1^2(k_{x'},k_y;z=b_2)\times H_{(0)}(k_{x'},k_y;z=L) \\ &= \frac{\Psi^{(0)}_{\text{input plane 2}}\left(\frac{k_x}{cos(\phi_{inc})cos(\phi_{\text{b}})},k_y\right)}{|cos(\phi_{inc})cos(\phi_{\text{b}})|} \\ &\times \frac{H_v\left(\frac{k_x}{cos(\phi_{inc})cos(\phi_{\text{b}})},k_y;z=\ b_2\right)}{|cos(\phi_{inc})cos(\phi_{\text{b}})|} \\ &\times \frac{H_{(0)}\left(\frac{k_x}{cos(\phi_{\text{b}})},k_y;z=\ L\right)}{|cos(\phi_{\text{b}})|}.\end{aligned} \tag{9.1-7}$$

The light field distribution at the input plane of the imaging lens is

$$\begin{aligned}\psi_2^{(0)}(x,y;z=\ c_1) &= \mathcal{F}^{-1}\left\{\Psi_2^{2(0)}(k_x,k_y)H_v(k_x,k_y;z=\ c_2)\right\} \\ &= \psi^{(0)}_{\text{input plane 2}}(cos(\phi_{inc})cos(\phi_{\text{b}})x,y) \\ &*h_v(cos(\phi_{inc})cos(\phi_{\text{b}})x,y;z=\ b_2) \\ &*h_{(0)}(cos(\phi_{\text{b}})x,y;z=L)*h_v(x,y;z=\ c_2),\end{aligned} \tag{9.1-8}$$

where as the light field distribution at the output plane of the imaging lens is

$$\begin{aligned}\psi^{(0)}_{\text{im}}(x,y) &= \mathcal{F}^{-1}\left\{\Psi_2^{2(0)}(k_x,k_y)H_v(k_x,k_y;z=\ c_2)\right\}e^{\left(j\frac{k_0}{2f'}[x^2+y^2]\right)} \\ &= \{\psi^{(0)}_{\text{input plane 2}}(cos(\phi_{inc})cos(\phi_{\text{b}})x,y) \\ &*h_v(cos(\phi_{inc})cos(\phi_{\text{b}})x,y;z=\ b_2) \\ &*h_{(0)}(cos(\phi_{\text{b}})x,y;z=L) \\ &*h_v(x,y;z=\ c_2)\}e^{\left(j\frac{k_0}{2f'}[x^2+y^2]\right)}\end{aligned} \tag{9.1-9}$$

The term $e^{\left(j\frac{k_0}{2f'}[x^2+y^2]\right)}$ expresses the phase change when the light field passes through the imaging lens; where f' is the focal length of the imaging lens. Finally, the light field distribution at the output plane is given by the following formalism

$$\begin{aligned}\psi^{(0)}_{\text{output plane 2}}(x,y) &= \mathcal{F}^{-1}\Big\{\Psi_2^{2^{(0)}}(k_x,k_y)H_v(k_x,k_y;z=\ c_2)\Big\} \\ & e^{\left(j\frac{k_0}{2f'}[x^2+y^2]\right)} * \mathcal{F}^{-1}\{H_v(k_x,k_y;z=\ d_2)\} \\ &= \Big\{\{\psi^{(0)}_{\text{input plane 2}}(cos(\phi_{inc})cos(\phi_{\text{b}})x,y) \\ & * h_v(cos(\phi_{inc})cos(\phi_{\text{b}})x,y;z=\ b_2) \\ & * h_{(0)}(cos(\phi_{\text{b}})x,y;z=L) * h_v(x,y;z=\ c_2)\} \\ & exp\left(j\frac{k_0}{2f'}\left[x^2+y^2\right]\right)\Big\} * h_v(x,y;z=\ d_2).\end{aligned} \tag{9.1-10}$$

The spatial frequency spectrum distribution of $\psi^{(0)}_{\text{output plane 2}}(x,y)$ is

$$\begin{aligned}\Psi^{(0)}_{\text{output plane 2}}(k_x,k_y) &= \left\{\Big\{\Psi_2^{2^{(0)}}(k_x,k_y)H_v(k_x,k_y;z=\ c_2)\Big\}\right. \\ & \left. * \frac{2jf'\pi}{k_o} e^{\left(j\frac{k_o}{2f'}[x^2+y^2]\right)}\right\} H_v(k_x,k_y;z=\ d_2) \\ &= \Big\{\{\frac{\Psi^{(0)}_{\text{input plane 2}}\left(\frac{k_x}{cos(\phi_{inc})cos(\phi_{\text{b}})},k_y\right)}{|cos(\phi_{inc})cos(\phi_{\text{b}})|} \\ & \times \frac{H_v\left(\frac{k_x}{cos(\phi_{inc})cos(\phi_{\text{b}})},k_y;z=\ b_2\right)}{|cos(\phi_{inc})cos(\phi_{\text{b}})|} \\ & \times \frac{H_{(0)}\left(\frac{k_x}{cos(\phi_{\text{b}})},k_y;z=\ L\right)}{|cos(\phi_{\text{b}})|} H_v(k_x,k_y;z=\ c_2)\} \\ & * \frac{2jf'\pi}{k_o} exp\left(j\frac{k_0}{2f'}\left[k_x^2+k_y^2\right]\right)\Big\} H_v(k_x,k_y;z=\ d_2).\end{aligned} \tag{9.1-11}$$

9.2 Realization of minus one order image processing

Figure $9.1-1$ represents the experiment setup for image high frequency noise reduction using the minus one diffracted order from two acousto-optic cells placed in series. The part of the image processing system from object plane 1 to image plane 1 has already analyzed in section 9.2. Again, the only thing that is left to be done is to analyze

the system from second object plane through second image plane. This can be done by first assuming that image located at image plane 1 is the same as at object plane 2. So the result in equation $8.2-11$ will be the image , $\psi^{(-1)}_{\text{input plane 2}}(x''', y)$, at input plane 2. The second acousto-optic modulator, AOM, is located between the object plane 2 and the second imaging lens. As stated earlier, the AOM has been rotated in the x-z plane clockwise by ϕ_{inc}. During the rotation of axes, we keep the x-z plane fixed. The distances from the object to the AOM, and from the AOM to the imaging lens are b_2 and c_2, respectively. The length of the AOM is denote by L. The distance between the image lens and the output plane (image plane) is d_2.

Assuming the light field distribution at input plane 2 to be $\psi^{(-1)}_{\text{input plane 2}}(x''', y)$ (amplitude distribution of the picture), the light field distribution as the image enters the AOM after propagating the distance b_2 is described as

$$\psi_1^2(x''', y; z = b_2) = \psi^{(-1)}_{\text{input plane 2}}(x''', y) * h_v(x''', y; z = b_2), \qquad (9.2-1)$$

where $*$ denotes convolution operation and $h_v(x''',y;z=b_2) = \frac{k_v}{j2\pi b_2} e^{-j\frac{k_v}{2b_1}\left[(x''')^2+y^2\right]}$ is the free-space impulse response function with k_v denoting the propagation constant in free space. So the spatial frequency spectrum distribution of $\psi_1^2(x''', y;z = b_2)$ is

$$\begin{aligned}\Psi_1^2(k_{x'''}, k_y;z = b_2) &= \mathcal{F}\{\psi_1^2(x''', y;z = b_2)\} \qquad (9.2-2)\\ &= \mathcal{F}\{\psi^{(-1)}_{\text{input plane 2}}(x''', y) * h_v(x''', y;z = b_2)\}\\ &= \psi^{(-1)}_{\text{input plane 2}}(k_{x'''}, k_y) * H_v(k_{x'''}, k_y;z = b_2),\end{aligned}$$

where $H_v(k_{x'''},k_y; z = b_1) = exp\left[\frac{j\left[(kx''')^2+ky^2\right]z}{2k_v}\right]$. Before applying the result in equation $9.2-2$ to the AOM, one must use a coordinate transformation, so that Ψ_1^2 is in the same coordinate system as the AOM. Using the coordinate transformation in equation $7.1-1a$ with z'=0, equation $9.2-1$ becomes

$$\begin{aligned}\psi_1^2(x', y; z = b_2) = \psi^{(-1)}_{\text{input plane 2}}&(cos(\phi_{inc})x', y) \qquad (9.2-3)\\ &* h_v(cos(\phi_{inc})x', y; z = b_2)\end{aligned}$$

So the spatial frequency spectrum distribution of $\psi_1^2(x', y; z = b_2)$ after the coordinate system transformation is

$$\begin{aligned}\Psi_1^2(k_{x'}, k_y; z = b_2) &= \mathcal{F}\{\psi_1^2(x', y; z = b_2)\} \\ &= \mathcal{F}\{\psi^{(-1)}_{\text{input plane 2}}(cos(\phi_{inc})x', y) \\ &* h_v(cos(\phi_{inc})x', y; z = b_2)\} \\ &= \left[\frac{\Psi^{(-1)}_{\text{input plane 2}}\left(\frac{k_{x'}}{cos(\phi_{inc})}, k_y\right)}{|cos(\phi_{inc})|}\right] \\ &\times \left[\frac{H_v\left(\frac{k_{x'}}{cos(\phi_{inc})}, k_y; z = b_2\right)}{|cos(\phi_{inc})|}\right].\end{aligned} \tag{9.2-4}$$

Using a transfer function, equation $(5.1.1-11)$, to model the AOM, the light field distribution of the minus one order as the light field exits the AOM is written as

$$\begin{aligned}\psi_2^{2(-1)}(x', y) &= \mathcal{F}^{-1}\{\Psi_1^2(k_{x'}, k_y; z = b_2) \\ &\times H_{(-1)}(k_{x'}, k_y; z = L)\} \\ &= \psi^{(-1)}_{\text{input plane 2}}(cos(\phi_{inc})x', y) \\ &* h_v(cos(\phi_{inc})x', y; z = b_2) * h_{(-1)}(x', y; z = L),\end{aligned} \tag{9.2-5}$$

where $h_{(-1)}(x', y; z = L) = \mathcal{F}^{-1}\{H_{(-1)}(k_{x'}, k_x; z = L)\}$, is called the spatial impulse response function of the AOM. The superscript or subscript (-1) corresponds to the minus one order diffracted light. The result in equation $9.2-5$ must be mapped to the coordinate system of the zeroth diffracted order. This can be done using the coordinate transformation in equation $7.1-2a$ with $z = 0$. Therefore equation $9.2-5$ becomes

$$\begin{aligned}\psi_2^{2(-1)}(x, y) &= \mathcal{F}^{-1}\{\Psi_1^2(k_{x'}, k_y; z = b_2) \\ &\times H_{(-1)}(k_{x'}, k_y; z = L)\} \\ &= \psi^{(-1)}_{\text{input plane 2}}(cos(\phi_{inc})cos(\phi_{\text{b}})x, y) \\ &* h_v(cos(\phi_{inc})cos(\phi_{\text{b}})x, y; z = b_2) \\ &* h_{(-1)}(cos(\phi_{\text{b}})x, y; z = L).\end{aligned} \tag{9.2-6}$$

The spatial frequency spectrum distribution of $\psi_2^{2^{(-1)}}(x,y)$ is

$$\begin{aligned}\Psi_2^{2^{(-1)}}(k_x,k_y) &= \Psi_1^2(k_x,k_y;z=b_2)\times H_{(-1)}(k_x,k_y;z=L) \\ &= \frac{\Psi^{(-1)}_{\text{input plane 2}}\left(\frac{k_x}{cos(\phi_{inc})cos(\phi_{\text{b}})},k_y\right)}{|cos(\phi_{inc})cos(\phi_{\text{b}})|} \\ &\times \frac{H_v\left(\frac{k_x}{cos(\phi_{inc})cos(\phi_{\text{b}})},k_y;z=\ b_2\right)}{|cos(\phi_{inc})cos(\phi_{\text{b}})|} \\ &\times \frac{H_{(-1)}\left(\frac{k_x}{cos(\phi_{\text{b}})},k_y;z=\ L\right)}{|cos(\phi_{\text{b}})|}.\end{aligned} \tag{9.2-7}$$

The light field distribution at the input plane of the second imaging lens is

$$\begin{aligned}\psi_2^{(-1)}(x,y;z=\ c_1) &= \mathcal{F}^{-1}\left\{\Psi_2^{2^{(-1)}}(k_x,k_y)H_v(k_x,k_y;z=\ c_2)\right\} \\ &= \psi^{(-1)}_{\text{input plane 2}}(cos(\phi_{inc})cos(\phi_{\text{b}})x,y) \\ &*h_v(cos(\phi_{inc})cos(\phi_{\text{b}})x,y;z=\ b_2) \\ &*h_{(-1)}(cos(\phi_{\text{b}})x,y;z=L)*h_v(x,y;z=\ c_2),\end{aligned} \tag{9.2-8}$$

where as the light field distribution at the output plane of the second imaging lens is

$$\begin{aligned}\psi_{\text{im}}^{(-1)}(x,y) &= \mathcal{F}^{-1}\left\{\Psi_2^{2^{(-1)}}(k_x,k_y)H_v(k_x,k_y;z=\ c_2)\right\}e^{\left(j\frac{k_0}{2f'}[x^2+y^2]\right)} \\ &= \{\psi^{(-1)}_{\text{input plane 2}}(cos(\phi_{inc})cos(\phi_{\text{b}})x,y) \\ &*h_v(cos(\phi_{inc})cos(\phi_{\text{b}})x,y;z=\ b_2) \\ &*h_{(-1)}(cos(\phi_{\text{b}})x,y;z=L)*h_v(x,y;z=\ c_2)\}e^{\left(j\frac{k_0}{2f'}[x^2+y^2]\right)}.\end{aligned} \tag{9.2-9}$$

The term $e^{\left(j\frac{k_0}{2f'}[x^2+y^2]\right)}$ expresses the phase change when the light field passes through the imaging lens; where f' is the focal length of the imaging lens. Finally, the light field

distribution at the second output plane is given by the following formalism

$$\psi^{(-1)}_{\text{output plane 2}}(x,y) = \mathcal{F}^{-1}\Big\{\Psi_2^{2^{(-1)}}(k_x,k_y)H_v(k_x,k_y;z=\ c_2)\Big\} \qquad (9.2-10)$$
$$e^{\left(j\frac{k_0}{2f'}\left[x^2+y^2\right]\right)} * \mathcal{F}^{-1}\{H_v(k_x,k_y;z=\ d_2)\}$$
$$= \Big\{\{\psi^{(-1)}_{\text{input plane 2}}(cos(\phi_{inc})cos(\phi_{\text{b}})x,y)$$
$$* h_v(cos(\phi_{inc})cos(\phi_{\text{b}})x,y;z=\ b_2)$$
$$* h_{(-1)}(cos(\phi_{\text{b}})x,y;z=L) * h_v(x,y;z=\ c_2)\}$$
$$exp\left(j\frac{k_0}{2f'}\left[x^2+y^2\right]\right)\Big\} * h_v(x,y;z=\ d_2)$$

The spatial frequency spectrum distribution of $\psi^{(-1)}_{\text{output plane 2}}(x,y)$ is

$$\Psi^{(-1)}_{\text{output plane 2}}(k_x,k_y) = \Big\{\Big\{\Psi_2^{2^{(-1)}}(k_x,k_y)H_v(k_x,k_y;z=\ c_2)\Big\} \qquad (9.2-11)$$
$$* \frac{2jf'\pi}{k_o} e^{\left(j\frac{k_o}{2f'}\left[x^2+y^2\right]\right)}\Big\} H_v(k_x,k_y;z=\ d_2)$$
$$= \Big\{\{\frac{\Psi^{(-1)}_{\text{input plane 2}}\left(\frac{k_x}{cos(\phi_{inc})cos(\phi_{\text{b}})},k_y\right)}{|cos(\phi_{inc})cos(\phi_{\text{b}})|}$$
$$\times \frac{H_v\left(\frac{k_x}{cos(\phi_{inc})cos(\phi_{\text{b}})},k_y;z=\ b_2\right)}{|cos(\phi_{inc})cos(\phi_{\text{b}})|}$$
$$\times \frac{H_{(-1)}\left(\frac{k_x}{cos(\phi_{\text{b}})},k_y;z=\ L\right)}{|cos(\phi_{\text{b}})|} H_v(k_x,k_y;z=\ c_2)\}$$
$$* \frac{2jf'\pi}{k_o} exp\left(j\frac{k_0}{2f'}\left[k_x^2+k_y^2\right]\right)\Big\} H_v(k_x,k_y;z=\ d_2)$$

9.3 Results from Series Acousto-Optic Image Processing System

The image processing system used in chapter 8 contained a single acousto-optic modulator and a single imaging lens. This section will present results from an optical image processing system that includes two AOMs and two imaging lenses (see figure $9.1-1$). In this particular experimental setup the following AOMs will be used: AOM_1 will have a RF center frequency of 80 MHz and AOM_2 will have an RF center frequency of 40 MHz. Figure $9.3-1$ shows the result of edge enhancement of a

rectangular image using this optical system. Figure $9.3-1$a is the result of high pass filtering after the image passes through AOM_1. Figure $9.3-1$b is the result of high pass filtering after the image passes through AOM_2. As you can see by looking at figure $9.3-1$, the edges of the rectangular image have been enhanced when you compare figure $9.3-1$a to figure $9.3-1$b. This is an expected result since the second acousto-optic modulator is reinforcing the effect of the first AOM. The Q and α values for the two AOMs are as follows: AOM_1: $Q=58$ and $\alpha=0.472\pi$, AOM_2: $Q=28$ and $\alpha=0.65\pi$.

A graph of the acousto-optic transfer function that corresponds to the result in figure $9.3-1$a is plotted in figure $8.3-10$. A graph of the combined transfer function for the AOM_1 and AOM_2 from figure $9.1-1$ that would yield the result in figure $9.3-1$ is given in figure $9.3-2$.

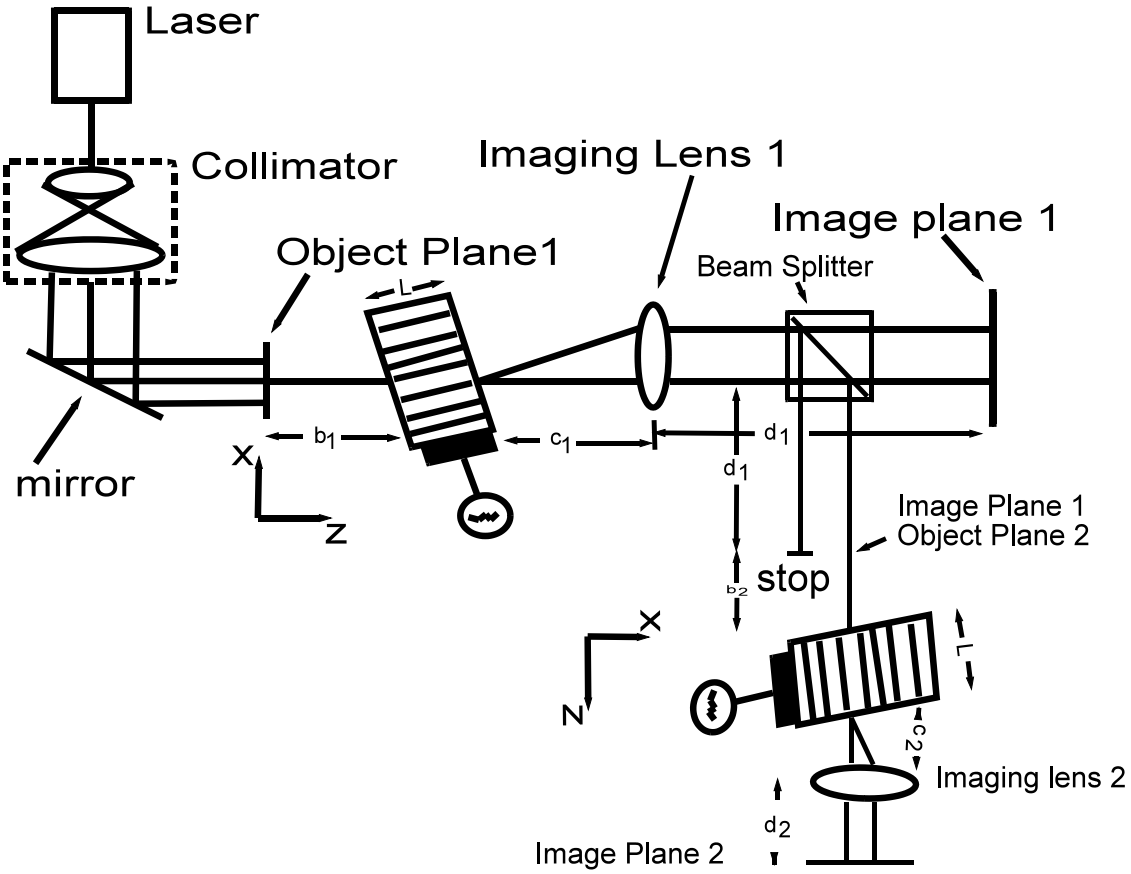

Figure 9.1 – 1: Series Acousto-Optic Image Processing System

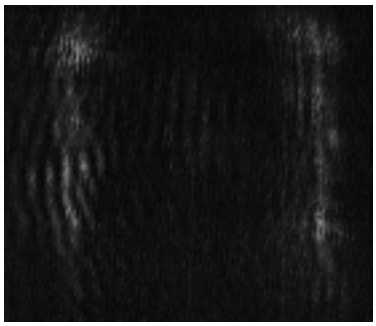

(a)

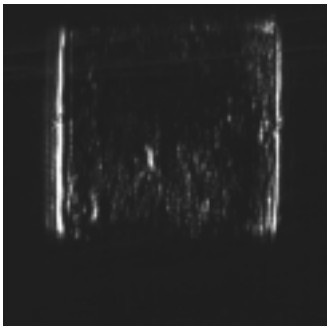

(b)

Figure 9.3 – 1: Photos of a rectangular image processed using a series acousto-optic system (a) processed image after first AOM , (b) processed image after second AOM

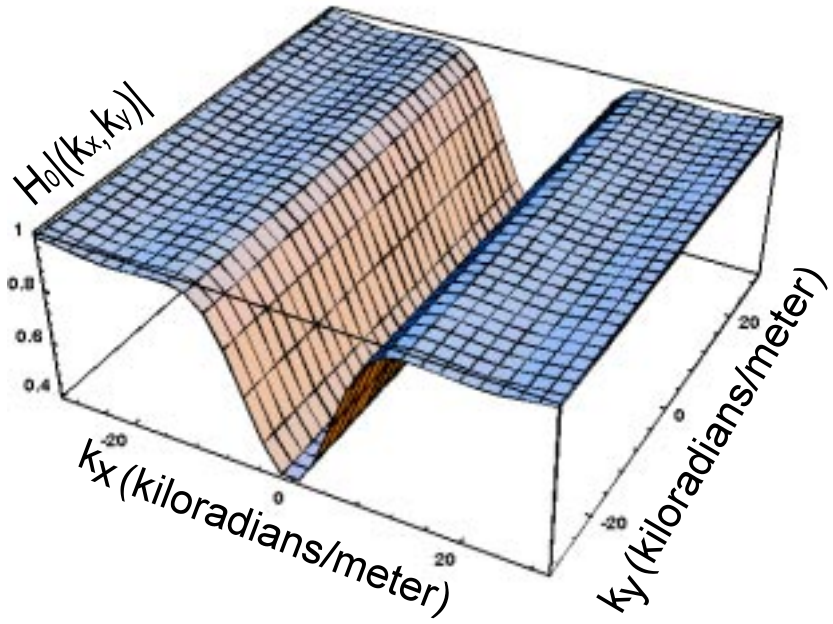

(a)

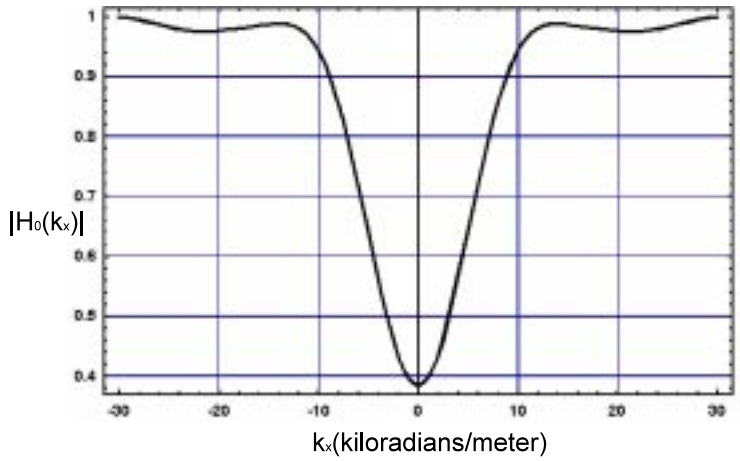

(b)

Figure $9.3-2$: Graph of the Acousto-Optic transfer function for the zeroth order for a series system (a) three dimensional and (b) two dimensional when AOM_1 has Q=58, $\alpha = 0.472\pi$, AOM_2 has Q=28, $\alpha = 0.65\pi$ and $L = 60mm$

Chapter 10.0 Detailed Analysis of the Parallel Acousto-Optic Image Processing System

10.1 Realization of zeroth order image processing

Figure $10.1-1$ represents the experiment setup for image edge enhancement using the zeroth diffracted order. The part of the image processing system that includes AOM_1 has already been analyzed in section 8.1. Therefore, this section will only analyze the light path that includes AOM_2 and combine this formalism with the formalism from section 8.1. The object (a transparency), $i(x, y''')$, is placed on the object plane and the Acousto-Optic Modulator, AOM_2, is located between the object and an imaging lens. Note that the AOM_2 has been rotated in the y-z plane counter clockwise by ϕ_{inc}. During the rotation of axes, we keep the y-z plane fixed. The distances from the object to the AOM_2, and from the AOM_2 to the imaging lens are $b_1 = b_{11} + b_{12}$ and $c_1 = c_{11} + c_{12}$, respectively. The length of the AOM_2 is denote by L. The distance between the image lens and the output plane (image plane) is $d_1 = d_{11} + d_{12} + d_{13}$.

Assuming the light field distribution on input plane to be $i(x, y''')$ (amplitude distribution of the transparent picture), the light field distribution at the entrance of the AOM_2 after propagating the distance $b_1 = b_{11} + b_{12}$ is described as

$$\psi_1(x, y'''; z = b_{11} + b_{12}) = i(x, y''') * h_v(x, y'''; z = b_{11} + b_{12}) \qquad (10.1-1)$$

where $*$ denotes convolution operation and $h_v(x,y''';z = b_{11} + b_{12}) = \frac{k_v}{j2\pi(b_{11}+b_{12})} e^{-j\frac{k_v}{2(b_{11}+b_{12})}\left[x^2+(y''')^2\right]}$ is the free-space impulse

response function with k_v denoting the propagation constant in free space. So the spatial frequency spectrum distribution of $\psi_1(x,y''';z = b_{11} + b_{12})$ is

$$\begin{aligned}\Psi_1(k_x, k_{y'''};z = b_{11} + b_{12}) &= \mathcal{F}\{\psi_1(x, y''';z = b_{11} + b_{12})\} \\ &= \mathcal{F}\{i(x, y''') * h_v(x, y''';z = b_1)\} \\ &= I(k_{x'''},k_y)H_v(k_{x'''},k_y; z = b_1),\end{aligned} \tag{10.1-2}$$

where $H_v(k_{x'''},k_y; z = b_1) = exp\left[\frac{j\left[(kx''')^2+ky^2\right]z}{2k_v}\right]$. Before applying the result in equation $10-2$ to the AOM, one must use a coordinate transformation, so that Ψ_1 is in the same coordinate system as AOM_2. Using the coordinate transformation in equation $7.1-1a$ with z'=0, equation $10-1$ becomes

$$\begin{aligned}\psi_1(x, y'; z = b_1) &= i(x, cos(\phi_{inc})y') \\ &\quad * h_v(x, cos(\phi_{inc})y'; z = b_1)\end{aligned} \tag{10.1-3}$$

So the spatial frequency spectrum distribution of $\psi_1(x, y'; z = b_1)$ is

$$\begin{aligned}\Psi_1(k_x, k_{y'};z = b_1) &= \mathcal{F}\{\psi_1(x, y';z = b_1)\} \\ &= \mathcal{F}\{i(x, cos(\phi_{inc})y') \\ &\quad * h_v(x, cos(\phi_{inc})y';z = b_1)\} \\ &= \left[\frac{I\left(k_x, \frac{k_{y'}}{cos(\phi_{inc})}\right)}{|cos(\phi_{inc})|}\right] \\ &\quad \times \left[\frac{H_v\left(k_x, \frac{k_{y'}}{cos(\phi_{inc})}; z = b_1\right)}{|cos(\phi_{inc})|}\right]\end{aligned} \tag{10.1-4}$$

Using a transfer function, equation $(5.1.1-12)$, to model the AOM_2, the light field distribution of the zeroth order as the light exits the AOM_2 is

$$\begin{aligned}\psi_2^{(0)}(x, y') &= \mathcal{F}^{-1}\{\Psi_1(k_x,k_{y'};z = b_1) \times H_0(k_x,k_{y'};z = L)\} \\ &= i(x, cos(\phi_{inc})y') \\ &\quad * h_v(x, cos(\phi_{inc})y';z = b_1) * h_0(x,y';z = L)\end{aligned} \tag{10.1-5}$$

where $h_0(x,y';z = L) = \mathcal{F}^{-1}\{H_0(k_x,k_{y'};z = L)\}$, is called the spatial impulse response function of the AOM_2; the superscript or subscript (0) corresponds to the zeroth order

light. The result in equation $10.1-5$ must be mapped to the coordinate system of the zeroth order. This can be done using the coordinate transformation in equation $7.1-9$a with $z=0$. Therefore equation $10.1-5$ becomes

$$\begin{aligned}\psi_2^{(0)}(x,y) &= \mathcal{F}^{-1}\{\Psi_1(k_x,k_y;z=b_1)\cdot H_{(0)}(k_x,k_y;z=L)\} \\ &= i(x,cos(\phi_{inc})cos(\phi_{\mathrm{b}})y) \\ &*h_v(x,cos(\phi_{inc})cos(\phi_{\mathrm{b}})y;z=\ b_1) \\ &*h_{(0)}(x,cos(\phi_{\mathrm{b}})y;z=L)\end{aligned} \qquad (10.1-6)$$

The spatial frequency spectrum distribution of $\psi_2^{(0)}(x,y)$ is

$$\begin{aligned}\Psi_2^{(0)}(k_x,k_y) &= \Psi_1(k_x,k_y;z=b_1)\times H_{(0)}(k_x,k_y;z=L) \\ &= \frac{I\left(k_x,\frac{k_y}{cos(\phi_{inc})cos(\phi_{\mathrm{b}})}\right)}{|cos(\phi_{inc})cos(\phi_{\mathrm{b}})|} \\ &\times \frac{H_v\left(k_x,\frac{k_y}{cos(\phi_{inc})cos(\phi_{\mathrm{b}})};z=\ b_1\right)}{|cos(\phi_{inc})cos(\phi_{\mathrm{b}})|} \\ &\times \frac{H_{(0)}\left(k_x,\frac{k_y}{cos(\phi_{\mathrm{b}})};z=\ L\right)}{|cos(\phi_{\mathrm{b}})|}\end{aligned} \qquad (10.1-7)$$

The light field distribution at the input plane of the imaging lens is

$$\begin{aligned}\psi_2^{(0)}(x,y;z=\ c_1) &= \mathcal{F}^{-1}\left\{\Psi_2^{(0)}(k_x,k_y)H_v(k_x,k_y;z=\ c_1)\right\} \\ &= i(x,cos(\phi_{inc})cos(\phi_{\mathrm{b}})y) \\ &*h_v(x,cos(\phi_{inc})cos(\phi_{\mathrm{b}})y;z=\ b_1) \\ &*h_{(0)}(x,cos(\phi_{\mathrm{b}})y;z=L)*h_v(x,y;z=\ c_1)\end{aligned} \qquad (10.1-8)$$

where as the light field distribution at the output plane of the imaging lens is

$$\begin{aligned}\psi_{\mathrm{im}}^{(0)}(x,y) &= \mathcal{F}^{-1}\left\{\Psi_2^{(0)}(k_x,k_y)H_v(k_x,k_y;z=\ c_1)\right\}e^{\left(j\frac{k_0}{2f'}[x^2+y^2]\right)} \\ &= \{i(x,cos(\phi_{inc})cos(\phi_{\mathrm{b}})y) \\ &*h_v(x,cos(\phi_{inc})cos(\phi_{\mathrm{b}})y;z=\ b_1) \\ &*h_{(0)}(x,cos(\phi_{\mathrm{b}})y;z=L)*h_v(x,y;z=\ c_1)\}e^{\left(j\frac{k_0}{2f'}[x^2+y^2]\right)}\end{aligned} \qquad (10.1-9)$$

The term $e^{\left(j\frac{k_0}{2f'}[x^2+y^2]\right)}$ expresses the phase change when the light field passes through the imaging lens; where f' is the focal length of the imaging lens. Finally, the light field

distribution at the output plane is given by the following formalism

$$\psi^{(0)}_{\text{image plane}}(x,y) = \mathcal{F}^{-1}\Big\{\Psi^{(0)}_{2}(k_x,k_y)H_v(k_x,k_y;z=\ c_1)\Big\} \qquad (10.1-10)$$
$$e^{\left(j\frac{k_0}{2f'}\left[x^2+y^2\right]\right)} * \mathcal{F}^{-1}\{H_v(k_x,k_y;z=\ d_1)\}$$
$$= \Big\{\{i(x,cos(\phi_{inc})cos(\phi_{\text{b}})y)$$
$$*h_v(x,cos(\phi_{inc})cos(\phi_{\text{b}})y;z=\ b_1)$$
$$*h_{(0)}(x,cos(\phi_{\text{b}})y;z=L)*h_v(x,y;z=\ c_1)\}$$
$$exp\left(j\frac{k_0}{2f'}\left[x^2+y^2\right]\right)\Big\}*h_v(x,y;z=\ d_1)$$

The spatial frequency spectrum distribution of $\psi^{(0)}_{\text{output plane 1}}(x,y)$ is

$$\Psi^{(0)}_{\text{image plane}}(k_x,k_y) = \Big\{\Big\{\Psi^{(0)}_{2}(k_x,k_y)H_v(k_x,k_y;z=\ c_1)\Big\} \qquad (10.1-11)$$
$$*\frac{2jf'\pi}{k_o}e^{\left(j\frac{k_o}{2f'}\left[x^2+y^2\right]\right)}\Big\}H_v(k_x,k_y;z=\ d_1)$$
$$= \Big\{\{\frac{I\left(k_x,\ \frac{k_y}{cos(\phi_{inc})cos(\phi_{\text{b}})}\right)}{|cos(\phi_{inc})cos(\phi_{\text{b}})|}$$
$$\times \frac{H_v\left(k_x,\ \frac{k_y}{cos(\phi_{inc})cos(\phi_{\text{b}})};z=\ b_1\right)}{|cos(\phi_{inc})cos(\phi_{\text{b}})|}$$
$$\times \frac{H_{(0)}\left(k_x,\ \frac{k_y}{cos(\phi_{\text{b}})};z=\ L\right)}{|cos(\phi_{\text{b}})|}H_v(k_x,k_y;z=\ c_1)\}$$
$$*\frac{2jf'\pi}{k_o}exp\left(j\frac{k_0}{2f'}\left[k_x^2+k_y^2\right]\right)\Big\}H_v(k_x,k_y;z=\ d_1)$$

As mentioned earlier, equation $10.1-11$ represents only one path of the parallel image processing system. Therefore, equation $10.1-11$ must be added to equation $8.1-9$ to form the complete mathematically formalism for this particular image processing system.

10.2 Realization of minus one order image processing

Figure $10.1-1$ represents the experiment setup for high frequency noise reduction in two dimension using the minus one diffracted order from each Acousto-Optic Modulator, AOM. The part of the image processing system that includes AOM_1 has already been analyzed in section 8.2. Therefore, this section will only analyze the light path that includes AOM_2 and combine this formalism with the formalism developed from section 8.2. The object (a transparency), $i(x, y''')$, is placed on the object plane and the AOM_2 is located between the object and an imaging lens. Note that the AOM_2 has been rotated in the y-z plane clockwise by ϕ_{inc}. During the rotation of axes, we keep the y-z plane fixed. The distances from the object to the AOM_2, and from the AOM_2 to the imaging lens are $b_1 = b_{11} + b_{12}$ and $c_1 = c_{11} + c_{12}$, respectively. The length of the AOM_2 is denote by L. The distance between the image lens and the output plane (image plane) is $d_1 = d_{11} + d_{12} + d_{13}$.

Assuming the light field distribution on input plane to be $i(x, y''')$ (amplitude distribution of the transparent picture), the light field distribution at the entrance of the AOM_2 after propagating the distance b_1 is described as

$$\psi_1(x, y'''; z = b_1) = i(x, y''') * h_v(x, y'''; z = b_1) \qquad (10.2-1)$$

where $*$ denotes convolution operation and $h_v(x,y''';z = b_1) = \frac{k_v}{j2\pi(b_{11}+b_{12})} e^{-j\frac{k_v}{2b_1}\left[x^2+(y''')^2\right]}$ is the free-space impulse response function with k_v denoting the propagation constant in free space. So the spatial frequency spectrum distribution of $\psi_1(x,y''';z = b_1)$ is

$$\begin{aligned} \Psi_1(k_x, k_{y'''}; z = b_1) &= \mathcal{F}\{\psi_1(x, y'''; z = b_1)\} \\ &= \mathcal{F}\{i(x, y''') * h_v(x, y'''; z = b_1)\} \\ &= I(k_{x'''}, k_y) H_v(k_{x'''}, k_y; z = b_1) \end{aligned} \qquad (10.2-2)$$

where $H_v(k_{x'''}, k_y; z = b_1) = exp\left[\frac{j\left[(kx''')^2+ky^2\right]z}{2k_v}\right]$. Before applying the result in equation $8.2.1-2$ to the AOM_2, one must use a coordinate transformation, so that Ψ_1 is in the

same coordinate system as the AOM_2. Using the coordinate transformation in equation $7.1-1a$ with z'=0, therefore equation 8.3.2.2-1 becomes

$$\psi_1(x,y';z=b_1) = i(x,cos(\phi_{inc})y') * h_v(x,cos(\phi_{inc})y';z=b_1) \qquad (10.2-3)$$

So the spatial frequency spectrum distribution of $\psi_1(x,y';z=b_1)$ is

$$\begin{aligned}\Psi_1(k_x,k_{y'};z=b_1) &= \mathcal{F}\{\psi_1(x,y';z=b_1)\} \\ &= \mathcal{F}\{i(x,cos(\phi_{inc})y') \\ &* h_v(x,cos(\phi_{inc})y';z=b_1)\} \\ &= \left[\frac{I\left(k_x,\frac{k_{y'}}{cos(\phi_{inc})}\right)}{|cos(\phi_{inc})|}\right] \\ &\times \left[\frac{H_v\left(k_x,\frac{k_{y'}}{cos(\phi_{inc})};z=b_1\right)}{|cos(\phi_{inc})|}\right]\end{aligned} \qquad (10.2-4)$$

Using a transfer function, equation $(5.1.1-11)$, to model the AOM_2, the light field distribution of the minus one order as the light exits the AOM_2 is

$$\begin{aligned}\psi_2^{(-1)}(x,y') &= \mathcal{F}^{-1}\Big\{\Psi_1(k_x,k_{y'};z=b_1) \\ &\times H_{(-1)}(k_x,k_{y'};z=L)\Big\} \\ &= i(x,cos(\phi_{inc})y') \\ &* h_v(x,cos(\phi_{inc})y';z=b_1) * h_{(-1)}(x,y';z=L)\end{aligned} \qquad (10.2-5)$$

where $h_{(-1)}(x,y';z=L) = \mathcal{F}^{-1}\big\{H_{(-1)}(k_x,k_{y'};z=L)\big\}$, is called the spatial impulse response function of the AOM_2; the superscript or subscript (-1) corresponds to the minus one diffracted order light. The result in equation $10.2-5$ must be mapped to the coordinate system of the zeroth order. This can be done using the coordinate

transformation in equation 7.1-9a with $z = 0$. Therefore equation $10.2 - 5$ becomes

$$\begin{aligned}\psi_2^{(-1)}(x,y) = \mathcal{F}^{-1}\Big\{ & \Psi_1(k_x,k_y;z = b_1) \\ & \times H_{(-1)}(k_x,k_y;z = L)\Big\} \\ & = i(x, cos(\phi_{inc})cos(\phi_{\mathrm{b}})y) \\ & *h_v(x, cos(\phi_{inc})cos(\phi_{\mathrm{b}})y;z = b_1) \\ & *h_{(-1)}(x,cos(\phi_{\mathrm{b}})y;z = L)\end{aligned} \tag{10.2-6}$$

The spatial frequency spectrum distribution of $\psi_2^{(-1)}(x,y)$ is

$$\begin{aligned}\Psi_2^{(-1)}(k_x,k_y) &= \Psi_1(k_x,k_y;z = b_1) \\ &\times H_{(-1)}(k_x,k_y;z = L) \\ &= \frac{I\Big(k_x, \frac{k_y}{cos(\phi_{inc})cos(\phi_{\mathrm{b}})}\Big)}{|cos(\phi_{inc})cos(\phi_{\mathrm{b}})|} \\ &\times \frac{H_v\Big(k_x, \frac{k_y}{cos(\phi_{inc})cos(\phi_{\mathrm{b}})};z = b_1\Big)}{|cos(\phi_{inc})cos(\phi_{\mathrm{b}})|} \\ &\times \frac{H_{(-1)}\Big(k_x, \frac{k_y}{cos(\phi_{\mathrm{b}})};z = L\Big)}{|cos(\phi_{\mathrm{b}})|}\end{aligned} \tag{10.2-7}$$

The light field distribution at the input plane of the imaging lens is

$$\begin{aligned}\psi_2^{(-1)}(x,y;z = c_1) &= \mathcal{F}^{-1}\Big\{\Psi_2^{(-1)}(k_x,k_y)H_v(k_x,k_y;z = c_1)\Big\} \\ &= i(x, cos(\phi_{inc})cos(\phi_{\mathrm{b}})y) \\ &*h_v(x, cos(\phi_{inc})cos(\phi_{\mathrm{b}})y;z = b_1) \\ &*h_{(-1)}(x,cos(\phi_{\mathrm{b}})y;z = L)*h_v(x,y;z = c_1)\end{aligned} \tag{10.2-8}$$

where as the light field distribution at the output plane of the imaging lens is

$$\begin{aligned}\psi_{\mathrm{im}}^{(-1)}(x,y) &= \mathcal{F}^{-1}\Big\{\Psi_2^{(-1)}(k_x,k_y)H_v(k_x,k_y;z = c_1)\Big\}e^{\left(j\frac{k_0}{2f'}[x^2+y^2]\right)} \\ &= \{i(x, cos(\phi_{inc})cos(\phi_{\mathrm{b}})y) \\ &*h_v(x, cos(\phi_{inc})cos(\phi_{\mathrm{b}})y;z = b_1) \\ &*h_{(-1)}(x,cos(\phi_{\mathrm{b}})y;z = L)*h_v(x,y;z = c_1)\}e^{\left(j\frac{k_0}{2f'}[x^2+y^2]\right)}\end{aligned} \tag{10.2-9}$$

The term $e^{\left(j\frac{k_0}{2f'}[x^2+y^2]\right)}$ expresses the phase change when the light field passes through the imaging lens; where f' is the focal length of the imaging lens. Finally, the light field

distribution at the output plane is given by the following formalism

$$\psi^{(-1)}_{\text{image plane}}(x,y) = \mathcal{F}^{-1}\Big\{\Psi_2^{(-1)}(k_x,k_y)H_v(k_x,k_y;z=\ c_1)\Big\} \qquad (10.2-10)$$
$$e^{\left(j\frac{k_0}{2f'}\left[x^2+y^2\right]\right)} * \mathcal{F}^{-1}\{H_v(k_x,k_y;z=\ d_1)\}$$
$$= \Big\{\{i(x, cos(\phi_{inc})cos(\phi_{\mathsf{b}})y)$$
$$*h_v(x, cos(\phi_{inc})cos(\phi_{\mathsf{b}})y;z=\ b_1)$$
$$*h_{(-1)}(x,cos(\phi_{\mathsf{b}})y;z=L) * h_v(x,y;z=\ c_1)\}$$
$$exp\left(j\frac{k_0}{2f'}\left[x^2+y^2\right]\right)\Big\} * h_v(x,y;z=\ d_1)$$

The spatial frequency spectrum distribution of $\psi^{(-1)}_{\text{output plane 1}}(x,y)$ is

$$\Psi^{(-1)}_{\text{image plane}}(k_x,k_y) = \Big\{\Big\{\Psi_2^{(-1)}(k_x,k_y)H_v(k_x,k_y;z=\ c_1)\Big\} \qquad (10.2-11)$$
$$*\frac{2jf'\pi}{k_o}e^{\left(j\frac{k_o}{2f'}\left[x^2+y^2\right]\right)}\Big\}H_v(k_x,k_y;z=\ d_1)$$
$$= \Big\{\{\frac{I\left(k_x,\ \frac{k_y}{cos(\phi_{inc})cos(\phi_{\mathsf{b}})}\right)}{|cos(\phi_{inc})cos(\phi_{\mathsf{b}})|}$$
$$\times \frac{H_v\left(k_x,\ \frac{k_y}{cos(\phi_{inc})cos(\phi_{\mathsf{b}})};z=\ b_1\right)}{|cos(\phi_{inc})cos(\phi_{\mathsf{b}})|}$$
$$\times \frac{H_{(-1)}\left(k_x,\ \frac{k_y}{cos(\phi_{\mathsf{b}})};z=\ L\right)}{|cos(\phi_{\mathsf{b}})|}H_v(k_x,k_y;z=\ c_1)\}$$
$$*\frac{2jf'\pi}{k_o}exp\left(j\frac{k_0}{2f'}\left[k_x^2+k_y^2\right]\right)\Big\}H_v(k_x,k_y;z=\ d_1)$$

As mentioned earlier, equation $10.2-11$ represents only one path of the image processing system. Therefore, equation $8.2-11$ must be added to equation $10.2-11$ to form the complete formalism for this particular image processing system.

10.3 Results of the Parallel Acousto-Optic Image Processing System

The optical image processing systems discussed in sections 8.1 and 8.2 performs only one dimensional image processing. The physical reason for this is due to the fact that

the ultrasonic sound wave travels only in the $x-$direction. Therefore, the image processing effect is in the $y-$direction.

The purpose of this section of the dissertation is to develop an acousto-optic image processing that will perform two dimensional image processing. Figure $10.3-1$ shows a proposed optical image processing system that is designed perform two dimensional image processing. As stated earlier, a single AOM is capable of performing one dimensional image processing. The AOM effect on the image is perpendicular to the direction of the sound wave. Therefore, if orientated the two AOM such that AOM_1 sound wave propagates in the $x-$direction and AOM_2 sound wave propagates in the $y-$direction. The processing of the image that passes through AOM_1 is in the $y-$direction and the processing of the image that passes through AOM_2 is in the $x-$direction. By combining these two results, I am able to produce an image that has been processed in two dimensions. Figure $10.3-2$a is the original image of a rectangle and figure $10.3-2$b shows two dimensional edge enhancement. Figure $10.3-3$a is the two dimensional edge enhancement of an image of a "2" and figure $10.3-3$b is the two dimensional edge enhancement of an image of a "5". Figure $10.3-4$a is the two dimensional edge enhancement of an image of a "17" and figure $10.3-3$b is the two dimensional edge enhancement of an image of a "7".

Figure $10.3-5$ shows the plot of the acousto-optic transfer function for the image processing system shown in figure $10.1-1$. Figure $10.3-5$a was obtained by graphing the magnitude of the mathematically formalism developed in section 10.2. Figure $10.3-5$ shows that the that the parallel image processing system developed in this chapter , gives us the ability to processes image in two spatial dimensions. This ability was lacking in the two previous optical image processing systems presented in this dissertation. Figure 10.3-5 shows that processing in both directions, x and y, is equal. Since the two acousto-optic modulators operator independently. They can be set to have two different processing characteristics.

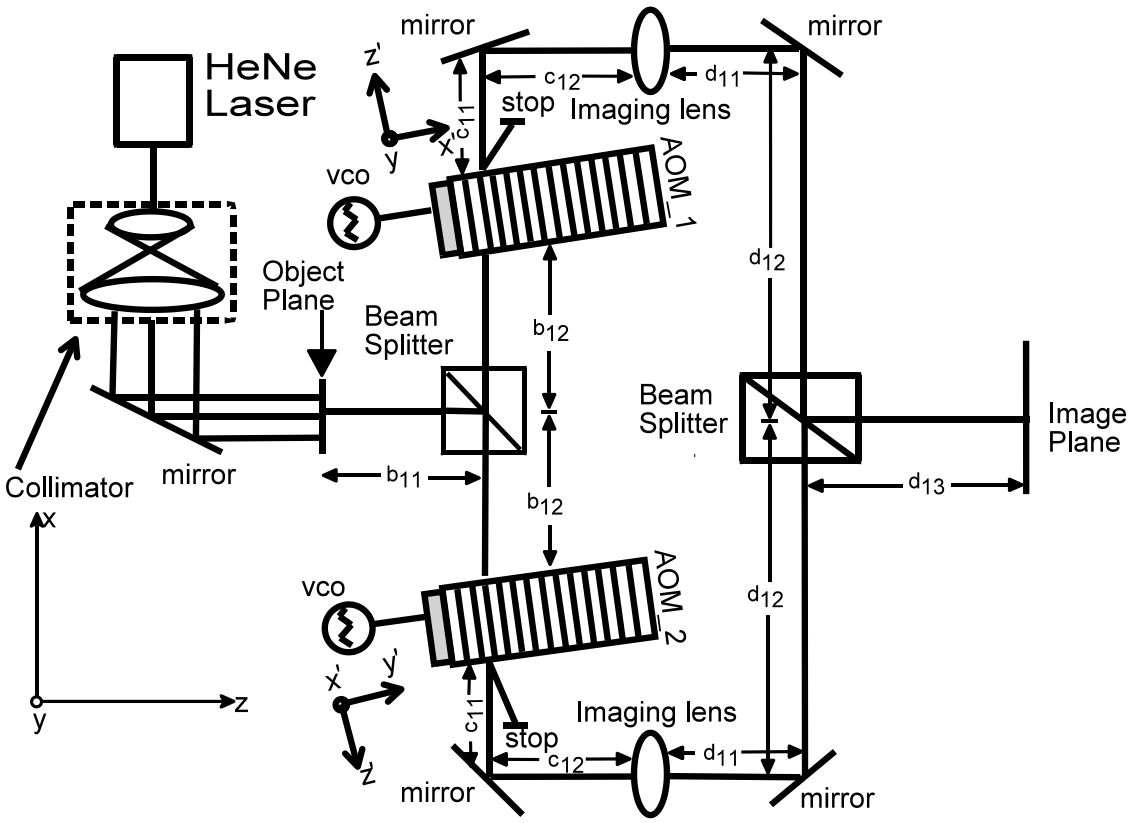

Figure 10.1 – 1: Parallel Acousto-Optic Image Processing System

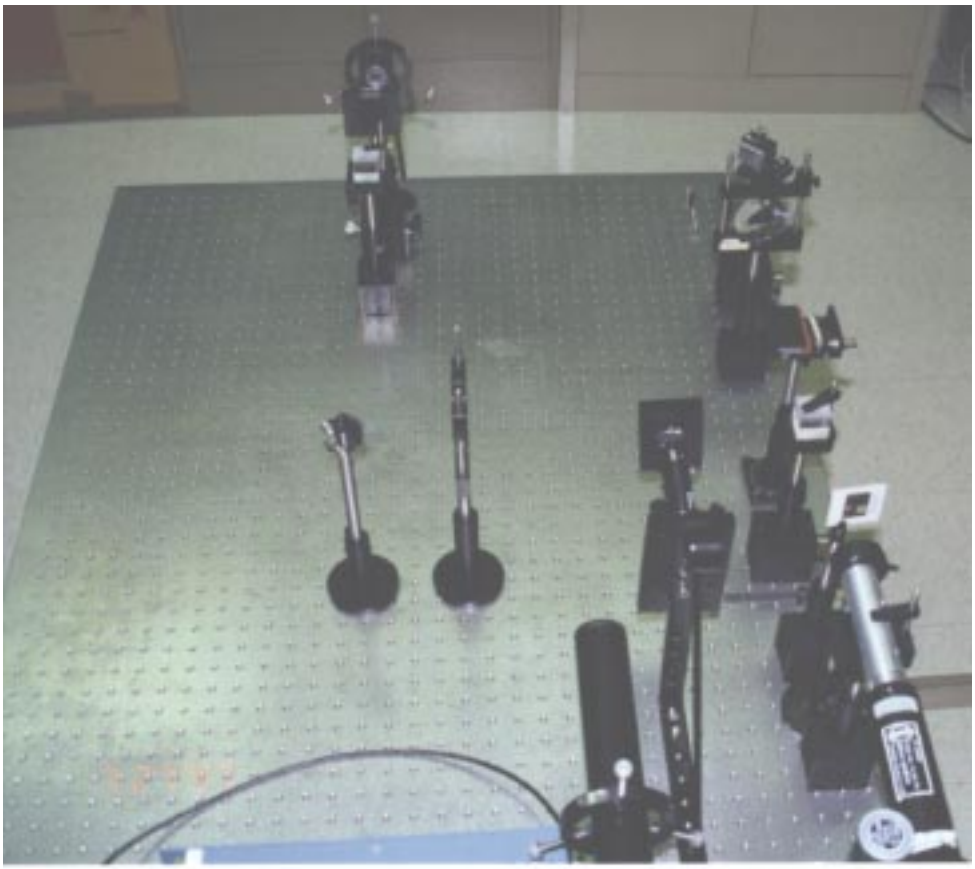

Figure $10.3 - 1$: Photo of the parallel AOM image processing system

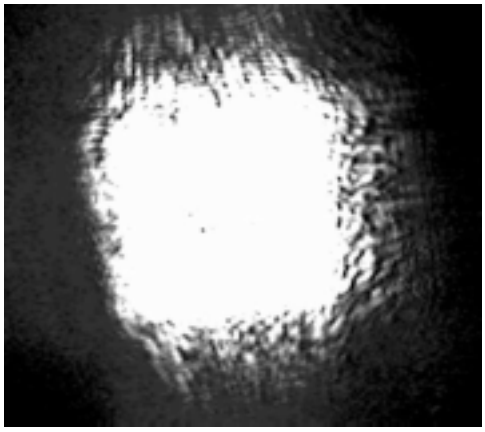

(a)

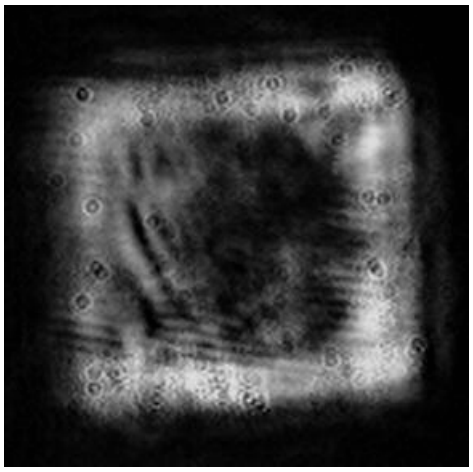

(b)

Figure $10.3-2$: Photos of rectangular image using two AOMs with RF center frequency of $40MHz$ (a) 2-D low pass image, (b) 2-D high pass filtered image

(a)

(b)

Figure $10.3-3$: Photos of edge detection using two AOMs with an RF center frequency of $40MHz$ (a) image of a 2 (b) image of a 5

(a)

(b)

Figure $10.3-4$: Photos of edge detection using two AOMs with an RF center frequency of $40MHz$ (a) image of a 17 (b) image of a 7

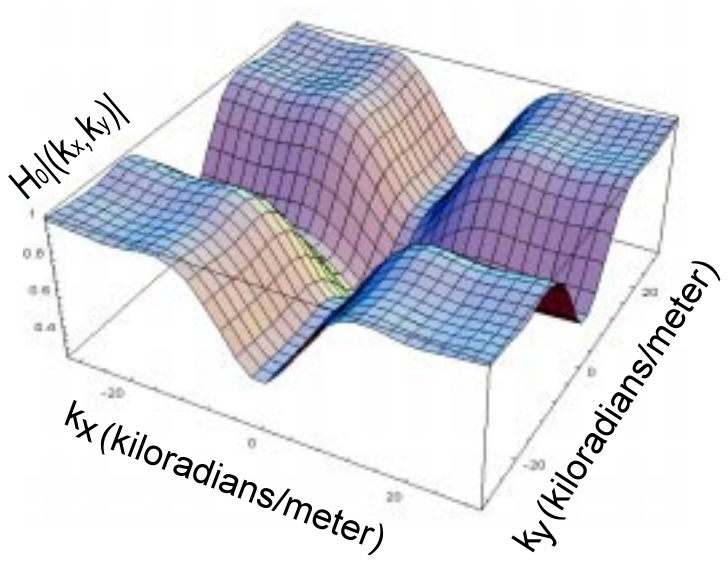

(a)

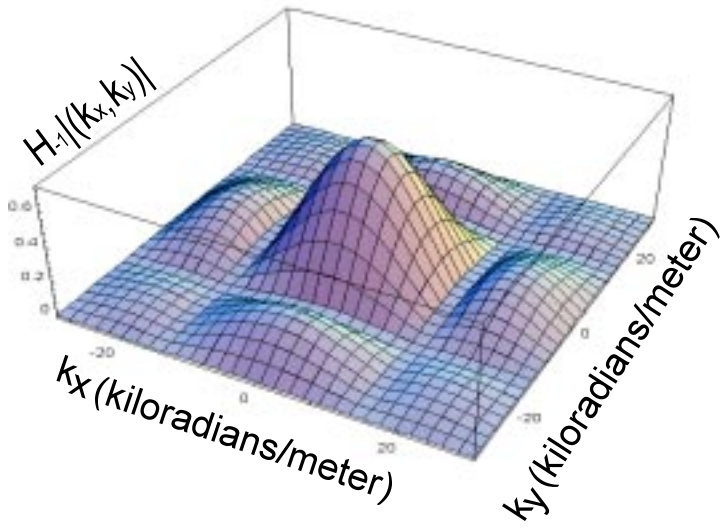

(b)

Figure $10.3-5$: Three dimensional graph of the Acousto-Optic transfer function for a parallel system (a) zeroth diffracted order and (b) minus one diffracted order when AOM_1 has Q=28, $\alpha = 0.65\pi$, AOM_2 has Q=28, $\alpha = 0.65\pi$ and $L = 60mm$

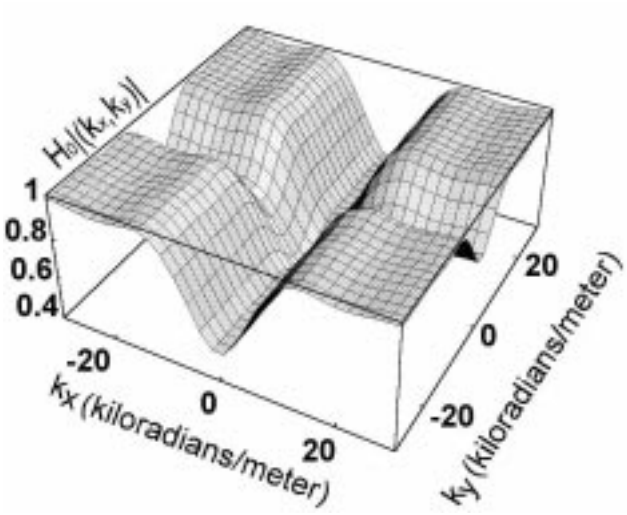

(a)

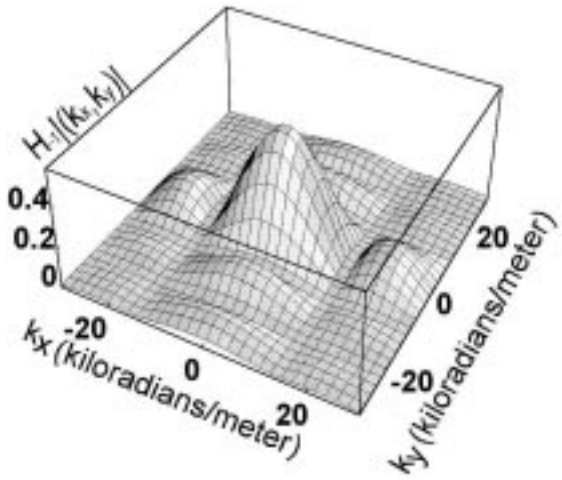

(b)

Figure $10.3-6$: Three dimensional graph of the Acousto-Optic transfer function for a parallel system (a) zeroth diffracted order and (b) minus one diffracted order when AOM_1 has Q=28, $\alpha = 0.65\pi$, AOM_2 has Q=58, $\alpha = 0.472\pi$ and $L = 60mm$

11.0 Conclusions and Direction of Future Research

11.1 General Discussion

This dissertation presents several acousto-optic systems that perform image processing. Each two-dimensional method agreed qualitatively with previously verified analytical results. This is the first time an analytical three-dimensional transfer function for strong acousto-optic interaction has been presented.

This dissertation presented an image processing technique based on the acousto-optic effect. Images were amplitude modulated onto a laser beam that interacted with acoustic waves inside a homogenous, isotropic, flint glass medium. The image entered the acousto-optic cell at the Bragg angle and the Bragg scattered light carried the processed images.

Several experimental setups were considered. The heart of each setups consisted of a system that contained one or two acousto-optic cell and a one or two imaging lenses. The first system consisted of an acousto-optic cell and an imaging lens. The second system consisted of two acousto-optic cells placed in series and with two imaging lens. The last experimental setup consisted of two acousto-optic cells place in parallel and perpendicular to each other with two imaging lenses. The first two systems performed one-dimensional image processing while the last system performed two-dimensional image processing.

In the image processing systems, we monitored the Bragg diffracted images and notice image enhancements. Laboratory experiments were performed and various image processing results were collected. These experimentally results were compared against

computer simulations of all the acousto-optic image processing systems using the transfer function that was derived by analytical means in chapter five.

11.2 Summary of Original Contributions

For the first time, we have presented analytical solutions to the three-dimensional strong acousto-optic interaction problem consisting of an arbitrary light envelope and rectangular sound column. In addition to solving the problem for interaction, I discussed in detailed the effect of the ultrasonic sound wave on the abilities of the acousto-optic systems to process images. I was also able to develop analytical formalism to describe the three acousto-optic image processing systems taking into account the effect of the different coordinate systems that the various system components are in. We were able to match the results of the analytical model to experimental results obtained. This achievement helped to validate the analytical spatial transfer function developed in chapter five.

11.3 Future Research Directions and Goals

Although we have modeled the three-dimensional strong interaction problem with the spatial transfer function developed in chapter 5, additional insights into the acousto-optic process is still needed. For example, the increasing use of acousto-optic cells in the area of image processing demands accurate three-dimensional models that predict how two-dimensional images will interact with sound fields of arbitrary profile. We need a generalized three-dimensional transfer function formalism similar to what is presented in chapter five for higher diffracted orders. Once the model is completed, diffracted orders and their prospective profiles can be immediately obtained from the knowledge of the transfer function. The major complication to date is that an analytically mathematically technique to solve the acousto-optic interaction problem and model the arbitrary three-

dimensional transfer functions is difficult to achieve. In addition to the mathematical modeling process, the need for the manufactor of acousto-optic cells capable of producing sound fields with arbitrary profiles must be achieved to accurately validate future theoretical methods. As for the work in this dissertation, additional experimental results need to be obtained for varying values of α and Q to identify cases where bandpass and bandstop image processing occurs. These results need to be compared with analytically results presented in this dissertation.

12.0 References

1. L. Brillouin, "Diffusion de la lumiere et des rayons X par un corps transparent homogene, " Ann. Phys. vol. 17, pp. 88-122, 1922.

2. L. I. Mandel'shtam,"Light scattering by an inhomogeneous medium"[in Russian], Vol.58, p 381, 1973; Complete Collected Works[in Russian], Vol. I, USSR, Moscow, 1948

3. L. Brillouin, "La diffraction de la lumiere par des ultrasons," Act. Sci. Indust. vol. 59, p 1,1933.

4. P. Debye, F. W. Sears, "On the scattering of light by supersonic waves," Proc. Nat. Acad. Sci. vol. 18, p 409, 1932.

5. R. Lucas, P. Biquard, "Proprietes optiques des milieux solides et liquides soumis aux vibration elastiques ultra sonores," J. Phys. Radium vol. 3, p 464, 1932.

6. C. V. Raman, N. S. Nagendra Nath, "The diffraction of light by high frequency sound waves, Proc. Ind. Acad. Sci. vol. 2, p 406, 1935.

7. Lord Rayleigh, "The theory of sound," vol. II, sect. 272a. Dover, New York, 1945.

8. C. V. Raman, N. S. Nagendra Nath, "The diffraction of light by high frequency sound waves," Proc. Ind. Acad. Sci. vol. 2, p 413, 1935.

9. C. V. Raman, N. S. Nagendra Nath, "The diffraction of light by high frequency sound waves, Proc. Ind. Acad. Sci. vol. 3, p 75, 1936.

10. C. V. Raman, N. S. Nagendra Nath, "The diffraction of light by high frequency sound waves, Proc. Ind. Acad. Sci. vol. 3, p 119, 1936.

11. C. V. Raman, N. S. Nagendra Nath, "The diffraction of light by high frequency sound waves, Proc. Ind. Acad. Sci. vol. 3, p 459, 1936.

12. P. H. Van Cittert, "Zur Theorie der Lichtbeugung and ultraschallwallen," Physica IV, p 540, 1937.

13. L. E. Hargrove,"Successive Diffraction Theory for Diffraction of Light by Ultrsonic Waves of Arbitrary Waveform", Journal of Acoustical Society of America, vol. 36, p 323-326, 1964

14. O. Nomoto, Y. Torikai,"Intensity distributation of ultrasonic light diffraction spectrum. Calculation by the method of successive diffraction", Acoustica, vol. 24, p 284-296,1771

15. D. Gasasent, Optical Data Processing Applications, Springer, Berlin, 1978.

16. P. Phariseau, "On the diffraction of light by progressive supersonic waves," Ind. Acad. Sci. vol. A44, p 165, 1956.

17. F.A. Jenkins, H.E. White, "Fundamentals of Optics" McGraw Hill, New York, 1965

18. W. R. Klein, B. D. Cook, "Unified approach to ultrasonic light diffraction." IEEE Trans. sonics untrson., vol. SU- 14, p 723, 1967.

19. B. Benlarbi, P. St. J. Russell, L. Solymar, "Bragg diffraction of finite beams by thick gratings: two rival theories," Appl. Phys. B vol. 28, p 63, 1982.

20. R. R. Aggarwal, "Diffraction of light by ultrasonic waves (deduction of different theories from the generalized theory of Raman and Nath) Proc. Ind. Acad. Sci. Sect. A vol. 37, p 417, 1950.

21. W. R. Klein, B. D. Cook,"Light Diffracted by Ultrasonic Gratings", Acoustica, vol. 15, p 67-74, 1965

22. W. R. Klein, B. D. Cook,"Unified Approach to Ultrasonic Gratings Light Diffraction", IEEE Trans. on Sonics and Ultrasonics, vol. SU-14, p 123-134, 1967

23. T. M. Smith, A. Korpel,"An Ultrasonic Light Deflectorion System", IEEE Journal of Quantum Electronics, vol. QE-1, p 60-61,1965

24. R.W. Dixon, M.G. Cohen,"A New Technique for Measuring Magnitudes of Photoelastic tensors and its application to Lithium Niobate", Applied Physics Letters, vol. 8, p. 205-207, 1966

25. G. Benedek, T. Greytak, Proc. IEEE. vol. 53, p 1623, 1965.

26. R. W. Dixon, E. I. Gordon, Bell System Tech. J. vol. 46, p 367, 1967.

27. D. H. McMahon, IEEE Trans. on UltraSonics, SU-16, p 41, 1969.

28. A. Korpel, IEEE Trans. Sonics Ultrason. SU-15, p 153, 1968.

29. E. I. Gordon, "A Review of acousto-optical deflection and modulation devices," Proc. IEEE, vol. 54, p 1391, 1966.

30. R. Adler, "Interaction between light and sound," IEEE Spectrum, vol. 69, p 48, 1981.

31. A. Korpel, "Acousto-optics, a review of fundamentals," Proc. IEEE vol. 69, p 48, 1981.

32. O. Leroy, J. Claeys, "Diffraction of light by profiled ultrasound," Acoustica vol. 55, p 21,1984.

33. R. Pieper, A. Korpel, W. Heremn, "Extension of the acousto-optic Bragg regime through a Hamming apodization ofthe sound field," J. Opt. Soc. Am. A, vol. 3, p 1608, 1986.

34. L. Magdich, V. Molchanov, "Diffraction of a divergent beam by a periodically modulated layer," Opt. Spectrosc. vol 42, pp. 299-302, 1977.

35. R. Chu, T. Tamir, "Bragg diffraction of Gaussian beams by periodically modulated media," J. Opt. Soc. Am. vol. 66, pp. 220-286, 1976.

36. R. Chu, T. Tamir, "Diffraction of Gaussian beams for incidence close to the Bragg angle," J. Opt. Soc. Am. vol. 66 pp. 1438-1440, 1976.

37. R. Chu, T. Tamir, "Diffraction of optical beams with arbitrary profiles by a periodically modulated media," J. Opt. Soc. Am. vol. 70, pp. 1-6, 1980.

38. M. R. Chatterjee, T.-C. Poon, & others "Transfer function formalism for strong acousto-optic Bragg diffraction of light beams with arbitrary profiles," Acoustica vol.71, p 81, 1990.

39. A. Korpel, W. Bridge, "A Monte Carlo simulation of the Feynman diagram approach in strong acousto-optic interaction," J. Opt. Soc. Am. A, vol. 7, p 1503, 1990.

40. A. Korpel, T.-C. Poon, "Explicit formalism for acousto-optic multiple plane wave scattering," J. Opt. Soc. Am. vol. 70, pp. 817-820, 1980.

41. P. K. Das, C. M. Decusatis, "Acousto-optic Signal Processing:Fundamentals and Applications," Artech House., 1991.

42. N. Uchida, N. Niizeki,"Acoustooptic deflection material and techniques", Proc. IEEE 61, p 1073-1089, 1973

43. R. Hardin, F. Tappert, "Applications of the split step Fourier method to the

numerical solution of nonlinear and variable coefficient wave equations," SIAM Review, vol. 15, 423, 1973.

44. A. Hasegawa, F. Tappert, "Transmission of stationary nonlinear optical pulses in dispersive dielectric fibers. I. Anomalous dispersion," Appl. Phys. Lett. vol. 23, p 142, 1973.

45. A. Hasegawa, F. Tappert, "Transmission of stationary nonlinear optical pulses in dispersive dielectric fibers. II. Normal dispersion, "Appl. Phys. Lett. vol. 23, p 171,1973.

46. R. A. Fisher, W. Bischel, "The role of linear dispersion in plane wave self Phase modulation," Appl. Phys. Lett. vol. 23, p 661, 1973.

47. N. N. Bojarski, "The K-space formulation of the scattering problem in the time domain," J. Acoust. Soc. Am. vol. 72, p 570, 1982.

48. P. P. Stepanichen, K. C. Benjamin, "Forward and Backward projection of acoustic fields using FFT methods," J. Acoust. Soc. Am. vol. 71, p 803, 1982.

49. G. L. Payne, D. R. Nicholson, R. M. Downie, "Numerical solution of the Zakharov equations," J. Comput. Phys. vol. 73, p 486, 1983.

50. D. Yevick, L. Thylen, "Analysis of gratings by the beam-propagating method", J. Opt. Soc. Am. vol. 72, p 1084, 1982.

51. C. Venzke, A. Korpel, D. Mehrl, "Improved space-marching algorithm for strong acousto-optic interaction of arbitrary fields," Appl. Opt. vol. 31, p 656, 1992.

52. A. R. Hare, G. R. Morrison, "Near-field soft X-ray diffraction modelled by the multislice method," J. Mod. Opt. vol. 41, p 31, 1994.

53. R. Wolfe, "Applied Solid State Science - Advances in materials and device research," Academic Press, New York, 1972.

54. T.-C. Poon, P. P. Banerjee,"Principles of Applied Optics", Aksen, 1990.

55. B. E. A. Saleh, M. C. Teich, "Fundamentals of Photonics," John Wiley and Sons, Inc., 1991.

57. H. Kogelnik, "Coupled wave theory for thick hologram gratings," Bell Syst. Tech J. Vol. 48, p 2908, 1969.

58. P. P. Banerjee, C. Tarn, "A Fourier transform approach to acousto-optic interaction in the presence of propagational diffraction," Acustica vol. 74, p 181, 1991.

59. S. Min, M. R. Chatterjee, "General integral formalism for acousto-optic and holographic Bragg scattering for arbitrary profiles and orientations," Acustica vol. 71, p 81, 1990.

60. M. D. McNeill, T.-C. Poon, "Gaussian beam profile shaping by acousto-optic Bragg diffraction," Appl. opt. vol. 33, p 4508, 1994.

61. A. Korpel, H. H. Lin, D. Mehrl, "A convenient operator formalism for Fourier optics and inhomogeneous and nonlinear wave propagation," J. Opt. Soc. Am. A vol. 6, p 630, 1989.

62. "Numerical Recipes in C, second edition."

63. "Numerical Recipes in FORTRAN, second edition."

64. Erich Zauderer, "Partial Differential Equations of Applied Mathematics, second edition."

65. Larry Nyhoff, Sanford Leestma, "FORTRAN 77 for Engineers and Scientists, second edition."

66. Donald W. Trim, "Applied Partial Differential Equations, second edition."

67. Ian N. Sheddon, "Fourier Transforms".

68. Mark D. McNeill, "3-D Strong Acousto-Optic Interaction Theory", Ph.D. Disseration, Virginia Polythenic Institute and State University, 1996.

69. E.C. Zachmanoglou, Dale W. Thoe, "Introduction to Partial Differential Equations with Applications".

70. Ruel V. Churchill, "Operational Mathematics".

71. Stanley J. Farlow, "Partial Differential Equations for Scientists and Engineers".

72. P. Banerjee, D. Cao, T.-C. Poon, "Basic image-processing operations by use of acousto-optics," Applied Optics, vol. 36, p 3086, 1997

73. S.-T.Chen, M. Chatterjee, "Dual-input hybird acousto-optic set-reset flip-flop and its nonlinear dynamics", Applied Optics, vol. 36, p 3147, 1997

13.0 Vita

Derrek Butler Dunn was born in Burlington, North Carolina on March 24,1968 to Samuel Jefferson and Roxie Butler Dunn. He went to public school in the Greensboro, North Carolina where he graduated from Greensboro Grimsely Senior High School in May, 1986.

Derrek B. Dunn received the Bachelor of Science in Mathematics from North Carolina A&T State University in December 1989. In December 1990, he completed all requirements for the Bachelor of Science in Electrical Engineering, also from North Carolina A&T State University. In June 1993, he received the Master of Science degree in Electrical Engineering, from Virginia Polytechnic Institute and State University. Derrek has recently completed a second Master of Science degree in Mathematics, also from Virginia Polytechnic Institute and State University in May 1995. He is presently completing the Doctor of Philosophy in Electrical Engineering at Virginia Polytechnic Institute and State University.

Derrek has worked three consecutive summers, from summer of 1991 to summer of 1993, as an intern at Honeywell Technology Center in Minneapolis, Minnesota. Honeywell Technology Center is the research and development division of Honeywell Inc.. He worked on several projects in the area of communication systems while interning at Honeywell.

Derrek is a member of Institute of Electrical and Electronic Engineers (I.E.E.E.), National Society of Professional Engineers (N.S.P.E.), the Optical Society of America (OSA) and the International Optical-Instrumentation Society (SPIE). Derrek has also been inducted into Alpha Lambda Delta, Alpha Chi, and Pi Mu Epsilon, the National Mathematics Honor Society. Derrek recently passed the Engineers in Training (EIT) Exam, the EIT is first step toward becoming a registered professional engineer, in April of 1995.

Derrek has presented a conference papers at the Southeastern Symposium on System Theory, Southeast con, and the Optical Society of America annual meeting. Derrek has given an invited lecture on satellite communication systems for the Virginia Space Grant Consortium's "Reaching for the Star" Video Teleconference in April of 1993.

Derrek has a keen interest in teaching at a college or university as a full-time faculty member. His brother, Dr. DeRome Osmond Dunn, is a faculty member at North Carolina A&T State University in the Mechanical Engineering Department. His father, Dr. Samuel Jefferson Dunn, taught in the School of Agriculture at N.C. A&T S.U. for thirty plus years. Derrek would like to continue this tradition of collegiate teaching that his father and brother have started.

Derrek started to consider a career in academia while he was in the ninth grade. Since that time he has taken steps to assure his ability to achieve this goal. These steps included going to summer school continuously from the summer before starting the tenth grade until he completed both of his Bachelors of Science degrees and taking night courses in addition to his regular classes while a student at Grimsely Senior High School.